DISSERTATION

GLIAL SIGNALING MECHANISMS IN THE PROGRESSION OF NEUROINFLAMMATORY INJURY

Submitted by

Katriana A. Popichak

Graduate Degree Program in Cell and Molecular Biology

In partial fulfillment of the requirements

For the Degree of Doctor of Philosophy

Colorado State University

Fort Collins, Colorado

Summer 2018

Doctoral Committee:

Advisor: Ronald B. Tjalkens

Gerrit J. Bouma
Laurie R. Goodrich
Marie E. Legare
Jennifer L. McLean

ABSTRACT

GLIAL SIGNALING MECHANISMS IN THE PROGRESSION OF NEUROINFLAMMATORY INJURY

The response of glial cells to foreign and endogenous stress signals is extensive. As a result, release of inflammatory factors as means of cellular communication and innate immune function, or neuroinflammation, can contribute to neurodegeneration and increased activation of surrounding glia, often associated with Parkinson's disease (PD). The identification of glial activation as an early event in the progression of neurodegenerative disease that precedes neuronal cell death presents an opportunity for better diagnostic markers, as well as new pathways that could be targeted therapeutically. The transcription factor, Nuclear Factor-kappa B (NF-κB), regulates the expression of multiple neuroinflammatory cytokines and chemokines in activated glial cells but the signaling factors modulating glial-glial and glial-neuronal signaling during neurotoxic injury are poorly understood. Thus, inhibition of NF-κB signaling in glial cells could be a promising therapeutic strategy for the prevention of neuroinflammatory injury. Recently, it was found that selected orphan nuclear receptors in the NR4A family (nerve growth factor-induced-β/NGFI-β), including NR4A1 (Nur77) and NR4A2 (Nurr1), can inhibit the inflammatory effects of NF-κB but there are no approved drugs that target these receptors. In the current studies, we utilized several experimental approaches to target neuroinflammation in cellular models of PD and manganese neurotoxicity in primary glia and in animal models. One of these studies demonstrated that a novel ligand of NR4A1 and NR4A2, 1,1-bis (3'-indolyl) -1-(p-methoxyphenyl) methane (C-DIM5), suppressed NF-κB-dependent inflammatory gene

expression in astrocytes following treatment with 1-methyl-4-phenyl-1, 2, 3, 6-tetrahydropyridine (MPTP) and the inflammatory cytokines, IFN-γ and TNF-α. These data were further supported by previous studies from our laboratory, which examined efficacy of multiple C-DIM compounds in PD animal and cellular models, including one (C-DIM12) identified as a modulator of Nurr1 activity that also inhibited NF-kB-dependent gene expression in glial cells. Collectively, these data demonstrate that NR4A1/Nur77 and NR4A2/Nurr1 dynamically regulated inflammatory gene expression in glia by modulating the transcriptional activity of NF-κB. An additional study examined the role of NF-κB in manganese (Mn)-induced neurotoxicity by exposing purified microglia, astrocytes (from both wild-type and an astrocyte-specific NF-kB (IKK2) knock-out (KO) mouse) and mixed glial cultures to varying Mn concentrations and then treated neurons with the conditioned media (GCM) of each cell type. In doing so, we showed that mixed glial cultures exposed to Mn enhanced glial activation and neuronal death compared to microglia, wild type astrocytes or IKK2-knockout astrocytes alone or in mixed cultures suggesting that astrocytes are a critical mediator of Mn neurotoxicity through enhanced expression of inflammatory cytokines and chemokines, including those most associated with reactive phenotype such as C3 and CCL2. Thus, these studies elucidate key mechanisms associated with neuroinflammation and present potential therapeutic targets in glial cells that regulate the progression of neuroinflammatory injury.

TABLE OF CONTENTS

CHAPTER 1

LITERATURE REVIEW

1.1 NEURODEGENERATIVE DISEASE

1.1.1 PARKINSON'S DISEASE

Parkinson's disease (PD) is a progressive, neurodegenerative disorder characterized by the loss of nigrostriatal dopaminergic neurons within the Basal Ganglia, the movement center of the brain (Kalia and Lang, 2015). While the overall cause of PD is largely unknown, there are multiple contributing factors including genetic predisposition and environmental exposure, which may synergistically contribute to disease etiology. According to the Parkinson's Disease Foundation, approximately 1 million people in the U.S. and 10 million worldwide live with the disease, with an estimated 60 thousand diagnosed annually in the U.S.

James Parkinson first described PD as a movement disorder 200 years ago and identified the neurological symptoms still recognized today. The first PD patients presented with "**…**involuntary tremulous motion, with lessened muscular power, in parts not in action and even when supported; with a propensity to bend the trunk forwards, and to pass from a walking to a running pace…" (Parkinson, 1817). The symptoms of a PD patient are progressive and debilitating, often contributing to rapid decline in quality of life. The primary motor symptoms include tremor of hands, arms, legs, jaw and face, bradykinesia (slowness of movement), rigidity of the limbs and trunk and postural instability (Jankovic, 2008). Other non-motor symptoms associated with PD include dementia, depression as well as gastrointestinal disturbances (Lozano et al., 1998; Weintraub et al., 2018).

Clinical presentation of disease occurs upon depletion of 60–70% dopaminergic neurons in the substantia nigra pars compacta, which leads to an 80% reduction in striatal dopamine levels (Lang and Lozano, 1998b). There is no treatment to halt neuronal degeneration, however there are drugs used to treat symptoms. Ultimately, there are no approved therapeutic agents to halt the progression of the disease.

The probability of developing PD often increases with age and male gender (Pringsheim et al., 2014), but the etiologic factors are still not completely understood. Environmental factors such as neurotoxicants (pesticides and heavy metals) (Baltazar et al., 2014; Di Monte et al., 2002), bacterial, viral and nutritive exposures (Liu et al., 2003), oxidative stress (Halliwell, 2006), mitochondrial dysfunction (Schapira, 2011) and gene mutation (Jankovic, 2008) are shown to play causative roles in neurodegeneration associated with PD. Genetic mutations in genes such as parkin, PTEN-induced kinase-1 (PINK1) and DJ-1 lead to an early onset for of Parkinsonism, whereas inherited mutations in leucine-rich repeat kinase 2 (LRRK2) and α-Synuclein cause late onset PD (Billingsley et al., 2018; Ferreira and Massano, 2016). Most intriguingly, however, is that there is increased support implicating glial inflammation in the brain as a major pathogenic factor in PD (Hirsch et al., 2003; Teismann and Schulz, 2004). An incomplete understanding of disease pathology associated with neuroinflammation has in part hindered the development of better treatment strategies. Observations made postmortem from the brains of individuals who suffered from PD have revealed a sustained inflammatory response within microglia and astrocytes in the SNpc that potentiates damage to neurons, thereby promoting progression of the disease (Hirsch et al., 2003; Pekny and Nilsson, 2005; Pekny et al., 2014; Teismann and Schulz, 2004).

A more complete appreciation of agents that promote neuroinflammation is therefore necessary to better understand pathogenic mechanisms associated with the progression of PD in order to identify neuroprotective therapeutic strategies to preserve neuronal function.

1.1.2 MANGANISM

Although Manganese (Mn) is an essential nutrient, excessive exposure to Mn is toxic and leads to a neurodegenerative disease called Manganism. It is characterized by motor deficits that are similar to those seen in idiopathic Parkinson's disease (PD), including gait disturbances, facial masking, speech problems, dystonia and action and postural tremor, as opposed to hallmark characteristic of resting tremor seen in idiopathic PD (Guilarte, 2010; Perl and Olanow, 2007). However, neurological variations from PD include an absence of resting tremor, dissimilar gait abnormalities and varied involvement of neurons in the substantia nigra pars compacta. These PD-like indicators can be attributed to neuropathological changes including irreversible neuronal loss, atrophy and glial- and neuro-inflammation within the globus pallidus (GP), substantia nigra pars reticulata (SNpr) and striatum (ST) of exposed individuals (Aschner and Aschner, 1991; Aschner et al., 2005; Aschner et al., 2007; Sigel, 2007).

The mechanisms of how Mn exposure leads to specific neurodegenerative changes in the basal ganglia of those exposed are less well understood. While it appears that Mn crosses the BBB through some facilitated diffusion and active transport, Mn preferentially accumulates in astrocytes due to their high-capacity transporters through mechanisms such as divalent metal transport 1 (DMT-1; also known as DCT-1/NRAMP2)-mediated transport as well as ZIP8- and transferrin (Tf)-dependent transport (Aschner et al., 2007)

The concentration of Mn in astrocytes is 50–60 times higher than in neurons; where the highest concentration of Mn is found in the mitochondria (Aschner et al., 1992; Morello et al.,

2008; Sidoryk-Wegrzynowicz and Aschner, 2013). Elevated levels of Mn are shown in the basal ganglia of exposed humans and animals (Olanow, 2004; Racette, 2014) and experimental evidence shows that Mn can be directly neurotoxic through inhibition of mitochondrial respiration leading to energy failure and oxidative stress (Zhang et al., 2003), as well as glial toxicity and neuroinflammation; which are all shown to contribute to Mn neurotoxicity, and thus, disease progression (Aschner and Aschner, 2005; Filipov and Dodd, 2012; Sigel, 2007).

1.2 NEURODEGENERATIVE DISEASE-CONTRIBUTING ENVIRONMENTAL EXPOSURES

1.2.1 MANGANESE

Manganese (Mn) is a ubiquitous trace element found in water, soil, air, and food (Bjørklund et al., 2017). As the fifth most abundant metal on earth, manganese is needed for proper fetal development (Mistry and Williams, 2011; Wood, 2009; Zota et al., 2009) and necessary for adult function, as well (Parmalee and Aschner, 2016), lending its role to the composition of metallo- proteins, including mitochondrial enzymes, superoxide dismutase (SOD) and pyruvate carboxylase, as well as glutamine synthetase (GS), which is specific to astrocytes in the CNS (Aschner et al., 2005; Aschner et al., 2007).

Approximately 90% of Mn intake is dietary, coming from plant-based foods such as avocados, blueberries, nuts and seeds, seaweed, egg yolks, whole grains, legumes, dried peas, green leafy vegetables and spices, and plant-derived beverages such as tea (Aschner, 2000; Lucchini et al., 2014). The average intake of Mn is between 2 and 9 mg/ day (for an average 70-kg person) (Aschner, 2000).

Exposure to high levels of Mn occurs in occupational settings such as factory work, mining and welding (Aschner et al., 2005; Bowler et al., 2006; Hua and Huang, 1991) but there is also more widespread exposure of Mn in the general population through well-water, aerosolized gasoline additive, MMT, and crops with residues of the Mn-containing pesticide Maneb (Santamaria, 2008). Additionally, dietary exposure includes high levels of Mn in soy-based infant formula (compared to breast milk) and well water in affected rural areas that are associated with cognitive and fine motor deficits in children (Bjørklund et al., 2017; Collipp et al., 1983).

There is increasing concern with chronic Mn exposure in children due to their lower ability to clear Mn (Collipp et al., 1983), higher levels of iron deficiency, shown to elevate brain Mn levels (Aschner and Aschner, 2005), and greater absorption of Mn from the GI tract (Neal, 2012). Epidemiological studies have reported cognitive deficits in children exposed to high levels of Mn in drinking water (Kim et al., 2009; Menezes-Filho et al., 2011; Riojas-Rodriguez et al., 2010), highlighting the need for future studies addressing the long-term consequences of these exposures. Additionally, iron deficiency, shown to increase Mn levels in the brain and considered the most common and widespread nutritional disorder in underdeveloped as well as industrial countries, is exacerbated by infection, ranging from parasitic to bacterial.

Additionally, glial response to Mn is especially prominent (Streifel et al., 2013; Verina et al., 2011). While it is shown that Mn exposures result in neurodegeneration (Zhao et al., 2009), glial activation in response increased Mn levels in the brain promotes neuroinflammation that may increase susceptibility to other neurotoxicants or neurological disease. This aspect of combinatorial environmental exposures that enhance risk for neurological disease has now

become a closely scrutinized area of biomedical research. This is further discussed later and investigated in Chapter 3.

1.2.2 BACTERIAL INFECTION-ENDOTOXIN

Gram-negative bacterial infections, in particular, range from food poisoning to gingivitis and periodontitis, which can cause severe meningitis, resulting from NF-κB-mediated cytokine expression in the peripheral immune system (Lee et al., 1993; Li et al., 2015a). Increasingly, there are reports of environmental exposures to endotoxin (LPS), including airborne exposures in sewage treatment plants, cotton textiles, metal working and even in the home (Block and Calderon-Garciduenas, 2009; Fang et al., 2003; Lange et al., 2003; THORN, 2002). Interestingly, normal flora in the gut consists of gram-negative bacteria, typically harmless to the host. Upon gram-negative bacterial infection, pro-inflammatory factors and cytokines produced peripherally communicate with the brain to change behavior through interaction with innate immune cells of the CNS including microglia (Villarán et al., 2010). In addition, systemic inflammatory mediators send signals to the brain through the compromised blood-brain barrier, ultimately activating perivascular macrophages and microglia, resulting in production of cytokines, prostaglandins and nitric oxide (NO) (Filipov et al., 2005). This systemic inflammation is part of the canonical immune response but can also exacerbate neurodegenerative disorders (Barhoumi et al., 2004). Microglia in aged rodents show increased activation and a more pronounced neuroinflammatory phenotype. Mn enhances LPS-induced production of proinflammatory cytokines in microglial cells and potentiates NF-κB-dependent expression of NOS2 in astrocytes (Zhang et al., 2010). LPS, especially in a capacity comparable to environmental exposure either directly or indirectly through bacterial infection, seems to contribute to persistent inflammation both peripherally and neurologically. Either way, these

effects of bacterial infection appear to work in a synergistic manner with other environmental exposures and the cooperation of various cell types to promote neurotoxic injury to the brain.

1.2.3 NEUROTOXICANT-MPTP

Other environmental neurotoxins associated with neurodegenerative diseases include various pesticides, such as paraquat, and recreational drugs such as opioids. One such drug, 1-methyl-4-phenyl-1, 2,3,6-tetrahydropyridine (MPTP), has proven beneficial for PD research.

In 1983, a number of young individuals accidentally injected themselves with MPTP. They rapidly displayed all the signs and symptoms typical of Parkinsonism, and they responded to treatment with levodopa (a synthetic dopamine) in the same manner, which idiopathic PD patients respond. Later, a neuropathologic study of the brains of those MPTP-exposed individuals demonstrated moderate to severe depletion of dopaminergic neurons in the substantia nigra, the specific region affected in PD, emphasizing the high degree of selectivity of MPTP toxicity (Di Monte et al., 2002).

More surprisingly, however, was that gliosis (glial inflammation) and clustering of microglia around nerve cells were present in the substantia nigra, suggesting, not only that MPTP, an environmental exposure, at least initially, could cause PD-like pathology, but that a neuroinflammatory glial response was also involved (Di Monte et al., 2002). Since then, MPTP has been widely utilized in *in vivo* PD models in both mice (Nagatsu and Sawada, 2005; Sugama et al., 2003) and primates (Di Monte et al., 2002), as well as extensive *in vitro* models, all of which collectively chronicle the response to MPTP ranging from behavioral (De Miranda et al., 2015b) to neuropathological studies, as well as RNA and protein profiling in varied cell types, such as glia (Carbone et al., 2009), in *in vitro* models (Chapter 2).

1.3 NEUROINFLAMMATION & GLIAL INVOLVEMENT

Neuropathology in neurodegenerative disease is associated with robust glial inflammation (Olanow, 2004). Glial-derived inflammatory cytokines and nitric oxide (NO) influence the progression of neuronal injury mediated by environmental exposures, genetic deficits and protein misfolding (Liu et al., 2006; Moreno et al., 2009; Moreno et al., 2008), leading to a state of neuroinflammation that furthers the progression of neuronal injury. This inflammatory glial response may additionally be triggered by signals emanating from neurons, creating a positive feedback signaling loop whereby glial activation and production of neurotoxic inflammatory mediators is worsened by the cellular damage cues from injured and dying neurons. Given the multiple functions of many inflammatory factors, it is difficult to pinpoint their roles in specific cell types such as glia, and ultimately different disease models

1.3.1 ASTROCYTE ROLE IN NEUROINFLAMMATION

Astrocytes are the most prominent cell type in the CNS composing up to 60-70% of total cell population in the brain (Verkhratsky, 2007). Throughout the CNS (Sofroniew and Vinters, 2010), astrocytes are often characterized by morphologic expression of the intermediate filament protein, glial fibrillary acidic protein (GFAP) and other known markers including glutamine synthetase (GS), S100 calcium binding protein β, vimentin and the high affinity glutamate transporters GLT-1/EAAT2 and GLAST/EAAT1 (Kimelberg, 2004). However, GFAP has been shown to be the most consistent marker in both physiological and pathological states (O'Callaghan and Sriram, 2005).

Initially, the role of astrocytes was thought to be simply structural or the ‘glue’ of the CNS, however it is increasingly apparent that their function is more than just scaffolding necessary to maintain neuronal circuitry (Verkhratsky, 2007). While astrocyte formation of a

continuous network is important for structural integrity of the brain, their dynamic networks help create specific micro and macro domains, create physical barriers between neuronal synapses (Sofroniew and Vinters, 2010; Verkhratsky, 2007), as well as contribute to the integrity of the blood-brain barrier (BBB) through astrocytic endfeet and ensheathing of blood vessels in the CNS (Carmignoto and Gomez-Gonzalo, 2010). They also contribute to neuronal function by lending nutritive and trophic support.

As a crucial component of the BBB, astrocytes help provide and mediate glucose and oxygen delivery from blood to neurons (Verkhratsky, 2007). Plus, astrocytes are capable of storing glucose in the form of glycogen and of *de novo* synthesis of glutamate (Parpura et al., 2012). Being the primary excitatory neurotransmitter in the brain, synaptic concentration of glutamate is tightly regulated by astrocytes, also. Among others, this metabolically coupled support pathway in astrocytes is critical for neuronal survival and is especially susceptible to injury upon neurotoxicant exposure such as manganese or MPTP. In addition to being critical for neuronal metabolism, astrocytes are required for normal synaptic transmission through regulation of neurotransmitters, ions, water, and extracellular pH (Sofroniew and Vinters, 2010; Verkhratsky, 2007). Dynamic communication between astrocytes is induced by neurotransmitter release which is important in modulation of synapses in learning and memory (Perea et al., 2009). Calcium-based communication in astrocytes plays a large role in synaptic plasticity and is vital to blood flow regulation in response to neuronal activity known as neurovascular coupling (Carmignoto and Gomez-Gonzalo, 2010; Sofroniew and Vinters, 2010), and how astrocytes prompt specific vasodilation versus vasoconstriction is still heavily researched.

Astrocytes are dynamic and diverse regulators of neuronal metabolism and activity in the CNS. They also play an important role in the developing CNS, through neuronal guidance and

synaptogenesis(Verkhratsky, 2007), and in adult neurogenesis (Doetsch, 2003). During development, astrocytes assist in the migration of axons and neuroblasts and synapse formation by establishing literal boundaries, as well. The origination and function of neurons is more dependent and interconnected with the vast and extensive physiology of astrocytes than is truly realized.

In vitro studies show that human astrocytes are the primary source of NO-induced neurotoxicity specifically through NOS2 induction (Streifel et al., 2012), more so than microglia. This suggests that astrocytes could be more central in neuroinflammatory-induced neuronal death than was initially shown in a rodent model (Lee et al., 1993). Another *in vitro* study demonstrated that Mn inhibits the ability of astrocytes to promote neuronal differentiation by a mechanism that involves oxidative stress and a reduction in levels of the extracellular matrix protein, fibronectin (Giordano et al., 2009). Oxidative stress in astrocytes, also, leads to dysfunction in the mitochondria and, not surprisingly, an energy shortage (Chen et al., 2006; Streifel et al., 2012).

Mn causes metabolic changes in astrocytic glucose metabolism by inhibition of the astrocyte-specific enzyme, Glutamine Synthetase (GS). Thereby, contributing to down-regulation of glutamate transporters and compromising glutamate uptake (Suarez-Fernandez et al., 1999; Verkhratski** and Butt, 2013; Verkhratsky et al., 2016; Yin et al., 2007). Additionally, Mn perturbs ATP-induced Ca^{2+} signaling and intercellular Ca^{2+} waves in astrocytes (Streifel et al., 2012). Because astrocytes cannot function and supply adequate neurotrophic support, overexposure to Mn causes excitotoxicity, neuronal death and imbalance of neurotransmission.

More surprisingly, however, are the increased inflammatory factors produced by astrocytes, which may contribute to further injury. These factors can vary from inflammatory

cytokines such as *Ccl2* and *Ccl5* to *Il6, Il1β, Tnf, Nos2* and, more recently, an astrocyte-specific inflammatory marker, the complement factor *C3 (*Liddelow et al., 2017*).* Astrocyte involvement is continually researched and more recently it has become apparent that cell-cell crosstalk may contribute to neuroinflammation. A recent study demonstrates that astrocyte-derived CCL2, in a model of surgery-induced cognitive dysfunction, causes additional neuroinflammation by also activating microglia (Xu et al., 2017) causing further injury. This, and many other studies, demonstrates that glial-glial crosstalk exacerbates neuroinflammation far more than just one cell type alone; very much in the same way that multiple environmental exposures and contributing factors may work synergistically as a potential cause for idiopathic disease.

1.3.2 MICROGLIAL ROLE IN NEUROINFLAMMATION

Microglia are often referred to as the resident immune cells of the brain having entered the CNS during embryonic development from a monocyte-derived cell type (Kim et al., 2005; Verkhratsky, 2007). Microglia respond rapidly to neurotoxicant exposure and injury with increased production of neuroinflammatory mediators. In the adult brain, microglia proliferate at low rates but their numbers can grow due to entering perivascular mononuclear phagocytes (Gehrmann et al., 1995).

Like astrocytes, they are heterogeneous throughout the adult brain, but only compose approximately 10-15% of all glial cells with most located in the grey matter (Verkhratsky, 2007). The majority of microglia (12%) are found within the olfactory bulb, hippocampus, basal ganglia and substantia nigra. They exist in three different morphological states: a ramified phenotype found within the neuropil, a rod-like state in fiber tracts, and a macrophage/amoeboid shape in areas with an incomplete BBB (Lawson et al., 1990). Microglia are constantly migrating and scanning their surroundings; distinct from different cells and without overlap (Gehrmann et al.,

1995; Verkhratsky, 2007). Their "immunosurveilance" entails debris clean up through their phagocytic function (Verkhratsky, 2007), however other microglial functions within the CNS are not yet fully elucidated (Block and Hong, 2005; Gonzalez-Scarano and Baltuch, 1999; Kim et al., 2005).

Microglia express a variety of receptors such as neurotransmitter and pattern recognition receptors (PRRs) necessary to sense disruption of brain homeostasis, presence of foreign matter and neuronal damage (Ransohoff and Perry, 2009; Streit, 2002; Verkhratski** and Butt, 2013; Webster et al., 2013). Microglia are involved in antigen presentation and important in recruitment of other immune cells such at T and B-lymphocytes to the sites of injury in the CNS (Gehrmann et al., 1995; Gonzalez-Scarano and Baltuch, 1999). Recent research has also found that microglia may contribute to neuronal development and migration, while amoeboid microglia are involved in synaptic remodeling and regulation of neuronal apoptosis by means of communicatory factors and pruning of synapses in late embryonic development through phagocytosis (Block and Hong, 2005; Verkhratsky, 2007). Additionally, studies have shown that microglia release neurotrophic factors necessary for synaptogenesis and neuronal function (Nakajima and Kohsaka, 1993).

Microglial cells are often the "first-responders" to foreign or endogenous materials in the brain, secreting several neuroinflammatory mediators and proinflammatory cytokines (e.g., tumor necrosis factor alpha (TNF-a); interleukins 1,6 and 1Beta (IL-1, IL-6, and IL-1β); reactive oxygen and nitrogen species (ROS and RNS), as well as lipid mediators; that can act on astrocytes to stimulate secondary inflammatory responses (Chao et al., 1992; Lee et al., 2012; Liu et al., 2003; Liu et al., 2006).

Because these cytokines are often upregulated early, this is indicated to directly lead to neuronal apoptosis and amplify inflammation upon recruitment of innate and adaptive immune cells (Gensel et al., 2012; Gonzalez-Scarano and Baltuch, 1999).

The second stage of microglial activation fosters phagocytosis, known to be significantly increased by LPS, but more recently shown to be potently induced by Mn and synergistically elevated by Mn and LPS co-treatment (Park and Chun, 2016). Transformation of microglia into a phagocytic M1 phenotype can lead to irreversible neuronal injury and dysfunction, not always due to direct microglial release of cytotoxic factors.

It is shown that apoptotic or necrotic neurons are rapidly removed through phagocytosis promoted by microglial activation. Consequently, neuronal loss due to neuroinflammation has always been assumed to be from phagocytosis, but more recently, it is shown that microglial activation and phagocytosis signal seemingly healthy neurons to express phosphatidylserine or the 'eat-me' signal for removal. Extraordinarily, the blockade of phagocytosis may prevent some forms of inflammatory neurodegeneration (Neher et al., 2011). Additionally, prevention of microglial activation by pharmacologic or genetic means protects against neuroinflammatory pathology, thus implicating microglial role in neuroinflammation to be crucial (Block and Hong, 2005; Cho et al., 2008; Neher et al., 2011).

In a ramified, or resting state, microglia release anti-inflammatory and neurotropic factors. Neurotoxic exposures are mediated by glial activation, often exhibiting an increase in nitric oxide (NO) production, especially injuring neurons in closest proximity to microglia (Filipov et al., 2005). Manganese combined with exposure to other microglial activators, such as lipopolysaccharide (LPS), further enhances microglial activation, which ultimately results in degeneration of the basal ganglia.

Like astrocytes, it is shown that microglia can both protect from and contribute to neuronal injury. In doing so, the question of glial-glial crosstalk is raised. Which cell type is first activated? Is it merely that simple? Some studies show that astrocyte activation can further activate microglia, but microglial role in inflammation and injury should not be discredited. A recent study from our laboratory has shown that microglia amplify inflammatory activation of astrocytes in manganese neurotoxicity (Kirkley et al., 2017), while another study showed that microglial response to LPS further amplifies astrocyte response (Saijo et al., 2009b). It especially seems that it isn't just one exposure, or one cell type, which contributes to disease. It may, in fact, be a compound effect.

1.4 CELLULAR SIGNALING & COMMUNICATION

1.4.1 NF-κB

Nuclear Factor-kappaB (NF-κB) is a dimeric transcription factor and key regulator of pro-inflammatory gene expression (Karin and Ben-Neriah, 2000). In PD and Manganism, NF-κB-regulated factors such as *Nos2, Tnf, Il6*, *Ccl2 and Ccl5,* in microglia and astrocytes especially (Bechade et al., 2014; Nagatsu and Sawada, 2005; Teismann and Schulz, 2004), are shown to contribute to neuroinflammation and disease progression (Frakes et al., 2014; Hirsch and Hunot, 2000; Karin, 2005). Pharmacologic and genetic inhibition of NF-κB in both microglia and astrocytes can decrease glial activation, expression of neuroinflammatory genes and neuronal cell death in glial-neuronal co-culture models (Kirkley et al., 2017), as well as in *in vivo* and *in vitro* models of neurodegenerative disease including PD, Manganism, Alzheimer's disease and Multiple Sclerosis (Liddelow et al., 2017; Moreno et al., 2011; Park and Chun, 2016; Rothe et al., 2017; Saijo et al., 2009b).

NF-κB responds to multiple intra- and extracellular stress signals including exposures such as Mn and MPTP through the activation of IκBα Kinase (IKK) complex, which phosphorylates the inhibitory subunit of NF-κB, IκBα, leading to its degradation in the 26S proteasome and permitting translocation of the p50/p65 active transcription factor to the nucleus (Karin, 1999; Karin and Ben-Neriah, 2000).

While it is shown that NF-κB is directly involved in neurodegenerative disease, being able to specifically halt its activation, via either pharmacologic or genetic means in varied cell types, not only further implicates NF-κB involvement in neuroinflammatory models, but also specifically implicates the role each cell type plays. One such study from our laboratory shows that astrocytes isolated from an astrocyte-specific IKK knockout (KO) mouse produce less inflammatory cytokines upon Mn exposure and ultimately decreases microglial activation upon exposure to astrocyte-conditioned media. This not only demonstrates that astrocytes drastically respond to Mn exposure, but that astrocyte-specific NF-κB mediates this response and further amplifies microglial response, as well (Kirkley et al., 2017). This glial-glial crosstalk mediated by NF-κB activation more specifically addressed in astrocytes is discussed in chapter 3. Studies of genetically modified mice and molecular pathways in activated glia are beginning to shed light on the role which glial-mediated inflammation plays in neurodegeneration. Altered expression of different inflammatory factors can either promote or offset neurodegenerative processes. Since many inflammatory responses are beneficial, directing and instructing an inflammatory system may be a better therapeutic objective than suppressing it.

1.4.2 NR4A ORPHAN NUCLEAR RECEPTORS AS MODULATORS OF NEUROINFLAMMATION

Because of the involvement of the NF-κB pathway in neuroinflammation, factors regulating this pathway in glia are considered to be important drug targets. Intriguingly, nuclear orphan receptors in the NR4A family, including NR4A1 (Nur77) and NR4A2 (Nurr1), constitutively antagonize the effects of NF-κB in inflammatory gene expression in glial cells. Nurr1, through a novel diindolylmethane drug ligand (C-DIM12), represses transcription of inflammatory genes in microglia by forming a complex with NF-κB and by stabilizing nuclear co-repressor proteins at NF-κB response elements that prevents the transcription of inflammatory genes (De Miranda et al., 2015a). Additionally, in a model of sepsis, Nur77 formed heterodimers with p65 to inhibit NF-κB from binding its *cis*-acting response element (Li et al., 2015a).

Extensive research has shown that these orphan receptors are rapidly induced upon multiple stimuli in many tissues and cell types. These responses play a role in managing both exogenous and endogenous stressors and the tissue-specific expression and induction of NR4A receptors especially contributes to their specificity. While these receptors have no known endogenous ligands, they may be novel therapeutic targets in various models ranging from cancer to inflammation (Safe et al., 2015).

Several recent studies have identified structurally diverse compounds that bind, activate or inactivate nuclear Nur77 or induce nuclear export of Nur77 allowing for its translocation from the nucleus to mitochondria for apoptosis initiation, and these compounds *para*-phenyl substituted diindolylmethanes (C-DIMs) show some promise in the treatment of conditions such as metabolic diseases and cancer (Chintharlapalli et al., 2005; Cho et al., 2007; Lin et al., 2004), While these studies, among many others, demonstrate Nur77 to be an important target for

treatment in various cancers, surprisingly, there are others, which demonstrate Nur77 to be protective in non-cancer cell models.

One such study shows that Nur77 can enhance resistance to lipopolysaccharide (LPS)-induced sepsis in mice by inhibiting NF-κB activity and suppressing aberrant cytokine production by direct binding with p65 to block its binding to the κB element (Li et al., 2015a). Additionally, we demonstrated in our laboratory, via pharmacologic activation by C-DIM12, Nurr1 demonstrates similar inhibition of NF-κB activity in multiple inflammatory models including LPS exposure in BV2 microglial cells (De Miranda et al., 2015a) and primary synovial fibroblasts and RAW macrophage cells (unpublished data) in an arthritic model.

Most intriguingly, however, is the interplay of both Nur77 and Nurr1 in inflammatory models of neurodegeneration. Recent evidence indicates that Nur77 and Nurr1 may have a compensatory relationship; supported by one study that Nur77 and Nurr1 present a contra-directional coupling interaction resulting in neuroprotection (Wei et al., 2016). This "push-pull" relationship is further evaluated in a glial model of MPTP and inflammatory cytokine exposure in Chapter 2.

Being able to specifically target and halt NF-κB-mediated inflammatory injury by genetic (Chapter 3) or pharmacologic (Chapter 2) means not only implicates glial involvement in neurotoxic models, but also provides insight into potential new therapeutic strategies, thus testing the overall hypothesis that glial signaling contributes to the progression of neuroinflammatory injury.

CHAPTER 2

COMPENSATORY EXPRESSION OF NUR77 AND NURR1 REGULATES NF-KB-DEPENDENT INFLAMMATORY SIGNALING IN

2.1 INTRODUCTION

Parkinson's disease (PD) is associated with selective degeneration of dopaminergic (DA) neurons within the substantia nigra *pars compacta* (SNpc) of the midbrain. The only available treatments are symptomatic, involving pharmacological replacement or augmentation of dopamine. However, patients become refractory to these interventions over time due to continued loss of dopaminergic neurons, resulting in dose escalations and debilitating drug-induced dyskinesia (Jankovic, 2008; Kalia and Lang, 2015; Panneton et al., 2010). Observations made postmortem from the brains of individuals who suffered from PD indicate a sustained inflammatory response within microglia and astrocytes in the SNpc associated with damage to neurons and disease progression (Hirsch et al., 2003; Pekny and Nilsson, 2005; Pekny et al., 2014; Teismann and Schulz, 2004).

The transcription factor, Nuclear Factor-kappa B (NF-κB), is an important regulator in microglia and astrocytes that modulates expression of inflammatory genes associated with neuronal damage and disease progression in PD (Bechade et al., 2014; Frakes et al., 2014; Hirsch et al., 2003; Hirsch and Hunot, 2000; Teismann and Schulz, 2004). Pharmacologic and genetic inhibition of NF-κB in microglia and astrocytes can decrease activation, expression of neuroinflammatory genes and neuronal cell death in glial-neuronal co-culture models (Kirkley et al., 2017), as well as in animal models of PD, Alzheimer's disease and Multiple Sclerosis (Liddelow et al., 2017; Rothe et al., 2017; Saijo et al., 2009b). NF-κB integrates multiple intra-

and extracellular stress signals through the IκBα Kinase (IKK) complex, causing translocation of the p50/p65 active transcription factor to the nucleus (Karin and Ben-Neriah, 2000). However, IKK is not a tractable drug target given that knockout mice for this pathway die *in utero* (Tanaka et al., 1999). More recently, it was reported that several nuclear receptors, including NR4A orphan receptors (nerve growth factor-induced-b receptors), can antagonize NF-κB signaling by stabilizing nuclear co-repressor protein complexes at NF-κB *cis*-acting elements in the promoter regions of inflammatory genes in macrophages and microglia (De Miranda et al., 2015a; De Miranda et al., 2015b; McEvoy et al., 2017; Saijo et al., 2013; Saijo et al., 2009b). However, there are no approved drugs that target NR4A receptors.

Based on these findings, we reported that a novel activator of NR4A2 (Nurr1), the *phenyl* substituted diindolylmethane derivative, 1,1-bis (3'-indolyl)-1-(*p*-chlorophenyl) methane (C-DIM12), prevented LPS-induced activation of NF-κB in BV-2 microglial cells by stabilizing the nuclear co-repressor proteins CoREST and HDAC at NF-κB binding sites in the promoter region of NOS2 (iNOS)(De Miranda et al., 2015a). Less is known regarding the anti-inflammatory activity of NR4A1 (Nur77), although a recent study demonstrated that loss of dopaminergic neurons induced by the neurotoxin, MPTP (1-methyl-4-phenyl-1, 2,3,6-tetrahydropyridine), is more severe in Nur77 knockout mice compared to wild-type mice and that MPTP-dependent down regulation of NR4A1 is associated with deprecations in neuronal cell differentiation and development (St-Hilaire et al., 2006). It has also been reported that homeostatic and anti-inflammatory functions of NR4A receptors extend to maintenance of neurological function and decreased injury in cardiovascular disease, as well as modulation of inflammatory immune responses in arthritis (McEvoy et al., 2017; Safe et al., 2015). Although recent studies suggest that NR4A1/Nur77 modulates lipopolysaccharide-induced inflammatory

signaling in microglia (Chen et al., 2017), it is not known whether NR4A1/Nur77 has a similar function in modulating NF-κB-dependent inflammatory signaling in astrocytes.

We therefore postulated that a novel ligand for both Nur77 and Nurr1 (1,1-bis (3'-indolyl)-1-(*p*-methoxyphenyl) methane (C-DIM5)) would suppress NF-κB-dependent inflammatory gene expression in astrocytes induced by treatment with MPTP and the inflammatory cytokines, IFN-γ and TNF-α. C-DIM5 suppressed the expression of multiple NF-κB-regulated neuroinflammatory genes in primary astrocytes without preventing translocation of p65 to nucleus following an inflammatory stimulus. In addition, C-DIM5 increased nuclear localization of both Nur77 and Nurr1, suggesting a nuclear mechanism of action. Interestingly, knockdown of either NR4A1/Nur77 or NR4A2/Nurr1 by RNA interference resulted in a compensatory increase in mRNA expression for the opposite receptor, but not for NR4A3/Nor1, indicating that these receptors are closely co-regulated in astrocytes. Genome-wide chromatin immunoprecipitation (ChIP)/Next Generation Sequencing (ChIP-Seq) analysis revealed that C-DIM5 modulates NF-κB/p65 transcription factor binding across multiple loci in astrocytes, including those regulating inflammation, cell division and neuronal trophic support. Thus, we demonstrate that pharmacologic modulation of NR4A receptors in glial cells may represent a promising approach to selectively inhibit glial inflammation in the prevention of neurotoxic and neuroinflammatory injury.

2.2 MATERIALS AND METHODS

Materials. DIM-C-pPhOCH3 was synthesized by Dr. Stephen Safe and characterized as previously described(Qin et al., 2004). All general chemical reagents including cell culture media, antibiotics, and fluorescent antibodies and dyes were purchased from Life Technologies (Carlsbad, CA) or Sigma Aldrich (St. Louis, MO) unless otherwise stated. TNFα and IFNγ were purchased from R&D Systems (Minneapolis, MN). Monoclonal antibodies against Nurr1 and Nur77 were purchased from Santa Cruz Biotechnology (Santa Cruz, CA) and horseradish peroxidase conjugated goat anti-mouse and goat anti-rabbit secondary antibodies were purchased from Cell Signaling (Danvers, MA). For immunofluorescence studies, antibodies against glial fibrillary acidic protein (GFAP), anti-FLAG, Beta-actin and p65 were purchased from Sigma Chemical Co. (St. Louis, MO) and Santa Cruz Biotechnology (Santa Cruz, CA) respectively. Antibodies used for ChIP analysis of p65 were purchased from Santa Cruz Biotechnology (Santa Cruz, CA) and Abcam (Cambridge, MA). Reagents utilized for transfection experiments were purchased from Mirus Bio (Madison, WI) for TransIT-X2 System reagent and Invitrogen (Carlsbad, CA) for Lipofectamine reagent. The NF-κB-293T-GFP-Luc reporter (HEK) cell line was purchased from System Biosciences (Mountain View, CA).

Primary Cell Isolation. Cortical glia were isolated from day-1 old C57Bl/6 or transgenic mouse pups according to procedures described previously(Aschner and Kimelberg, 1991), and purity confirmed through immunofluorescent staining using antibodies against GFAP and IBA1(Carbone et al., 2009). Briefly, pups were euthanized by decapitation under isofluorane anesthesia and cortices (astrocytes) were rapidly dissected out, and meninges removed. Tissue was subject to digestion with Dispase (1.5 U/ml), and selection of astrocytes was performed by

complete media change 24 hrs after plating to remove non-astroglial cell types. Astrocyte cultures were maintained at 37°C and 5% CO2 in minimum essential media supplemented with 10% heat-inactivated fetal bovine serum and a penicillin (0.001 mg/ml), streptomycin (0.002 mg/ml), and neomycin (0.001) antibiotic cocktail. Cell media was changed 24 hr prior to all treatments. All animal procedures were approved by the Colorado State University Institutional Animal Care and Use Committee and were conducted in accordance with published NIH guidelines.

Gene Knockdown Assays. RNA interference (siRNA, small interfering RNA) sequences were acquired from Integrated DNA Technologies (IDT DNA, Coralville, IA). Nurr1 and Nur77 RNAi duplexes were designed against splice common variants of the target gene and were validated using a dose-response assay with increasing concentrations of the suspended oligo (900-1200 ng/ml) using a standard scrambled dicer- substrate RNA (DsiRNA) as control. Astrocytes were transfected with RNAi oligonucleotides using the TransIT-X2 delivery system (Mirus Bio, Madison, WI) 48 hr before treatment with MPTP (10 μM) and the inflammatory cytokines TNFα (10 pg/ml) and IFNγ (1 μg/μl), with or without DIM-C-pPhOCH3 (10 μM) treatment or vehicle control (DMSO) for 4 hr. Separate siRNA systems were used to ensure specific knockdown of Nurr1 and Nur77 mRNA, while limiting off-target effects on other nuclear receptor family members (Nur77 or Nurr1, respectively, and Nor1). The Nurr1 dsiRNA duplex sequences are (5'→3') CUAGGUUGAAGAUGUUAUAGGCACT; AGUGCCUAUAACAUCUUCAACCUAGAA (IDT DsiRNA; denoted siNurr1) and the Nur77 DsiRNA duplex sequences (5'→3') UCGUUGCUGGUGUUCCAUAUUGAGCUU; AGCAACGACCACAAGGUAUAACUCG (IDT DsiRNA; denoted siNur77).

Flow Cytometry. The percent of astrocytes in confluent mixed glial (astrocyte and microglia) cultures before and after transfections with siNur77 and/or siNurr1 were determined by immunophenotying using direct labeling with anti-GLAST-PE (Miltenyi Biotec, San Diego, CA) and anti-Cd11b-FITC (BD Biosciences, San Jose, CA) followed by flow cytometric analysis as described{Kirkley:2017ef}. Briefly, cells were labeled using the mouse anti-GLAST-PE (20 μg/mL) and mouse anti-CD11b-FITC (10 μg/mL) at room temperature for 1 h. After labeling, the cells were washed twice in incubation buffer and resuspended at a final volume of 500 μL of PBS and stored at 37 °C until analysis. Flow cytometry was performed on a Beckman Coulter CyAn ADP flow cytometer operated with Summit software for data collection at Colorado State University's Flow Cytometry Core Facility. All further data analysis was done utilizing FlowJo software (version 10.1; FlowJo, Ashland, OR).

Real-Time RT-PCR and qPCR arrays. Confluent astrocytes were treated with MPTP (10 μM) and the inflammatory cytokines TNFα (10 pg/ml) and IFNγ (1 μg/μl), after a one-hour pretreatment with or without DIM-C-pPhOCH3 (1 or 10μM) or a DMSO vehicle control, for four hours prior to RNA isolation. RNA was isolated using the RNEasy Mini kit (Qiagen, Valencia, CA), and purity and concentration were determined using a Nanodrop ND-1000 spectrophotometer (NanoDrop Technologies, Wilmington, DE). Following purification, RNA (250-1000ng) was used as template for reverse transcriptase (RT) reactions using the iScript RT kit (BioRad, Hercules CA). The resulting cDNA was immediately profiled for *Nos2* gene expression (forward: 5'-TCACGCTTGGGTCTTGTT-3'; reverse: 5'-CAGGTCACTTTGGTAGGATTT-3') using β-Actin as a housekeeping gene (forward: 5'-GCTGTGCTATGTTGCTCTAG-3'; reverse: 5'-CGCTCGTTGCCAATACTG-3') according to

the 2-ΔΔCT method (Livak and Schmittgen, 2001). Primer sequences of additional genes profiled are presented in Table 2. Pre-designed quantitative PCR arrays profiling components of NF-κB target pathway were purchased in a 384-well format from SA Biosciences (Frederick, MD) and processed according to the manufacturer's instructions using a Roche Light Cycler 480 (Indianapolis, IN). Array data were analyzed using an online software package accessed through SA Biosciences.

Western Blotting. Confluent glia were treated with MPTP (10 μM) and the inflammatory cytokines TNF-α (10 pg/ml) and IFN-γ (1 ng/ml), with or without DIM-C-pPhOCH3 (10 μM) or a DMSO vehicle control for eight hours or, to ensure effective overexpression of Nur77/NR4A1, NF-κB-293T-GFP-Luc reporter (HEK) cells were transfected for 24 hours with human-NR4A1-FLAG/FLAG-TRE or human-empty-FLAG prior to protein harvesting. Cells were lysed with RIPA buffer, quantified via Pierce BCA Protein Assay kit (Thermo Scientific), and combined with SDS-PAGE loading buffer (1x final concentration), and equal volumes/total protein were separated by standard SDS-PAGE using a 10% acrylamide gel (BioRad, Hercules CA) followed by semi-dry transfer to polyvinylidene fluoride (PVDF) membrane (Pall Corp., Pensacola, FL). All blocking and antibody incubations were performed in 5% non-fat dry milk in tris-buffered saline containing 0.2% Tween-20. Protein was visualized on film using enhanced chemiluminescence (Pierce, Rockford, IL) on a Chemidoc XRS imaging system (Biorad, Hercules, CA). Membranes were stripped of antibody and reprobed against ß-Actin to confirm consistent protein loading among sample groups.

NF-κB Reporter Assays. For green fluorescent protein/49,6-diamidino-2-phenylindole (GFP/DAPI) and luminescence/protein expression assays, NF-κB-GFP/Luc reporter cells were grown in DMEM (Life Technologies) supplemented with 10% FBS and 1x PSN (as described earlier) on 96-well black-walled plates (Thermo Scientific, Waltham, MA). Cells were plated 24 hours before transfection with FLAG-TRE or Empty-FLAG with Lipofectamine reagent for 24hrs prior to 24-hour treatment with 10 ng/ml TNFα with or without 1μM of C-DIM5. Cells were washed with 1x phosphate-buffered saline (PBS) and stained with Hoechst 33342 (Molecular Probes/Life Technologies, Eugene, OR) in Fluorobrite DMEM (Life Technologies) incubated at 37°C, 5% CO_2 for 5 minutes, then washed again with 1x PBS. The medium was replaced with fresh Fluorobrite DMEM before reading the plate at 488/519 nm for GFP fluorescence expression and 345/478 nm for DAPI fluorescence expression on a Cytation3 Cell Imaging Multi-Mode Reader (BioTek Instruments, Winooski, VT). The GFP expression intensity values were divided over the DAPI expression intensity values for quantitative analysis. Luciferase assays were run according to the protocol provided by the luciferase assay kit utilized in which Bright-Glo lysis buffer (Promega, Madison, WI) was added after PBS wash, additionally, total protein was ascertained via BCA assay. Chemiluminescence was also detected on Cytation3 plate reader. All chemiluminescent values were divided over total amount of protein (μg/mL) for quantitative analysis.

Immunofluorescence Microscopy of Nurr1 (hNR4A1), Nur77, p65 shuttling. Primary astrocytes or hNR4A1-FLAG-transfected human embryonic kidney (HEK) cells were grown to confluence on 20 mm serum-coated glass coverslips and treated with saline or MPTP (10 μM), TNF-α (10 pg/ml), IFN-γ (1 ng/ml) for glia or TNF-α (10ng/ml) for transfected HEK cells with

or without DIM-C-pPhOCH3 (1μM or 10 μM), or a DMSO vehicle control for a time course of 24 hours for p65 and transfected HEK cells, and then 30 minutes for remaining IF in glia. Blocking and antibody hybridization was conducted in 1% goat/donkey serum in PBS, and all washes were conducted in PBS. Coverslips were mounted in Vectashield Mounting medium containing DAPI (Vector Laboratories, Burlingame, CA). Slides were imaged using a Zeiss Axiovert 200M inverted fluorescence microscope equipped with a Hammamatsu ORCA-ER–cooled charge-coupled device camera (Hammamatsu Photonics, Hamamatsu City, Japan) using Slidebook software (version 5.5; Intelligent Imaging Innovations, Denver, CO) and 6 – 8 microscopic fields were examined per treatment group over no less than three independent experiments. Quantification of protein was determined by measuring the fluorescence intensity of p65, Nurr1, Nurr7, GFP or FLAG expression within the boundary of each cell, defined by DAPI counterstain, and segmented using Slidebook 5.0 software function for fluorescence intensity minus background (F/F_O).

Chromatin Immunoprecipitation-Next Generation Sequencing (ChIP-Seq). Primary mixed glia were grown to confluence in 10-cm tissue culture plates (approximately $2x10^7$cells) and treated 30 minutes with MPTP (10 μM) and the inflammatory cytokines TNF-α (10 pg/ml) and IFN-γ (1 ng/ml), with or without DIM-C-pPhOCH3 (10 μM) or a DMSO vehicle control before cross-linking with 1% formaldehyde (Thermo Scientific) for 10 minutes. The remaining steps were adapted from the Chromatrap ChIP (chromatin immunoprecipitation) protocol, which accompanies the Chromatrap Pro-A Premium ChIP Kit (Chromatrap, Wrexham, United Kingdom). DNA was sheared into approximately 500 bp fragments before removing 10% (200 ng) for input controls, and 2 mg of chromatin was loaded into the immunoprecipitation reaction

with 2 mg precipitating antibody (as suggested by Chromatrap) anti-p65 (372) from Santa Cruz Biotechnology.

Next generation sequencing performed by the Infectious Diseases Research Center Next Generation Sequencing Core at Colorado State University using the Applied Biosystems SOLiD 3 Plus System. Fragment sequencing library preparation performed by the Next Generation Sequencing Core following standard SOLiD protocols (http://solid.appliedbiosytems.com). Each sample was deposited on a quadrant of the sequencing slide to achieve a bead density of ~65,000 beads per quadrant. Sequencing was conducted resulting in 35-bp reads that were filtered for high quality and aligned to the reference genome (GenBank). Reference genome alignments of the resulting ChIP-seq tags file provided the specific regions of protein binding in the genome.

ChIP Sequence Analysis of p65 DNA binding. ChIP-Seq reads were mapped to the mouse genome (v10mm) using StrandNGS software. The raw reads were aligned with minimum of 90% identity; maximum of 5% gaps and 30 bp as the minimum aligned read length. Post alignment, peak detection was detected using PICS algorithm. A significant peak located in a window size of 250 bases per gene. Duplicates were filtered to avoid redundancy. Using StrandNGS software, GO analysis was performed and unique terms were sorted.

Modeling. Molecular modeling was performed at the Computational Chemistry and Biology Core Facility at the University of Colorado Anschutz Medical Campus.All molecular modeling studies were conducted using Accelrys Discovery Studio 4.5 (Accelrys Inc., San Diego, CA) and the crystal structure coordinates for the NR4A1 and NR4A2 ligand binding domains (PDB IDs: 1OVL, 1YJE)(Flaig et al., 2005; Wang et al., 2003) were downloaded from the protein data bank

(http://www.rcsb.org/pdb). The protein was prepared and subjected to energy minimization utilizing the conjugate gradient minimization protocol with a CHARMm force field (Brooks et al., 2009) and the Generalized Born implicit solvent model with simple switching (GBSW)(Feig et al., 2004) that converged to an RMS gradient of < 0.01 kcal/mol. The Flexible Docking protocol(Koska et al., 2008), which allows flexibility in both the protein and the ligand during the docking calculations, was used to predict the c-DIM-5 binding mode in either the ligand binding site of NR4A1 or the coactivator binding pocket of NR4A2. Predicted binding poses were energy minimized *in situ* using the CDOCKER protocol(Wu et al., 2003) prior to final ranking of docked poses via consensus scoring that combined the Jain(Jain, 1996) PLP(Parrill and Reddy, 1999), and Ludi (Böhm, 1994) scoring functions. Interaction energies were calculated using implicit distance-dependent dielectrics.

Statistical Analysis. Experiments were performed no less than three times, with replicates consisting of independent cultures using a minimum of four plates or cover slips per replicate study. Comparison of two means was performed by Student's t-test, while comparison of three or more means was performed using one-way ANOVA followed by the Tukey-Kramer multiple comparison post-hoc test using Prism software (v6.0h, Graphpad Software, Inc., San Diego, CA). For all experiments, $p < 0.05$ was considered significant, although the level of significance was often much greater.

2.3 RESULTS

C-DIM5 reduces NF-κB-mediated inflammatory gene expression in primary mixed glial cultures.

The purity of mixed glial cultures was assessed by flow cytometry (Fig. 2.1A), demonstrating the cellular composition to be 78.8% astrocyte (Glast PE+) and 12.0% microglia (Cd11b FITC+). Primary culture mixed glia was treated with MPTP (10μM) and cytokines TNFα (10pg/ml) and IFNγ (1ng/ml) or C-DIM5 (10μM) alone for 24 hrs and mRNA expression of Nr4a1/Nur77 and Nr4a2/Nurr1, as well as multiple inflammatory cytokines and chemokines, was assessed by real-time qPCR (Fig. 2.1B,C). Nur77 mRNA levels were strongly induced by treatment with MPTP+TNF/IFN by 4 hrs. Treatment with C-DIM5 (10 μM) also induced expression of Nur77 mRNA by approximately 10-fold over control and combined treatment with both MPTP+TNF/IFN further increased expression of Nurr7 mRNA (Fig. 2.1B). In contrast, there was little or no increase in expression of Nurr1 mRNA with either treatment group (Fig. 2.1C). Following treatment with MPTP+TNF/IFN, levels *of Nos2, Ccl2, Il6 and Tnf* peaked at 4 hrs and levels of *Ccl5* mRNA were maximal at 24 hrs post-treatment (Fig. 2.1D). Treatment with C-DIM5 alone did not significantly increase expression of any cytokines or chemokines examined (Fig. 2.1D), whereas combined treatment with MPTP+TNF/IFN and C-DIM5 strongly suppressed mRNA expression of all inflammatory genes examined (Fig. 2.1E). To determine whether the observed inhibitory effect of C-DIM5 on transcript levels also occurred at a protein level, several NF-κB-regulated secreted cytokines were measured in the media of mixed glial cultures by multiplex ELISA following 24 hrs treatment with MPTP+TNF/IFN in the presence or absence of C-DIM5 or vehicle control (DMSO). As shown in Table 1, treatment of primary mixed glia with MPTP+TNF/IFN caused an increase in the inflammatory cytokines and

chemokines IL6, IL-12p70, MIP-1a, CCL5 and TARC, with a trend towards increasing levels of IL2 as well. Co-treatment with C-DIM5 inhibited expression of each cytokine or chemokine examined.

C-DIM5 inhibits NF-κB activity through a nuclear specific mechanism.

To examine the capacity of C-DIM5 to functionally inhibit NF-κB-dependent gene expression, immortalized human embryonic kidney (HEK) cells stably expressing an NF-κB-GFP-Luciferase reporter were transfected with a construct to overexpress FLAG-tagged human NR4A1/Nurr7 (hNR4A1-FLAG, Fig. 2.2A). HEK cells transfected with a control vector containing only FLAG expressed very low amounts of endogenous Nur77 protein, which was highly overexpressed in cells transfected with the NR4A1-FLAG construct (Fig. 2.2A). The subcellular localization of transfected hNR4A1-FLAG was examined in HEK reporter cells by immunofluorescence to determine the effect of treatment with inflammatory cytokines and C-DIM5 on movement of this receptor (Fig. 2.2B). In HEK cells transfected with hNR4A1-FLAG, treatment with 30 ng/ml TNF caused increased expression of NF-κB-GFP and concomitant redistribution of Nur77 from the nucleus to the cytoplasm. Treatment with TNF in the presence of C-DIM5 or treatment with C-DIM5 alone inhibited subcellular redistribution of Nur77 and reduced NF-κB-dependent expression of GFP. In contrast, HEK cells transfected with the control FLAG vector showed high expression levels of GFP following treatment with TNF (Fig. 2.1B). Expression of both NF-κB-Luc and NF-κB-GFP was quantified in Fig. 2.2C. Treatment with TNF strongly induced expression of both NF-κB-Luc and NF-κB-GFP that was not inhibited by C-DIM5 except in cells, which overexpressed Nur77 (Fig. 2.2C,D) demonstrating that the inhibitory response was both ligand and receptor-dependent. To determine if C-DIM5 inhibited

nuclear translocation of NF-κB/p65, the mean fluorescence intensity of nuclear p65 was determined by immunofluorescence following treatment with MPTP+TNF/IFN in the presence and absence of C-DIM5. MPTP+TNF/IFN induced rapid movement of p65 to the nucleus of astrocytes within 30 minutes of treatment that was not inhibited by C-DIM5 (Fig. 2.2E). Representative immunofluorescence images of astrocytes with p65 (red) and GFAP (green) are presented in Fig. 2.2F.

C-DIM5 stabilizes nuclear localization of both Nur77 and Nurr1 in primary astrocytes.

Given that C-DIM5 increased *Nur77* mRNA expression with MPTP+TNF/IFN treatment and inhibited expression of multiple neuroinflammatory genes without preventing nuclear translocation of NF-κB, we assessed the effect of treatment with C-DIM5 on the subcellular localization of Nur77 and Nurr1 by immunofluorescence microscopy (Figure 2.3). In astrocytes treated with MPTP+TNF/IFN, Nur77 translocated from the nucleus to cytoplasm, whereas treatment with C-DIM5, alone or in the presence of MPTP+TNF/IFN, kept Nur77 sequestered in the nucleus (Fig. 2.3A-B) as observed in HEK cells (Fig 2.2B). In control astrocytes, Nurr1 was largely present in the cytoplasm. Treatment with MPTP+TNF/IFN caused a modest but significant increase in nuclear levels of Nurr1, however, treatment with C-DIM5 resulted in marked redistribution of Nurr1 to the nucleus, irrespective of inflammatory stimulus (Fig. 2.3C-D).

Modulation of NF-κB-regulated inflammatory genes in primary glia by C-DIM5 involves compensatory regulation of Nur77 and Nurr1.

Previous studies demonstrated that C-DIM5 activates Nur77 to modulate gene transcription in pancreatic cancer cells (Yoon et al., 2011). We also reported that a chlorinated diindolylmethane analog of C-DIM5, 1,1-bis (3'-indolyl)-1-(p-chlorophenyl) methane, effectively suppressed LPS-induced NF-κB signaling in BV-2 microglial cells by stabilizing transcriptional co-repressor protein complexes at p65 binding sites on inflammatory gene promoters (De Miranda et al., 2015a) in a Nurr1-dependent manner. Based on these findings, we postulated that the observed inhibition of inflammatory gene expression in primary astrocytes treated with C-DIM5 involved activation of Nur77 that subsequently inhibited expression of NF-κB-regulated inflammatory genes. To test this hypothesis, we used RNAi to sequentially knock down expression of Nur77 and Nurr1 in primary astrocytes and then examined the capacity of C-DIM5 to inhibit the expression of several NF-κB-regulated inflammatory cytokines and chemokines (Figure 2.4). Expression of each NR4A family member was examined following RNAi directed against either Nur77 or Nurr1. Following transfection of primary astrocytes with siRNA oligonucleotides directed against *Nr4a1/Nur77,* mRNA levels were reduced by ~90%, *Nr4a3*/*Nor1* mRNA was unaffected whereas mRNA levels of *Nr4a2*/*Nurr1* doubled (Fig. 2.4A). Similarly, knockdown of Nr4a2*/Nurr1* had no effect on *Nor1/Nr4a3* mRNA but caused a compensatory increase in *Nr4a1/Nur77* mRNA levels 4-fold (Fig. 2.4B). Double knockdown of both *Nur77* and *Nurr1* effectively reduced mRNA for both receptors by ~60% (Fig. 2.4C) without affecting expression of *Nor1* (data not shown). We next examined protein expression of Nur77 and Nurr1 in highly purified cultures of astrocytes. Following removal of microglial cells, flow cytometric analysis indicated that cultures were >97% pure astrocytes, based upon

immunoreactivity for the high affinity glutamate transporter SLC1A3/GLAST (Fig. 2.4D). Following 24 hrs treatment with C-DIM5, protein levels of Nur77 were more robustly increased over control than were levels of Nurr1 (Fig. 2.4E). Astrocytes were next transfected with control siRNA oligonucleotides or siRNA oligonucleotides directed against Nur77 or Nurr1 singly (KD) or in combination (double KD) for 48 hrs and then examined for expression of the NF-kB-regulated inflammatory genes *Nos2*, *Il1b*, *Il6* and *Tnf* following inflammatory stimulus with MPTP+TNF/IFN for 4 hrs in the presence or absence of C-DIM5 (Fig. 2.4F). In pure astrocyte cultures transfected with control siRNA and treated with MPTP+TNF/IFN, C-DIM5 inhibited expression of *Nos2* mRNA but had less inhibitory effect on expression of mRNA for *Il1b*, *Il6* and *Tnf* compared to KD of *Nur77* alone, which enhanced suppression of mRNA expression for each gene examined following C-DIM5 treatment. Whereas *Nurr1* KD alone resulted in little to no change in inflammatory gene expression upon C-DIM5 treatment. However, double KD of both *Nur77* and *Nurr1* completely abolished the capacity of C-DIM5 to suppress inflammatory gene expression of *Nos2*, *Il1b*, *Il6* and *Tnf* following treatment with MPTP+TNF/IFN (Fig. 2.4F, last bar in each graph).

ChIP-Seq and qPCR array analysis in primary astrocytes demonstrates that C-DIM5 transcriptionally modulates the expression of multiple genes regulating inflammation, cell death and neuronal trophic support.

To identify unknown genes that interact with p65 in astrocytes in response to C-DIM5 during inflammatory activation, we conducted a genome-wide analysis of p65 binding to NF-κB consensus sequences of annotated genes in the mouse genome using ChIP-Seq (Figure 2.5). By investigating regions of the genome bound by p65 in cells treated with MPTP+TNF/IFN plus

DMSO (vehicle control) in comparison to cells treated with MPTP+TNF/IFN plus C-DIM5, we identified 34 loci bound to p65 in both treatment groups, 36 unique loci bound to p65 in the MPTP+TNF/IFN vehicle control group (DMSO) and 21 loci bound to p65 unique to cells treated with MPTP+TNF/IFN+C-DIM5 (Fig. 2.5A). The loci bound to p65 that are statistically significant ($p< 0.05$) and unique to the C-DIM5-treated group correspond to a number of pathways important for neuronal function and survival, including neuronal development and morphogenesis, regulation of cellular differentiation, protein tyrosine kinase activity and dendritic process development (Fig. 2.5B). Amongst these genes, Ppp1r9a, involved in a number of functions including axonogenesis (Nakabayashi et al., 2004) and neuron projection development(Nakanishi et al., 1997), had higher RPKM values for p65 binding in the C-DIM5 group, whereas binding of p65 to *Rps6ka3*, involved in Nur77 activation leading to apoptosis, had fewer sequenced reads in treated vs. control cells (Fig. 2.5C).

We also used a targeted qPCR array to identify patterns of mRNA expression in primary astrocytes for 86 NF-κB-regulated genes following treatment with MPTP+TNF/IFN in the presence or absence of C-DIM5 (Fig. 2.5D,E). Ontology analysis revealed that the MPTP/TNF/IFN+C-DIM5 group clustered with the Control group, distinct from the patterns of gene expression in astrocytes treated with MPTP/TNF/IFN+DMSO (Fig. 2.5D). A comparison of transcripts differentially expressed between groups ($p<0.05$) is depicted in Fig. 2.5E, representing genes involved in inflammation, cell growth and apoptosis. *Tnf* was the most highly induced transcript in cells treated with MPTP+TNF/IFN, followed by *Ifnb1*, *Birc3*, *Ccl12* and *Cxcl1* (Fig. 2.5E, top graph). Each of these genes was down regulated following treatment with MPTP+TNF/IFN in the presence of C-DIM5 (Fig. 2.5E, middle graph). A comparison of the MPTP+TNF/IFN and Control (DMSO) groups indicated little differential expression of

transcripts, except for moderate induction of *Tnf* and *Ifng*, albeit at lower levels than in the MPTP+TNF/IFN group (Fig. 2.5E, lower graph).

Molecular *in silico* modeling identifies potential interactions for C-DIM5 with both Nur77 and Nurr1.

To examine potential differences in C-DIM5 binding affinity between Nur77 and Nurr1, we conducted flexible small molecule docking studies to predict its binding manner at either the NR4A1 ligand binding site or the NR4A2 coactivator-binding site. The modeling results indicated that C-DIM5 was predicted to bind with good affinity to NR4A1 (interaction energy: -46.7 kcal/mol), with one of the indole groups buried further into the region of the binding site corresponding to the ligand binding pocket in a classical nuclear receptor with both indoles participating in pi-alkyl interactions with Leu569 and hydrogen bonds with Glu444 and Asp 593 (Figure 2.6). The methoxybenzene moiety was predicted to face towards the exterior of the pocket and form two hydrogen bonds with both the side chain and backbone amines of His515 and a pi-cation interaction with Arg514 (Fig. 2.6A-C). Additionally, C-DIM5 was predicted to bind the co-activator site of NR4A2 with the para-methoxy substituted benzene of C-DIM5 involved in a hydrogen bond with Lys590, a pi-pi interaction with Phe439, and hydrophobic interactions with Mse414, while the indole moieties participated in both hydrophobic and pi-cation interactions with Arg418 (Fig. 2.6D-F). However, due to fewer predicted hydrogen bonds and electrostatic interactions as compared to NR4A1, the interaction energy was somewhat less favorable (-34.2 vs -46.7 kcal/mol). All demonstrating that C-DIM5 binds both receptors.

2.4 DISCUSSION

Neuronal cell death is accompanied by activation of microglia and astrocytes, resulting in the coordinated expression of multiple NF-κB-regulated inflammatory genes (Bechade et al., 2014; Murphy and Crean, 2015; Verkhratsky and Butt, 2007). In the present study, we demonstrated that a novel substituted diindolylmethane compound, C-DIM5, inhibits NF-κB-mediated glial inflammation in primary astrocytes by compensatory regulation of the orphan nuclear receptors, Nur77 and Nurr1. Direct treatment of astrocytes with C-DIM5 caused an increase in *Nr4a1*/*Nur77* mRNA without affecting expression of *Nr4a2*/*Nurr1* (Fig 2.1B), suggesting that this compound has some level of selectivity towards Nur77, as revealed by previous studies in pancreatic cancer cells demonstrating that C-DIM5 is a transcriptional activator of Nur77 (Lee et al., 2014; Yoon et al., 2011). We saw similar results in HEK NF-κB-eGFP-luciferase reporter cells, which express extremely low levels of Nur77 and were refractory to the anti-inflammatory effects of C-DIM5 until transfected with human Nur77 (hNR4A1/TRE-FLAG, Figure 2.2). In cells overexpressing Nur77, C-DIM5 inhibited TNF-induced NF-κB activity and increased nuclear Nur77, suggesting that this compound likely interacts directly with the receptor to stabilize it in the nucleus. Such a nuclear-specific mechanism of action is also supported by the data in Fig. 2.2E,F, which demonstrated that C-DIM5 had no effect on translocation of NF-κB/p65 from the cytoplasm to the nucleus in GFAP+ astrocytes treated with MPTP+TNF/IFN. This indicates that inhibition of NF-κB transcriptional activity was not due to interference with upstream activating kinases nor inhibition of nuclear translocation.

In primary astrocytes treated with MPTP+TNF/IFN, Nur77 redistributed to the cytosol from the nucleus (Fig. 2.3A,B). C-DIM5 prevented loss of nuclear Nur77 in astrocytes and similarly increased nuclear levels of Nurr1 (Fig. 2.3C,D). This finding is consistent with

previous data from our laboratory which demonstrated that a related C-DIM (1,1-bis (3'-indolyl)-1-(*p*-chlorophenyl) methane; C-DIM12) inhibited NF-κB in BV-2 microglial cells by a mechanism involving inhibitory interactions between Nurr1 and p65 at NF-κB transcriptional response elements (De Miranda et al., 2015a). We also separately reported that C-DIM12 increased Nurr1 levels in the nucleus of dopaminergic neurons in the SNpc in mice lesioned with MPTP over a period of 14 days (De Miranda et al., 2013). Thus, the capacity of C-DIM5 to sequester both Nur77 and Nurr1 in the nucleus of astrocytes supports a similar mechanism of inhibition involving receptor-ligand interactions that stabilize the nuclear localization of NR4A1/2. Although Nur77 can translocate to the mitochondria of cancer cells to activate the intrinsic apoptotic pathway through interactions with Bcl-2 family proteins (Beard et al., 2015; Chintharlapalli et al., 2005; Cho et al., 2007; Lin et al., 2004), in normal tissues Nur77 has anti-inflammatory activity. Studies in cell types ranging from monocytes and T-cells to neurons and microglia report that Nurr77 can interact with NF-κB/p65 to limit expression of inflammatory genes (Chen et al., 2017; Harant and Lindley, 2004; Li et al., 2015a; McEvoy et al., 2017; Murphy and Crean, 2015; Wei et al., 2016), consistent with the data presented here in primary astrocytes.

To determine whether the observed anti-inflammatory effects of C-DIM5 on NF-κB-regulated genes required Nur77, we used RNA interference (RNAi) directed towards either Nur77 or Nurr1 in highly purified astrocyte cultures stimulated cells with MPTP+TNF/IFN in the presence or absence of C-DIM5 (Figure 2.4). Knockdown of either *Nur77* or *Nurr1* resulted in a compensatory increase in mRNA levels for the other receptor (Fig. 2.4A,B), whereas knockdown of *Nr4a3/Nor1* had no effect on expression of *Nur77* or *Nurr1*. This is a novel observation in astrocytes and suggests that these receptors are transcriptionally co-regulated,

likely because of the importance of Nur77 and Nurr1 in modulating inflammatory signaling in glial cells, which is critical to neuronal survival. C-DIM5 treatment also selectively increased Nur77 proteins levels in astrocytes without an apparent effect on Nurr1, similar to the effect of C-DIM5 on *Nurr1* mRNA levels observed in Fig. 2.1C. When purified astrocytes were treated with MPTP+TNF/IFN in the presence of C-DIM5, there was only a modest decrease in inflammatory gene expression (Fig. 2.4F), likely due to the absence of microglia, which are sensitive to inhibition of inflammatory gene expression by C-DIM compounds (De Miranda et al., 2015a) and can also enhance inflammatory gene expression in astrocytes through cell-cell signaling (Kirkley et al., 2017). Knockdown of Nur77 did not prevent the anti-inflammatory effects of C-DIM5 in purified astrocytes, whereas selective knockdown of Nurr1 partially prevented the inhibitory effects of C-DIM5 on inflammatory gene expression. However, double knockdown of both Nur77 and Nurr1 completely abolished the anti-inflammatory effects of C-DIM5 (Fig. 2.1F, last bar in each graph), supporting a compensatory role for these receptors in regulating inflammatory gene expression in astrocytes, as well as suggesting that C-DIM5 likely acts as a ligand toward both receptors. Because Nurr1 is a potent antagonist of NF-κB-regulated gene expression in macrophages, as well as microglia and astrocytes (De Miranda et al., 2015a; Saijo et al., 2013; Saijo et al., 2009b), the compensatory increase in expression of Nurr1 that occurs upon knockdown of Nur77 in purified astrocyte cultures therefore likely increased the anti-inflammatory activity of C-DIM5 toward expression of *Nos2*, *Il1b*, *Il6* and *Tnf* following treatment with MPTP+TNF/IFN. The favorable binding energies calculated for interactions between C-DIM5 for both Nur77 and Nurr1 (Figure 2.6) support such a mechanism of interaction.

Using ChIP-Seq and qPCR array analysis, we identified NF-κB-regulated loci modulated by C-DIM5 (Figure 2.5). VENN diagram analysis of ChIP-Seq data identified unique loci bound by p65 following treatment with MPTP+TNF/IFN + C-DIM5, including several important to neuron projection and morphogenesis, as well as regulation of neuronal differentiation and ATP binding (Fig. 2.5A,B). Amongst these, Ppp1r9a displayed higher RPKM read counts in the MPTP+TNF/IFN+C-DIM5 group and Rps6ka3 had fewer RPKM read counts following inflammatory stimulus in the presence of C-DIM5 (Fig. 2.5C). Increased p65 binding to Ppp1r9a (Neuroabin 1) could positively influence the effects of astrocytes on a number of key cellular functions in neurons, including axonogenesis and actin filament organization (Nakabayashi et al., 2004), as well as neuron projection development (Nakanishi et al., 1997). The positive trophic effects of C-DIM5 were also evident in decreased p65 binding to Rps6ka3 (RSK2), which is involved in the phosphorylation and activation of Nur77 leading to its mitochondrial translocation and loss of its ability to interact with NF-κB/p65 (Kurakula et al., 2014; Wang et al., 2009; Wingate et al., 2006). Thus, C-DIM5 appeared to enhance p65 binding to loci in astrocytes that trophically support neurons while simultaneously decreasing binding of p65 to loci that could enhance inflammation (Harant and Lindley, 2004; Hong et al., 2004; Li et al., 2015a).

These findings were further supported by qPCR array data of NF-κB-regulated genes (Fig. 2.5D,E), which indicated that transcripts in the MPTP+TNF/IFN+C-DIM5 group statistically clustered with control cells, distinct from gene expression patterns in cells treated only with MPTP+TNF/IFN (Fig. 2.5D). A number of differentially expressed inflammatory genes were down-regulated by C-DIM5, including *Tnf*, *Stat3*, *Ifnb1* and complement component *c3*, which is uniquely expressed by activated astrocytes in the CNS and correlates closely with a

neurotoxic inflammatory phenotype (A1 astrocytes)(Liddelow et al., 2017). *Nr4a2/Nurr1*, which is also regulated by NF-κB, was down regulated in both control and MPTP+TNF/IFN groups but up regulated in the MPTP+TNF/IFN+C-DIM5 group. These data support the conclusion that C-DIM5 suppresses inflammatory genes regulated by NF-κB, and positively regulates a number of genes important for cell survival and neuronal trophic support.

Computational-based small molecule docking studies predicted binding between C-DIM5 and Nur77 and Nurr1 in either the ligand-binding site or the co-activator binding site, respectively (Figure 2.6). Modeling results indicated that C-DIM5 binds with moderately high affinity to the ligand-binding site of Nur77 but also to the co-activator site of Nurr1. Energy minimization data indicate that C-DIM5 likely has binding affinity for both Nur77 and Nurr1 but suggests a greater potency towards Nur77. These findings are in agreement with our previously published data demonstrating that various *para*-phenyl substituted diindolylmethane analogs directly bind Nur77 and modulate its transcriptional activity(Chintharlapalli et al., 2005; Cho et al., 2010; Lee et al., 2014; Safe et al., 2015). Functionally, this suggests that activation of Nur77 and Nurr1 by C-DIM5 globally suppresses the expression of inflammatory genes in primary astrocytes, which is consistent with previous studies from our laboratory indicating that C-DIM5 protects dopamine neurons in mice lesioned with MPTP and prevents inflammatory activation of both microglia and astrocytes in the striatum and substantia nigra (De Miranda et al., 2015b). Given that C-DIM5 has favorable pharmacokinetic distribution to brain following oral dosing (De Miranda et al., 2013), this compound would likely be suitable for further development for small molecule-based approaches targeting neuroinflammation. Collectively, the data presented here suggest that Nur77 and Nurr1 are important modulators of inflammatory signaling in astrocytes that can be pharmacologically targeted to inhibit NF-κB-regulated genes. The specific

mechanisms underlying the capacity of C-DIM5 and related compounds to modulate protein-protein and protein-DNA interactions between NR4A receptors and various transcriptional regulatory factors remain to be elucidated.

2.5 FIGURES

Table 1. Reduction in secreted cytokines by C-DIM5. Inflammatory cytokines secreted upon MPTP/IFNγ/TNFα treatment are significantly reduced upon addition of C-DIM5.

Secreted Cytokine Concentration (pg/ml)

Group	IL2	IL6	IL-12p70	CCL2	MIP-1a	CCL5	TARC
Control	-	1.9±0.65*	-**	13.2±0.67 **	-*	5.7±0.52 **	9.6±0.47*
MPTP/TNF/IFN	3.1±0.24	84.6±1.13	7.4±0.33	750.4±7.58	4.1±1.09	1916±153.55	18.4±0.80
MPTP/TNF/IFN+ C-DIM5	2.6±0.15	55.1±2.53 **	2.4±0.27 **	279.5±5.74 **	- *	111.2±3.08 **	16.6±1.46*

- Result lower than limit of detection

* P<0.01, ** P<0.001 Statistical significance from MPTP/TNF/IFN group

Table 2. List of qPCR primer sequences. Primer sequences of measured genes in qPCR experiments separate from the SABiosciences NF-κB-targeted gene array.

Gene	Accession No.	Primer Sequence (5' - 3')	Length (bp)
NOS2	NM_010927.3	For: TCA CGC TTG GGT CTT GTT Rev: CAG GTC ACT TTG GTA GGA TTT	149
TNFα	NM_013693.3	For: CTT GCC TGA TTC TTG CTT CTG Rev: GCC ACC ACT TGC TCC TAC	140
IL-1β	NM_008361.3	For: GCA GCA GCA CAT CAA CAA G Rev: CAC GGG AAA GAC ACA GGT AG	90
NURR1/NR4A2	NM_001139509.1	For: GTG TTC AGG CGC AGT ATG G Rev: TGG CAG TAA TTT CAG TGT TGG T	153
CCL2	NM_011331.2	For: TTAAAAACCTGGATCGGAACCAA Rev: GCATTAGCTTCAGATTTACGGGT	121
CCL5	NM_013653.3	For: GCT GCT TTG CCT ACC TCT CC Rev: TCG AGT GAC AAA CAC GAC TGC	104
IL-6	NM_031168.1	For:CTG CAA GAG ACT TCC ATC CAG Rev:AGT GGT ATA GAC AGG TCT GTT GG	131
β-ACTIN	NM_007393.3	For: GCT GTG CTA TGT TGC TCT AG Rev: CGC TCG TTG CCA ATA GTG	117
HPRT	NM_013556.2	For: TCA GTC AAC GGG GGA CAT AAA Rev: GGG GCT GTA CTG CTT AAC CAG	142
NOR1/NR4A3	XM_006537657.3	For: TGC GTG CAA GCC CAG TAT AG Rev: ATA AGT CTG CGT GGC GTA AGT	60
NUR77/NR4A1	NM_010444.2	For: TTG GGG GAG TGT GCT AGA AG Rev: GTA GGC TTG CCG AAC TCA AG	202

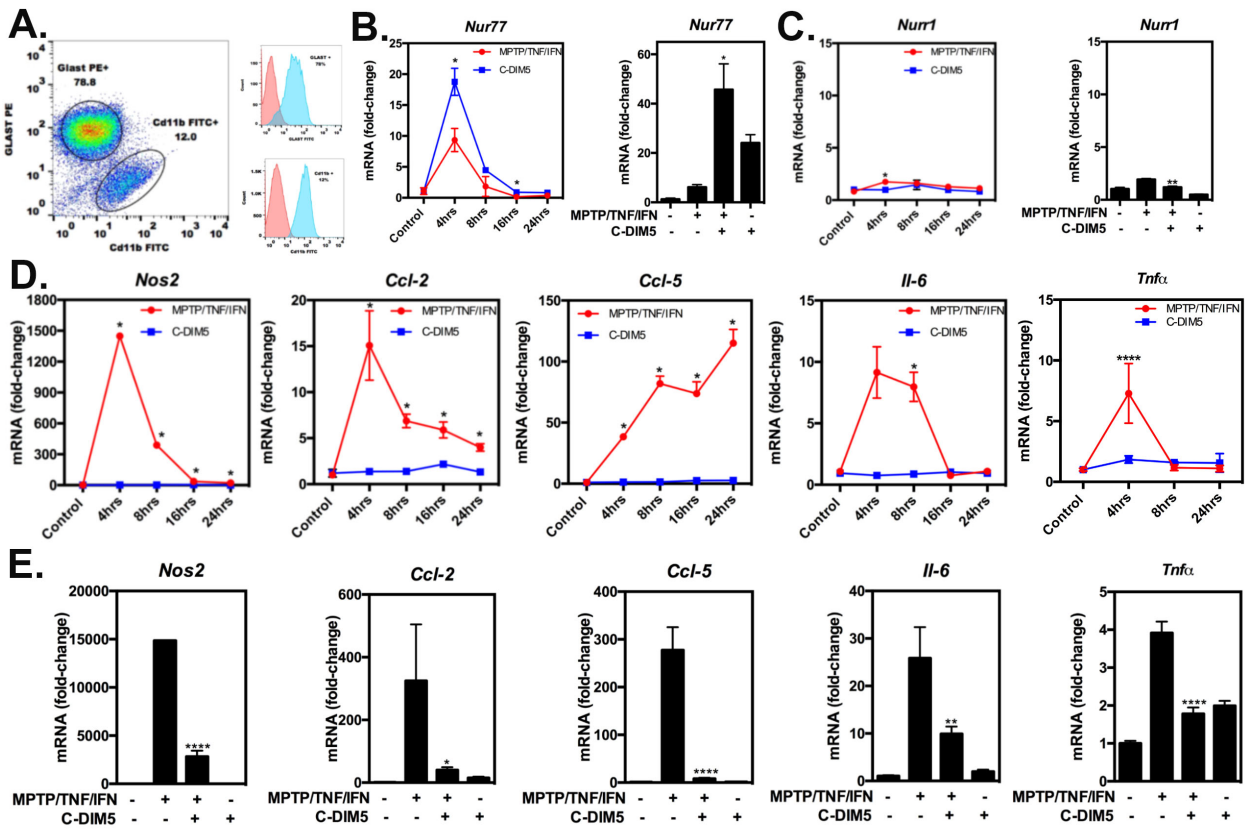

Figure 2.1. C-DIM5 alone and MPTP/IFNγ/TNFα-induced mRNA expression in primary mixed glia over a time course of 24 hours. (A) Flow cytometry scatter plots show the percentage of Cd11b (microglia-12%) or GLAST-positive (astrocytes-78.8%) cells in mixed glial cultures. **(B)** C-DIM5 alone increases *Nur77* mRNA at 4 hours and MPTP/IFNγ/TNFα mildly activates *Nur77*, while both synergistically show an increase. **(C)** C-DIM5 alone does not increase *Nurr1*. **(D)** A time course over 24 hours demonstrates the most inflammatory gene expression at 4 hours, while C-DIM5 does not. **(E)** C-DIM5 suppresses inflammatory gene expression at 4 hours.

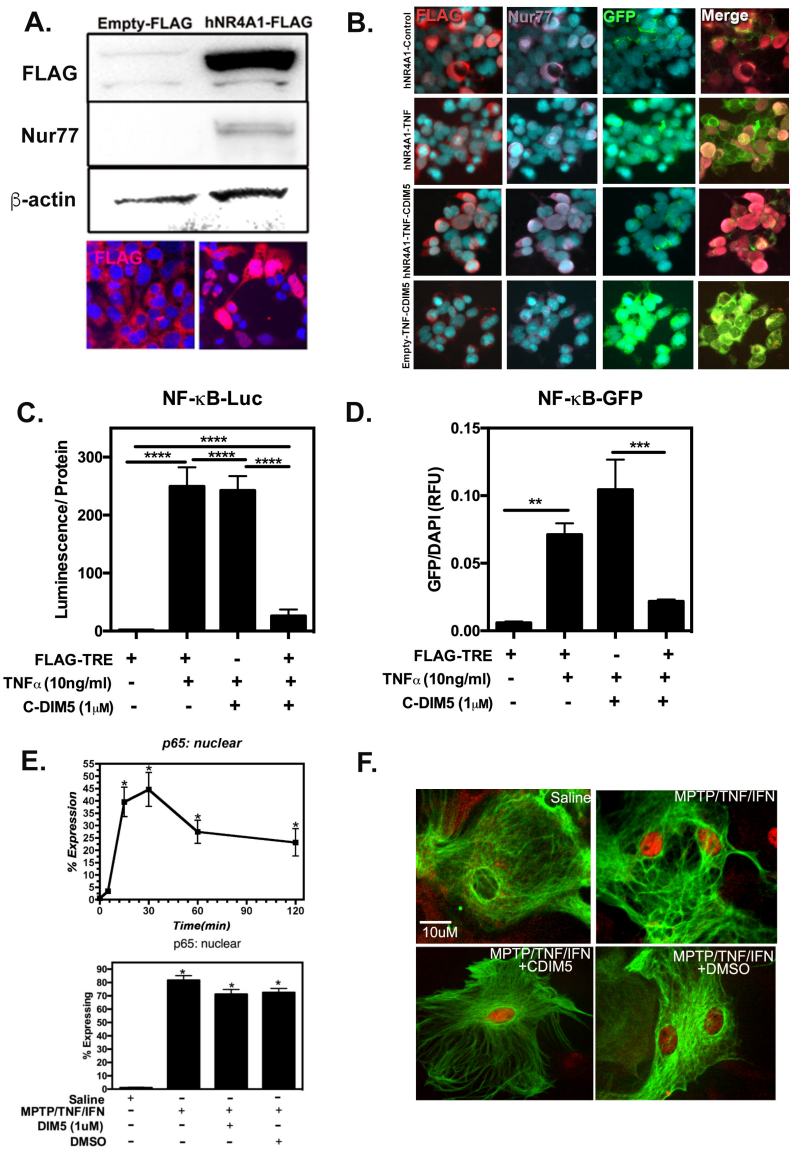

Figure 2.2. C-DIM5 inhibits NF-κB activity in HEK NF-κB-GFP/luciferase reporter cells upon hNR4A1-FLAG (Nur77) overexpression, through a nuclear specific mechanism exhibited in primary astrocytes. **(A)** Western blot and representative images demonstrating increased Nur77 and FLAG in HEK dual-reporter cells. **(B)** Representative images demonstrating increased nuclear Nur77, upon overexpression in the presence of C-DIM5, after TNF treatment in HEK cells. **(C-D)** Quantitative graphs demonstrate decreased NF-κB activity via luciferase and GFP expression. **(E)** A time course graph demonstrating increased nuclear p65 expression under the influence of MPTP and IFNγ/TNFα at 30min in primary astrocytes. Additionally, C-DIM5 does not suppress p65 translocation. **(F)** Representative images of p65 translocation in astrocytes under basal conditions and/or stimulation with MPTP (10μM) and TNF-α (10pg/ul)/IFN-γ (1ng/ul) in the absence or presence of 1 uM C-DIM5.

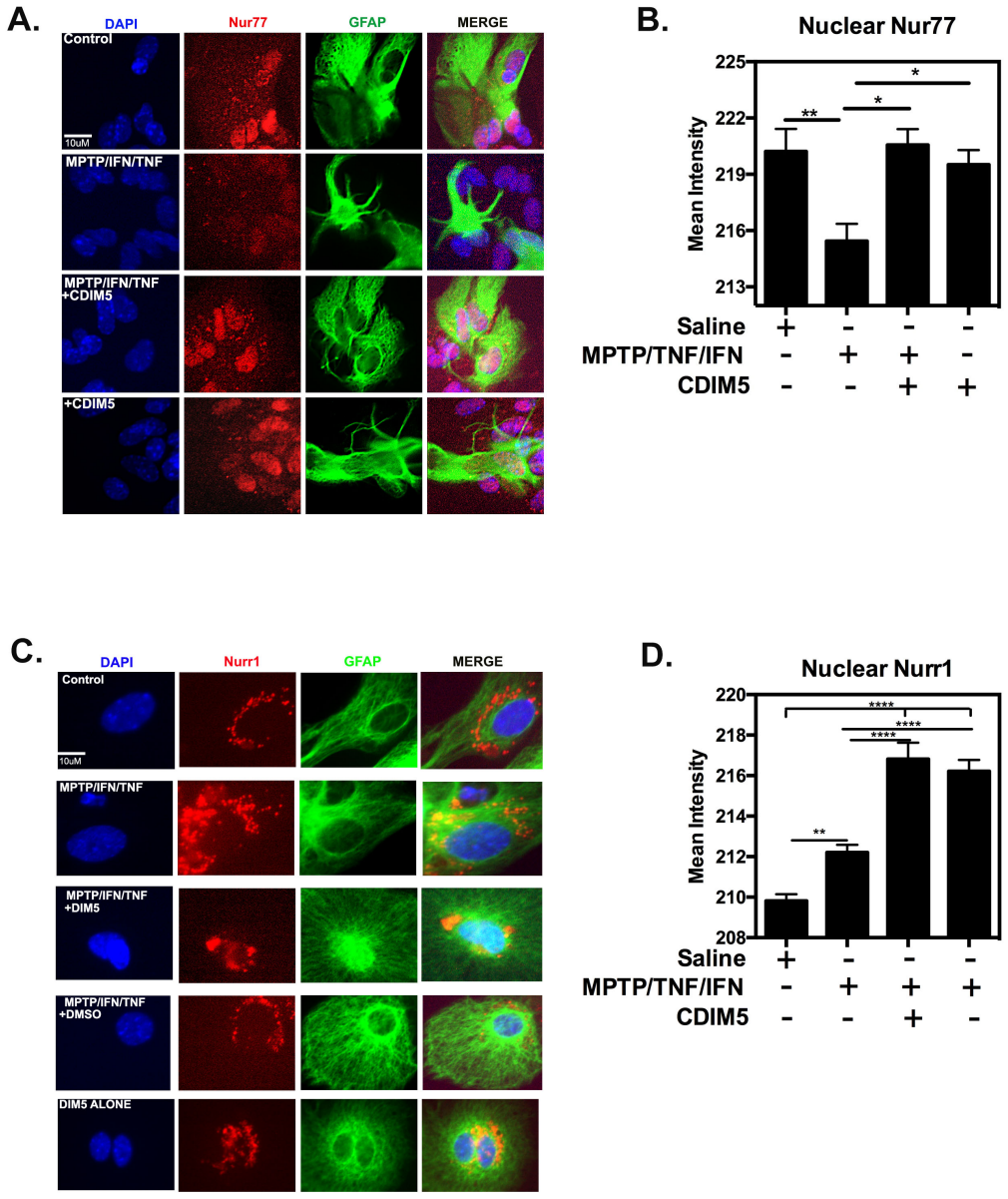

Figure 2.3. C-DIM5 prevents Nur77 (NR4A1) from translocating to the cytoplasm and shuttles Nurr1 (NR4A2) to the nucleus under inflammatory stimuli. (A) Representative images of Nur77 translocation in astrocytes under control (saline) conditions and/or stimulation with MPTP/IFNγ/TNFα in the absence or presence of C-DIM5. **(B)** A quantitative figure demonstrating nuclear Nur77 expression at time point 30min upon inflammatory stimuli and/or CDIM5 treatment. **(C)** Representative images of Nurr1 translocation in astrocytes under control (saline) conditions and/or stimulation with MPTP/IFNγ/TNFα in the absence or presence of C-DIM5. **(D)** A quantitative figure demonstrating nuclear Nurr1 expression at time point 30min upon inflammatory stimuli and/or C-DIM5 treatment or DMSO-vehicle control treatment.

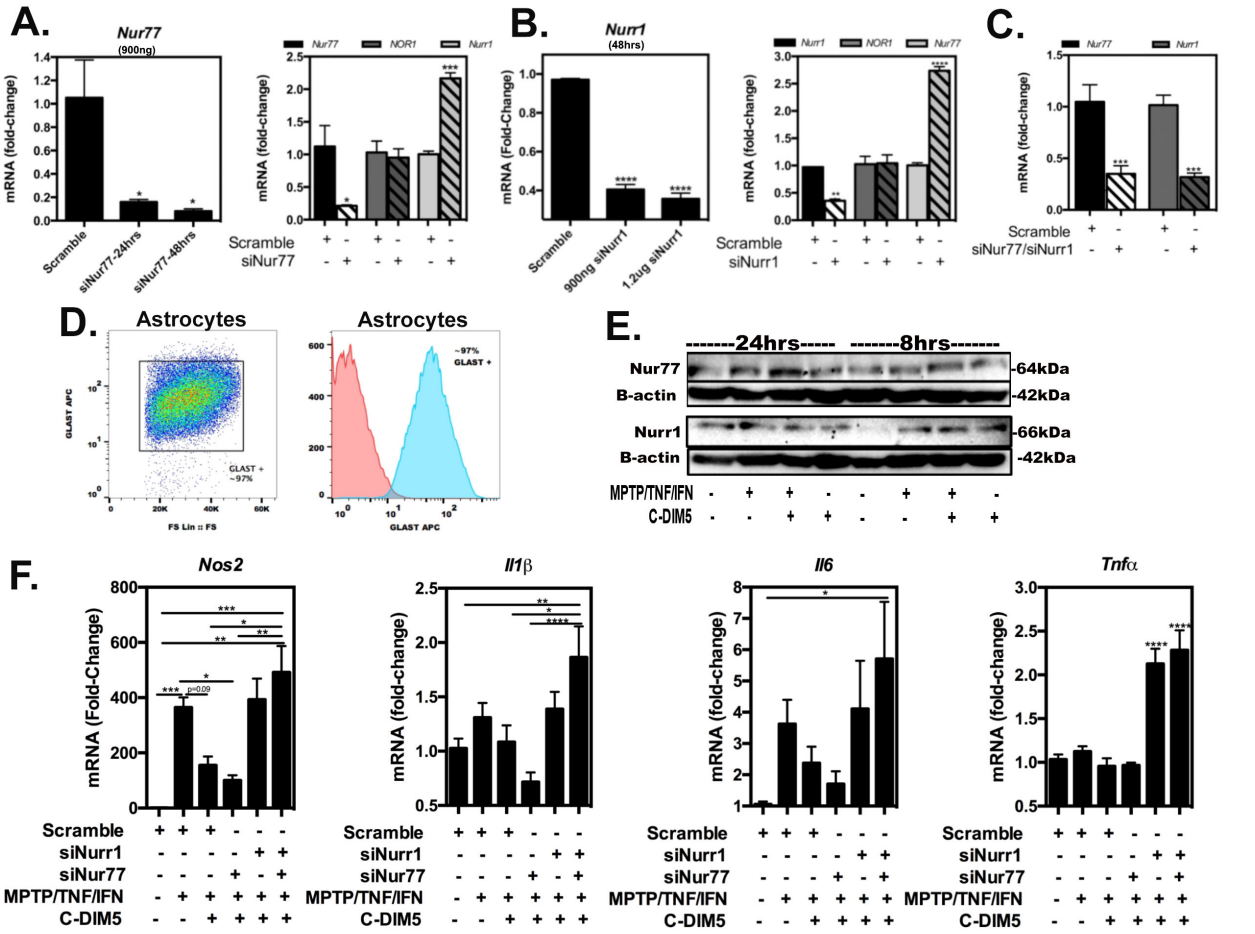

Figure 2.4. RNAi targeted toward Nur77 and Nurr1 effectively knocks down Nur77 and Nurr1 mRNA expression in primary pure astrocytes, respectively. (A) Nur77 is silenced alone at 48hrs, which selectively increases expression of NR4A2/Nurr1 without affecting expression of NR4A3/NOR1 **(B)** Nurr1 is silenced alone which selectively increases expression of NR4A1/Nur77 without affecting expression of NR4A3/NOR1 **(C)** Double knockdown of both Nur77 and Nurr1 effectively suppresses Nur77 and Nurr1, respectively. **(D)** Transfecting primary mixed glia effectively removes microglia yielding pure GLAST-positive primary astrocytes, as demonstrated by flow cytometry. **(E)** 24hr treatment with C-DIM5 alone or with MPTP-cytokines shows increased Nur77 protein compared to less Nurr1 protein. Double knockdown prevents *Nos2* suppression by C-DIM5 with MPTP-cytokines. C-DIM5 effectively increases Nur77 at 24hrs versus 8hrs, while Nurr1 expression is expressed more at 8hrs.

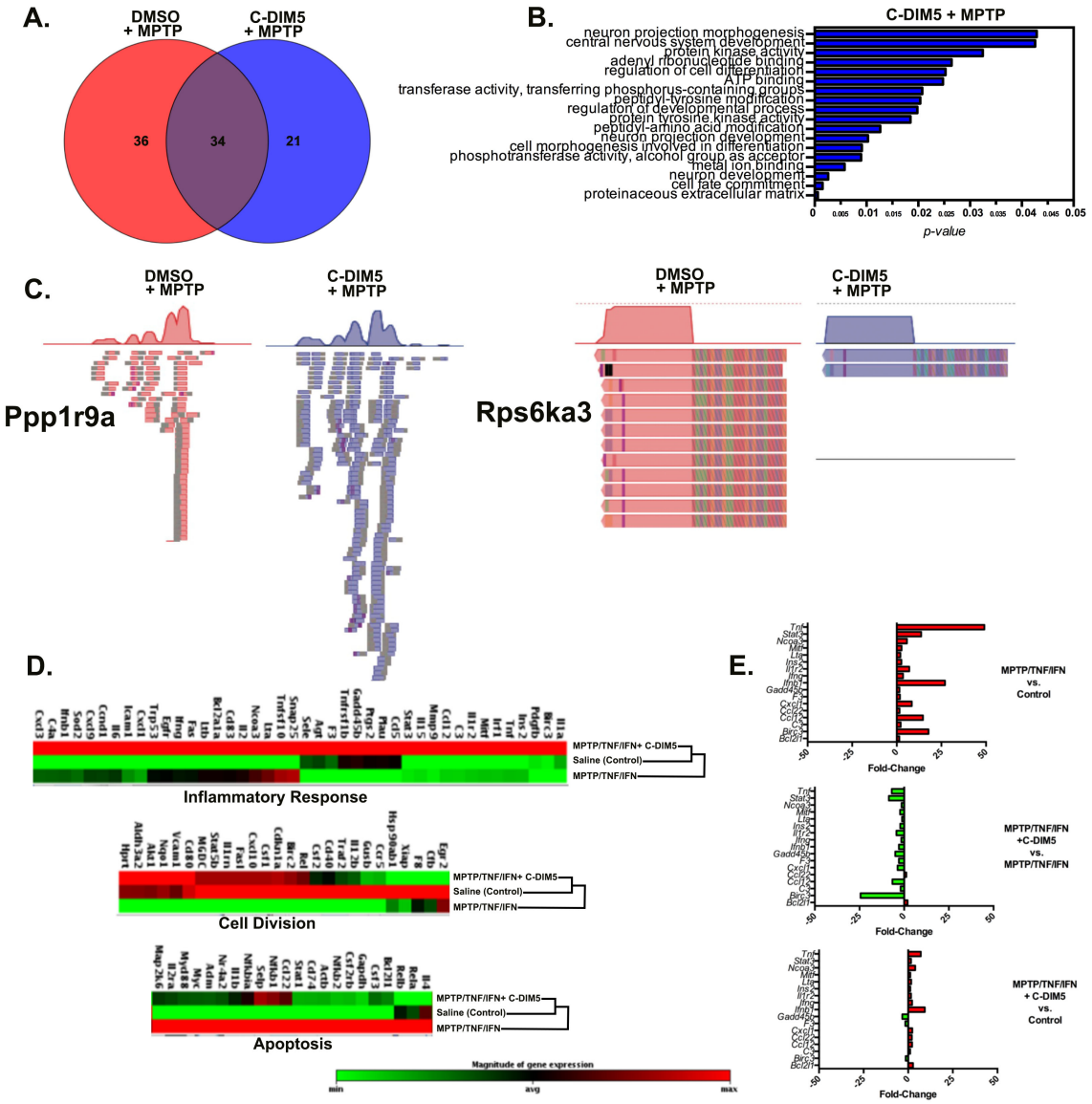

Figure 2.5. ChIP-seq analysis of p65 bound genes in C-DIM5 treated MPTP exposed astrocytes. C-DIM5 largely restores NF-κB-mediated inflammatory and apoptosis gene expression back to control levels as measured by a qPCR array study. **(A)** Venn diagram depicting unique and over-lapping genes bound to p65 in C-DIM5 and vehicle (DMSO) treated MPTP exposed astrocytes. (**B**) GO analysis of biological processes found to be statistically unique in the C-DIM5 treated MPTP exposed astrocytes. P- value used to rank degree of enrichment. (**C**) Genome browser view of distribution of the ChIP-seq reads of represented genes in both C-DIM5 and DMSO treated MPTP exposed astrocytes. **(D)** A cluster gram and heat map demonstrate gene pattern expression similarities among treatment groups, MPTP/IFNγ/TNFα+C-DIM5 clusters with control (saline) levels, while MPTP/IFNγ/TNFα clusters alone. **(E)** MPTP/IFNγ/TNFα increases gene expression from control, while C-DIM5 decreases MPTP/IFNγ/TNFα -induced gene expression. MPTP/IFNγ/TNFα +C-DIM5 has minimal changes in gene expression compared to control.

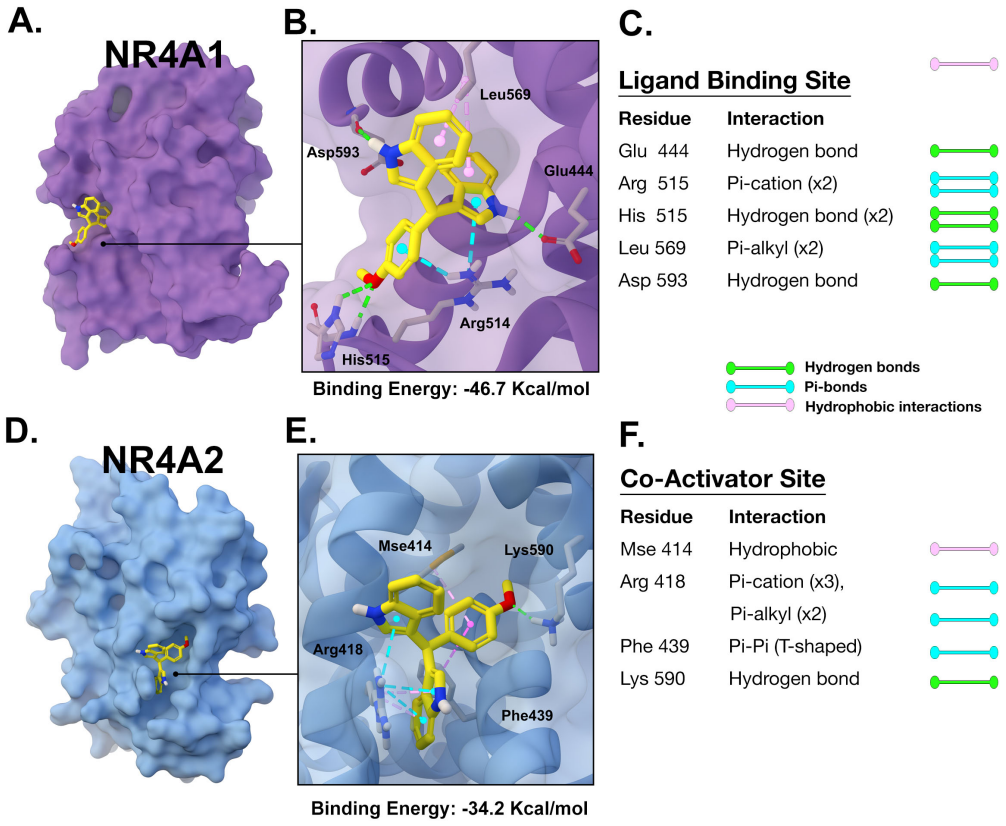

Figure 2.6. Small molecule docking of C-DIM5. Predicted binding orientation of C-DIM5 (yellow) at either **(A)** the ligand-binding site of NR4A1 (purple) or **(B)** the coactivator-binding site of NR4A2 (blue). Insets depict the specific residues of each respective binding site (gray) and their predicted interactions with C-DIM5 as dashed lines (pink=hydrophobic/pi-alkyl, purple=pi-sigma, cyan=pi-cation/pi-anion, and green=hydrogen bonds).

CHAPTER 3

GLIAL-NEURONAL SIGNALING MECHANISMS UNDERLYING THE NEUROINFLAMMATORY EFFECTS OF MANGANESE

3.1 INTRODUCTION

Manganese (Mn) is an essential trace element primarily acquired through diet. However, increased exposures ranging from soy-based infant formula (Collipp et al., 1983) and well water (Woolf et al., 2002) to mining (Riojas-Rodriguez et al., 2010) and industrial settings such as welding (Hua and Huang, 1991), both in juveniles and adults, leads to inflammation and neuronal injury in the cortex and basal ganglia, that cause an irreversible neurodegenerative disorder known as manganism. Activation of astrocytes and microglia in response to Mn neurotoxicity can lead to overproduction of neurotoxic levels of reactive oxygen and nitrogen species (ROS, RNS) (Filipov and Dodd, 2012), as well as inflammatory cytokines such as TNF (Kirkley et al., 2017). An additional study indicates that Mn specifically injures astrocytes by a mechanism, which likely involves oxidative stress, ultimately affecting their ability to promote neuronal health and differentiation (Giordano et al., 2009; Sidoryk-Wegrzynowicz and Aschner, 2013). This may lead to consequential activation of surrounding glia ultimately creating a feedback loop culminating in neuronal cell death, further.

A number of studies have demonstrated that Mn-induced glial activation is exacerbated by glial derived pro-inflammatory factors that damage neurons. Data from our laboratory recently demonstrated that NF-κB signaling in microglia plays an essential role in inflammatory responses in Mn toxicity by regulating cytokines and chemokines that amplify the activation of astrocytes (Kirkley et al., 2017). Although this reveals the importance of NF-κB-mediated

microglial communication with astrocytes, the effects that astrocytes have on microglia and ultimately neuronal cell death is less well known. It was reported that Mn exposure induces activation of microglia and signs of dystrophy including increase in iron-mediated oxidative stress in the substantia nigra of non-human primates (Verina et al., 2011), as well as microgliosis-induced degeneration of dopaminergic neurons in rats (Zhao et al., 2009). Previous studies from our laboratory and others demonstrated that Mn-induced NO from inducible nitric oxide synthase (iNOS/NOS2) production in astrocytes causes injury to surrounding neurons (Liu et al., 2006; Moreno et al., 2009; Spranger et al., 1998; Streifel et al., 2012). NOS2 and many other pro-inflammatory factors are highly regulated in glial cells by NF-kB, consistent with data reporting that the NF-κB-mediated pro-inflammatory cytokines CCL2, CCL5 and TNF released by astrocytes are associated with Mn neurotoxicity in *in vitro* studies of murine glia (Filipov and Dodd, 2012; Filipov et al., 2005; Moreno et al., 2008).

However, only recently has research begun to establish how the communication between both glial cell types ultimately affects Mn-induced neuronal injury(Chen et al., 2006). One study especially emphasizes how the NF-κB-mediated astrocyte-specific chemokine, CCL2, induces microglial activation in a surgery-induced cognitive dysfunction and neuroinflammatory model, suggesting not only that astrocytes and microglia communicate in injurious models, but NF-κB-mediated factors contribute to glial inflammation, as well. NF-κB is activated in glia in response to Mn, oxidative stress and other neurotoxic exposures (Barhoumi et al., 2004; Filipov et al., 2005; Moreno et al., 2008). We recently reported that NF-κB activation in microglia amplifies the inflammatory response of astrocytes to Mn toxicity, resulting in overproduction of inflammatory cytokines and chemokines such as TNF, IL1 and IL6 (Kirkley et al., 2017). However, it remains to be determined what NF-κB signaling in astrocytes plays in modulating

the inflammatory response of mixed cultures of microglia and astocytes, as well as the effect of this signaling on neuronal injury.

We, therefore, examined the role of NF-κB in Mn-induced neurotoxicity by exposing pure microglia, astrocytes (from wild-type and astrocyte-specific IKK/ NF-κB knockout mice) and mixed glial cultures to varying concentrations of Mn and then treating neurons with the resultant glial conditioned media (GCM) of each cell type. We hypothesized that mixed cultures of astrocytes and microglia exposed to Mn (0-100μM) would display enhanced expression of inflammatory cytokines compared to pure microglia or astrocytes, leading to neuronal death. Under these conditions, we measured expression of NF-κB-regulated inflammatory genes by qPCR in glial cells, as well as levels of secreted cytokines in GCM from both WT or IKK KO astrocytes and microglia using spotted array-based ELISA's. In mixed glial cultures, Mn exposure enhanced expression of multiple inflammatory cytokines and chemokines, which was inhibited by pharmacologic inhibition of NF-κB in cultures of mixed glia or pure astrocytes, as well as by gene deletion of IKK2 in astrocytes. Additionally, the resultant GCM decreased neuronal viability and increased neuronal apoptosis, while NF-κB inhibition, both pharmacologically and genetically astrocyte-specific, decreased neuronal death, suggesting that NF-κB activation in astrocytes is the primary mediator in Mn neurotoxicity.

3.2 MATERIALS AND METHODS

Materials. All general chemical reagents including $MnCl_2$, cell culture media, antibiotics, and fluorescent antibodies and dyes were purchased from Life Technologies (Carlsbad, CA) or Sigma Aldrich (St. Louis, MO) unless otherwise stated. Neuro-2a cells (N2A) were cultured as previously described (Li et al., 2015b). For immunofluorescence studies, antibodies against glial

fibrillary acidic protein (GFAP) and ionized binding adaptor protein-1 (IBA1) were purchased from Sigma Chemical Co. (St. Louis, MO) and Santa Cruz Biotechnology (Santa Cruz, CA) respectively. For flow cytometric experimentation, Annexin V-iFluor^{TM} 647 conjugate was purchased from AAT Bioquest (Sunnyvale, CA) and Propidium Iodide was purchased from Life Technologies (Carlsbad, CA).

Primary Glial and Neuronal Isolation. Cortical glia and neurons were isolated from day-1 old C57Bl/6 or transgenic mouse pups according to procedures described previously(Aschner and Kimelberg, 1991), and purity confirmed through immunofluorescence staining using antibodies against GFAP and IBA1 (Carbone et al., 2009). Briefly, pups were euthanized by decapitation under isofluorane anesthesia and cortices (astrocytes) were rapidly dissected out, and meninges removed. Tissue was subject to digestion with Dispase (1.5 U/ml), and a complete media change 24 hrs after plating to remove non-glial cell types. Glial cultures were maintained at 37°C and 5% CO2 in minimum essential media supplemented with 10% heat-inactivated fetal bovine serum and a penicillin (0.001 mg/ml), streptomycin (0.002 mg/ml), and neomycin (0.001) antibiotic cocktail. Cell media was changed 24 hrs prior to all treatments. All animal procedures were approved by the Colorado State University Institutional Animal Care and Use Committee and were conducted in accordance with published NIH guidelines.

Real-Time RT-PCR and qPCR array analysis. Confluent mixed glia, purified astrocytes, or purified microglia were treated with $MnCl_2$ (0-100μM) for eight hours prior to RNA isolation. RNA was isolated using the RNEasy Mini kit (Qiagen, Valencia, CA), and purity and concentration were determined using a Nanodrop ND-1000 spectrophotometer (NanoDrop Technologies, Wilmington, DE). Following purification, RNA (250-1000ng) was used as

template for reverse transcriptase (RT) reactions using the iScript RT kit (BioRad, Hercules CA). The resulting cDNA was immediately profiled for mRNA expression according to the 2-ΔΔCT method (Livak and Schmittgen, 2001) See primer table for primer sequences of additional genes profiled.

Presto Blue Viability Assay. N2A cells or primary neurons were grown or plated on 96-well plates for 24 h or 10 days, respectively, before treatment with GCM. After 48 hrs, cells were imaged using the PrestoBlue Cell viability reagent (Life Technologies, Carlsbad, CA) per the manufacturer's protocol.

Spotted protein array ELISA assays. Measurement of cytokines in glia-conditioned media was sampled from glia prior to application on neurons and stored at −80 °C. Stored media was thawed, and cytokines were measured using a mouse 14-plex ELISA (Q-Plex™ Mouse Cytokine Arrays, Quansys Biosciences, Logan, UT) according to manufacturer instructions and imaged on a ChemiDoc XRS (Life Science Research, Hercules, CA) to capture images. Levels of cytokines and chemokines were calculated from standard curves using Q-View imaging software (Quansys Biosciences).

RNA interference. RNA interference (siRNA, small interfering RNA) oligonucleotides were purchased from Integrated DNA Technologies (IDT DNA, Coralville, IA). RNAi duplexes were designed against splice common variants of the target gene and were validated using a dose-response assay with increasing concentrations of the suspended oligo (900-1200 ng/ml) using a standard scrambled dicer- substrate RNA (DsiRNA) as control. RNAi oligonucleotides were transfected using the TransIT-X2 delivery system (Mirus Bio, Madison, WI) 48 hours before

100μM $MnCl_2$ treatment. Separate siRNA systems were used to ensure specific knockdown of *Ccl2* and *C3* mRNA. The Ccl2 dsiRNA duplex sequences are (5'→3') UGAAGCUAAUGCAUCCACUACCUTT; UAAACAAUACCUUGGAAUCUCAAACAC (IDT DsiRNA; denoted siCcl2). The C3 dsiRNA duplex sequences are (5'→3') UAAUAAAGCUUCAGUUGUAUUUCAA; UUGAAAUACAACUGAAGCUUUAUUAGA (IDT DsiRNA; denoted siC3).

Flow Cytometry. The percent of Annexin-V positive (+) and Propidium Iodide positive (+) in neuroblastoma (N2A) cultures before and after treatment with or without conditioned-media or $MnCl_2$ for 48hrs followed by flow cytometric analysis as described{Kirkley:2017ef}. Briefly, cells were labeled using Annexin-V and PI at room temperature for 1 h. After labeling, the cells were washed twice in incubation buffer and resuspended at a final volume of 500 μL of PBS and stored at 37 °C until analysis. Flow cytometry was performed on a Beckman Coulter CyAn ADP flow cytometer operated with Summit software for data collection at Colorado State University's Flow Cytometry Core Facility. All further data analysis was done utilizing FlowJo software (version 10.1; FlowJo, Ashland, OR).

Statistical Analysis. Experiments were performed no less than three times, with replicates consisting of independent cultures using a minimum of four plates or cover slips per replicate study. Comparison of two means was performed by Student's t-test, while comparison of three or more means was performed using one-way ANOVA followed by the Tukey-Kramer multiple comparison post-hoc test using Prism software (v6.0h, Graphpad Software, Inc., San Diego,

CA). For all experiments, $p < 0.05$ was considered significant, although the level of significance was often much greater.

3.3 RESULTS

$MnCl_2$ exposure induces increased inflammatory gene expression in mixed glial cultures.

To assess inflammatory gene expression upon $MnCl_2$ exposure, mixed primary glial cultures containing astrocytes and microglia, pure astrocytes or pure microglia were treated for 24 hrs prior to profiling expression of inflammatory genes by qPCR. Mn exposure enhanced expression of inducible nitric oxide synthase (*Nos2*) and multiple inflammatory cytokines and chemokines, including the astrocyte-specific inflammatory complement factor, *C3*, *Tnf*, *Ccl2* and its receptor *Ccr2, Ccl5, Il6* and *Il1β*. These genes showed dose-dependent expression in mixed glia, with maximal gene expression at 100μM $MnCl_2$ (Fig. 3.1a.). Pure astrocytes (Fig. 3.1b.) showed less increase in gene expression compared to mixed glia and pure microglia (Fig. 3.1c) displayed less gene expression compared to the other two cell populations.

Glia-conditioned media (GCM) causes more neuronal cell death than astrocyte-conditioned media (ACM) or microglia-conditioned media (MCM).

To ascertain whether $MnCl_2$ exposure causes the release of soluble neurotoxic factors from glia, cultures of mixed glia, pure astrocytes or pure microglia were treated with 0-100 μM $MnCl_2$ for 24hrs and the resultant glia-conditioned media (GCM) added to cultured neurons (Figure 3.2). Conditioned media from Mn-treated mixed glia (GCM) decreased neuronal viability in a dose-dependent manner following 24 hr incubation in culture and was further decreased at 48 hrs (Fig. 3.2a, left panel). Neuronal cell death following 48 hr exposure to

100μM $MnCl_2$-treated conditioned media was greater for GCM (~30% decreased viability) than for either astrocyte-conditioned media (ACM) (~15% decreased viability) or microglia-conditioned media (MCM) (~10% decreased viability) (Fig. 3.2b, left panel). Flow cytometric analyses of neuronal cells treated for 48 hrs with GCM-100uM $MnCl_2$ indicated an increase in apoptotic neurons, based on staining for Annexin V and Propidium Iodide (PI), as indicated by quantification bar graphs and depicted in representative histograms. GCM-100uM $MnCl_2$ resulted in 38.98% Annexin positive and 38.81% PI positive neurons (Fig. 3.2c, top panel) as depicted in representative histograms (Fig. 3.2d, top panel) compared to AMC-100uM $MnCl_2$ which resulted in 11.11% Annexin positive and 11.13% PI positive neurons (Fig. 3.2c-d, middle panel). While MCM-100uM $MnCl_2$ resulted in 16.2% Annexin positive and 17.66% PI positive neurons (Fig. 3.2c-d, bottom panel).

Pharmacologic inhibition of NF-kB decreases inflammatory gene expression in mixed glia and pure astrocytes upon $MnCl_2$ exposure.

To determine the function of NF-κB in $MnCl_2$-induced inflammatory gene expression in mixed glia or pure astrocytes, we pretreated cell cultures with the NF-κB inhibitor, Bay 11-7082 (Bay-11) [(E)- 3-(4-methylphenyl) sulfonylprop-2-enenitrile], or the vehicle control, dimethylsulfoxide (DMSO), prior to treatment with 100μM $MnCl_2$. Pretreatment with Bay-11 broadly suppressed expression of inflammatory genes in mixed glia following exposure to 100μM $MnCl_2$ (Fig. 3.3a.). 100μM $MnCl_2$ exposure in pure astrocytes resulted in significant increase in most genes compared to mixed glia (Fig. 3.3b). *Nos2*, *Il6*, *Ccl5*, and *Ccl2* in pure astrocytes had a larger mRNA fold-change compared to mixed glia, while NF-kB inhibition is less effective in decreasing some inflammatory gene expression. However, NF-kB inhibition

diminished *Nos2*, *Ccl5*, and *Ccl2* in pure astrocytes (Fig. 3.3b), drastically, however the affects were less potent compared to mixed glia in which NF-kB inhibition caused more statistically significant suppression of *Nos2*, *Il6*, *Ccl5*, and *Ccl2.*

Pharmacologic inhibition of NF- B in glia is neuroprotective.

To determine how glia-released factors modulate neuronal viability following exposure to MnCl2, we examined the effect of Bay-11 treatment in glia on neuronal viability following incubation with GCM or ACM (Figure 3.4). Pretreatment of mixed glia cultures with Bay-11 protected against Mn-induced loss of neuronal viability following incubation with GCM from Mn-treated glia, 105.2% viable compared to GCM-Saline (Fig. 3.4a), whereas pre-treatment of mixed glia with vehicle control (DMSO) showed no protective effect and caused neuronal viability to decrease by ~23% compared to GCM-Saline. There was an insignificant decrease in neuronal viability following incubation with ACM from Mn-treated astrocyte cultures, however the presence of Bay-11 showed neuroprotection indicated by an increase in neuronal viability to 106.3% compared to ACM-Saline, while DMSO showed no neuroprotective effect (Fig. 3.4b). To identify direct effects of Mn on neurons, N2A cells were incubated for 48 hrs with $MnCl_2$ (1 – 1000 μM) and examined for viability. Treatment with increasing doses of $MnCl_2$ resulted in loss of neuronal viability, with an LD50 value of approximately 30 μM (Fig. 3.4c). Analysis of N2A cells by flow cytometry following direct treatment with $MnCl_2$ demonstrated increased numbers of apoptotic (+Annexin V) cells and a modest increase in dead (+Propidium Iodide (PI)) neurons (Fig. 3.4e-d). The magnitude of neuronal apoptosis following direct treatment with $MnCl_2$ was markedly less that than that induced by GCM or ACM. Flow cytometric analysis also demonstrated that NF-κB inhibition upon 100 **μ**M $MnCl_2$ exposure in mixed glia or pure

astrocytes produces more neuroprotective GCM (Fig. 3.4f,h) and ACM (Fig. 3.4g,i), respectively, as shown by +Annexin V and +PI staining.

Genetic inhibition of IKK (NF-κB) in astrocytes (in a mixed glial population) decreases inflammatory gene expression.

To specifically asses the role that NF-κB plays in astroglial-glial communication, we treated mixed glial cultures containing IKK knockout (KO) astrocytes and wild-type microglia with 100 μM $MnCl_2$. 8 hrs later we assayed mRNA expression of inflammatory genes and showed that astrocyte-specific IKK knockout drastically decreases inflammatory gene expression (Fig. 3.5a.) compared to mixed glia containing both littermate control wild-type astrocytes and microglia (Fig. 3.5a. *Nos2* & *Ccl2)*.

Genetic inhibition of astrocyte-specific NF-κB in glia is neuroprotective.

In order to fully elucidate the role that astrocytes play in glial-mediated neuronal cell death we assessed N2A cell viability and death after exposure to GCM from mixed glia (containing IKK KO astrocytes and wild-type microglia) treated with saline or 100 μM $MnCl_2$. We showed that GCM-100 μM $MnCl_2$ (from mixed glia containing IKK KO astrocytes) almost completely preserved N2A cell viability, which caused only ~5% reduction in viability (Fig. 3.6a. white bars) compared to exposure to GCM (from mixed glia containing wild-type astrocytes) in which there was ~20% reduction in N2A cell viability (Fig. 3.6a. black bars). Flow cytometric analysis of N2A cells exposed to IKK KO astrocyte GCM demonstrated statistically significant decrease in apoptotic (4.47% Annexin V +) (Fig. 3.6b. white bars) and

dead (4.62% PI +) (Fig. 3.6c. white bars) N2A cells compared to wild-type GCM-100 **μ**M $MnCl_2$ (12.33% Annexin V +) and (9.14% (Fig. 3.6b-c. black bars).

Genetic inhibition of IKK (NF-κB) in astrocytes (in a mixed glial population) is neuroprotective to primary neurons.

Additionally, we wanted to assess the effects that GCM from mixed glia (containing IKK KO astrocytes and wild-type microglia) would have on primary neurons (Figure 3.7). To do so, we exposed primary neurons to GCM (either from Mn-treated mixed glia, wild-type astrocytes + wild-type microglia or IKK KO astrocytes + wild-type microglia) for 48hrs, similar to treatments done in N2A cells. Representative images of live-cell imaging of primary neurons exposed to GCM (from wild-type mixed glia) for 48hrs showed a visual increase in apoptotic cells (Annexin V +), dead cells (PI+) and caspase staining (Bis-Rhodamine +) (top 2 rows) compared to primary neurons treated with GCM (from IKK KO astrocyte containing mixed glia), which visually exhibited a decrease in apoptotic cells (Annexin V +), dead cells (PI+) protease staining (Bis-Rhodamine +) (bottom 2 rows).

Knockdown (KD) of both C3 and CCL2 in mixed glia does not inhibit Mn-induced inflammatory gene expression.

To determine whether C3 or CCL2 gene expression mediates Mn-induced inflammatory gene expression, we knocked down both C3 (~90% KD; Fig. 3.8a) and CCL2 (~95% KD; Fig. 3.8b) separately in mixed glial cultures prior to Mn exposure (Fig. 3.8). Rather than causing a decrease in inflammatory gene expression of the other inflammatory genes, KD of C3 (Fig. 3.8a)

and CCL2 (Fig. 3.8b), once treated with Mn, resulted in either no change or greater inflammatory gene induction compared to scramble control Mn treated.

3.4 DISCUSSION

Mn-induced neurotoxicity in humans and in animal models is accompanied by reactive gliosis and inflammation that is damaging to surrounding neurons. But how this inflammation mediates neurodegeneration in Manganism is less understood. Multiple studies have reported that microglia and astrocytes respond to Mn exposure with elevated levels of NF-κB-regulated inflammatory cytokines and other inflammatory mediators (Chang and Liu, 1999; Chen et al., 2006; Spranger et al., 1998). Furthermore, other studies have evaluated glial response as a result of Mn-induced neuronal cell death (Streifel et al., 2012), however research assessing the role that glial-glial and glial-neuronal communication plays in neurodegeneration in a model of Manganism is lacking.

To determine glial factors involved in neurodegeneration as a result of Mn exposure, we first assessed Mn-induced inflammatory gene expression in three glial populations. We treated astrocytes and microglia, either together or separately, for 8 hrs with 0, 30, or 100μM $MnCl_2$. While, overall, we showed a dose-dependent increase in a handful of key NF-κB-mediated inflammatory genes including *Nos2, Il6* and *Il1β*, surprisingly, mixed glia (Fig. 3.1a) demonstrated drastically more fold-change mRNA than pure astrocytes (Fig. 3.1b.) or pure microglia alone (Fig. 3.1c.), suggesting that microglia and astrocytes, together, respond to Mn injury more potently than either cell type alone. Intriguingly, the complement component *c3* gene, which is uniquely expressed by activated astrocytes in the CNS and correlates closely with a neurotoxic inflammatory phenotype (A1 astrocytes) (Liddelow et al., 2017), was more highly

induced in mixed glia (~4-fold more in 100μM compared to 0μM) than pure astrocytes alone (only ~2-fold increase), while pure microglia showed a dose-dependent-decrease upon Mn-exposure. This demonstrates that *c3* is induced in astrocytes following Mn exposure and also that microglia potentiate expression of inflammatory gene expression in astrocytes, similar to in vivo studies reporting that release of the inflammatory cytokines C1q, IL1a and TNF by microglia induces reactive astrocytosis *in vivo* (Liddelow et al., 2017). Additionally, the chemokine, *Ccl2*, was induced following Mn exposure in mixed glia and in pure astrocytes but not in pure microglial cultures, supporting studies which show that *Ccl2* is astrocyte-derived and revealed to increase microglial activation and neuroinflammation (Liu et al., 2017; Xu et al., 2017), ultimately suggesting that glial-glial communication in a diverse, mixed glial population promotes an increase in astrocytic-specific inflammatory gene expression compared to astrocyte cultures alone. The studies by Xu et al., 2017 also implicated CCL2-CCR2 signaling in astrocyte-mediated microglial activation in central nervous system (CNS) inflammation, suggesting that the increase in both *Ccl2* and *Ccr2* in mixed glia is what contributes to an increased inflammatory gene response due to Mn treatment.

To assess the role that C3 and CCL2 play in astrocyte-microglial signaling, we knocked each gene down in mixed glia prior to Mn treatment and then assessed gene expression of additional inflammatory genes. While it was expected that a loss of C3 or CCL2 would result in a decrease of other inflammatory genes due to their astrocyte specificity, unexpectedly, it resulted in additional increase in Mn-induced gene expression, indicating that additional signaling factors are likely involved in glial cross-communication leading to further activation in mixed glia.

In addition to assessing gene expression in 8 hr Mn-exposed glia, we removed conditioned-

media from mixed glia (GCM), astrocytes (ACM), or microglia (MCM) to treat N2A neuroblastoma cells to emulate what's seen in the brain to further assess glial released inflammatory mediators. Since mixed glia expressed the most inflammatory gene expression upon Mn treatment, we wanted to assess whether glia release neurotoxic factors as a result of Mn exposure. We showed that 48hrs of the 100μM-GCM caused the largest decrease (~20% compared to 0μM) (Fig. 3.2a, right panel) compared to 24hrs exposure (Fig. 3.2a, left panel). In separate experiments comparing GCM (Fig. 3.2b, left panel) to ACM (Fig. 3.2b, middle panel) and MCM (Fig. 3.2b, right panel) at 48hrs, we showed that all three conditioned media caused statistically significant decrease in N2A viability, establishing that mixed glia, pure astrocytes alone and pure microglia alone produce neurotoxic mediators in response to Mn. This is consistent with other studies that show Mn causes an increase in inflammatory cytokines and chemokines (Chen et al., 2006; Filipov and Dodd, 2012; Filipov et al., 2005). However, mixed glia (100μM Mn) produced more potent or possibly more varied detrimental inflammatory mediators compared to pure astrocytes or pure microglia alone. Flow cytometric analysis also supports these findings by measuring N2A cell death as designated by Annexin V positive and/or Propidium Iodide (PI) positive staining, indicative of apoptotic and/or necrotic cells, respectively (Fig. 3.2c-d). GCM-exposed N2A cells stained the most positive for Annexin (~40%) and PI (~38%) compared to ACM (~10%, respectively) and MCM (~18% and 19%, respectively), suggesting that mixed glia produce more potent mediators than astrocytes or microglia alone, possibly due to glial-glial communication intensifying glial activation, and ultimately increased neurotoxic mediator production.

NF-κB is shown to be up regulated in Mn-induced glial activation as indicated by increased NOS2, NO and other cytokine production in astrocytes (Chang and Liu, 1999; Moreno

et al., 2011; Moreno et al., 2008). Based off the exacerbated increase in inflammatory gene expression in mixed glia, as well as the resultant N2A cell death from conditioned media, we wanted to determine the signaling pathways regulating astrocyte cross-communication with microglia. So, we treated pure astrocytes and mixed glia with the NF-κB inhibitor, Bay 11-7082, prior to treatment with 100μM Mn and collection of ACM and GCM (Fig. 3.3-3.4). Inhibition of astrocyte NF-κB signaling using the IKK complex inhibitor, Bay 11-7082, resulted in significant reduction in astrocyte and mixed glial activation in our model. The inflammatory genes up regulated (*Nos2, C3, Il6, Il1β, Ccl5, Ccl2, Ccr2,* and *Tnfα*) by Mn exposure were significantly decreased in both mixed glia and pure astrocytes, suggesting that Mn-induced inflammatory gene expression in mixed glia and especially astrocytes is coordinated by Mn-induced NF-κB activation.

To then evaluate the role that NF-κB plays in glial released neurotoxic factors, we exposed N2A cells to the resultant GCM and ACM. Bay-11 treatment in Mn-treated glia was significantly neuroprotective (Fig. 3.4a) while ACM showed a similar, less potent trend (Fig. 3.4b.). Additionally, we exposed N2A cells to direct Mn treatment and demonstrated that the LD50 was 30μM as well as increased apoptotic (Annexin V positive) and necrotic (PI positive) staining from direct 100μM Mn treatment (Fig. 3.4c-e), revealing that N2A cells respond to direct Mn-exposure, however, conditioned media from Mn-treated glia cause more N2A cell death and decreased N2A viability. This insinuates that there are additional factors in the media, aside from Mn, which contribute to N2A death. Our laboratory has ascertained that glial uptake of Mn is ~70%, leaving behind ~30% of Mn in the conditioned-medium (Kirkley et al., 2017), thus uptake of 70% of 100μM Mn treatment would result in ~30μM in the resultant conditioned media. It's also shown that astrocytes not only transport Mn, but are also heavily involved in

metabolism (Aschner et al., 1992; Sidoryk-Wegrzynowicz and Aschner, 2013) thus added Mn is taken up by astrocytes and further contributes to glial injury. Uniquely, direct treatment of 30μM Mn (LD50) does not cause the same decrease in N2A viability (~20%) as 100μM-GCM (~30%), while direct treatment of N2A cells with 100μM Mn doesn't prompt as much Annexin V or PI positive staining as conditioned media, ultimately suggesting that the resultant N2A cell death from conditioned media exposure is not solely due to residual Mn in the media, but is in part due to glial-released inflammatory factors, most likely controlled by NF-κB. This is further supported by the flow cytometric analysis of GCM and ACM from Bay-11 experiments in which there is increased neuroprotection as demonstrated by the significant decrease in apoptotic (Annexin V) and necrotic (PI) positive staining for GCM (Fig. 3.4f,h) and similar, but less significant trend in ACM (Fig. 3.4g,i). Altogether, this insinuates the involvement of NF-κB activation in neurotoxicity by demonstrating that pharmacologic inhibition of NF-κB in glia is anti-inflammatory and furthermore, neuroprotective.

While we established that NF-κB is directly involved in Mn-induced glial inflammation and neuronal cell death by pharmacologic inhibition, we wanted to further establish its role in astrocyte-mediated glial communication. We, therefore, isolated primary mixed glia from astrocyte-specific IKK knockout (KO) mice and exposed the mixed glia (containing IKK KO astrocytes and wild-type microglia) to 100μM Mn for 8 hrs. We showed that there was a significant decrease in inflammatory gene expression (Fig. 3.5) suggesting that not only is NF-κB directly involved in Mn-induced inflammatory gene expression, but also, by genetically inhibiting NF-κB in astrocytes in a mixed glial culture, we show that astrocytes are most significantly involved in glial communication consequential to Mn exposure.

Additionally, astrocyte-specific genetic inhibition of IKK resulted in almost complete

neuroprotection in GCM treated N2A cells as depicted by significant prevention of decreased viability (Fig. 3.6a), and significantly diminished apoptotic (Annexin V) and necrotic (PI) staining (Fig. 3.6b-c) as well as primary neuronal cells as depicted by representative images from live-cell imaging experimentation (Figure 3.7), suggesting that astrocytes are the key mediators involved in Mn-induced glial activation, and ultimately increased release of neurotoxic mediators.

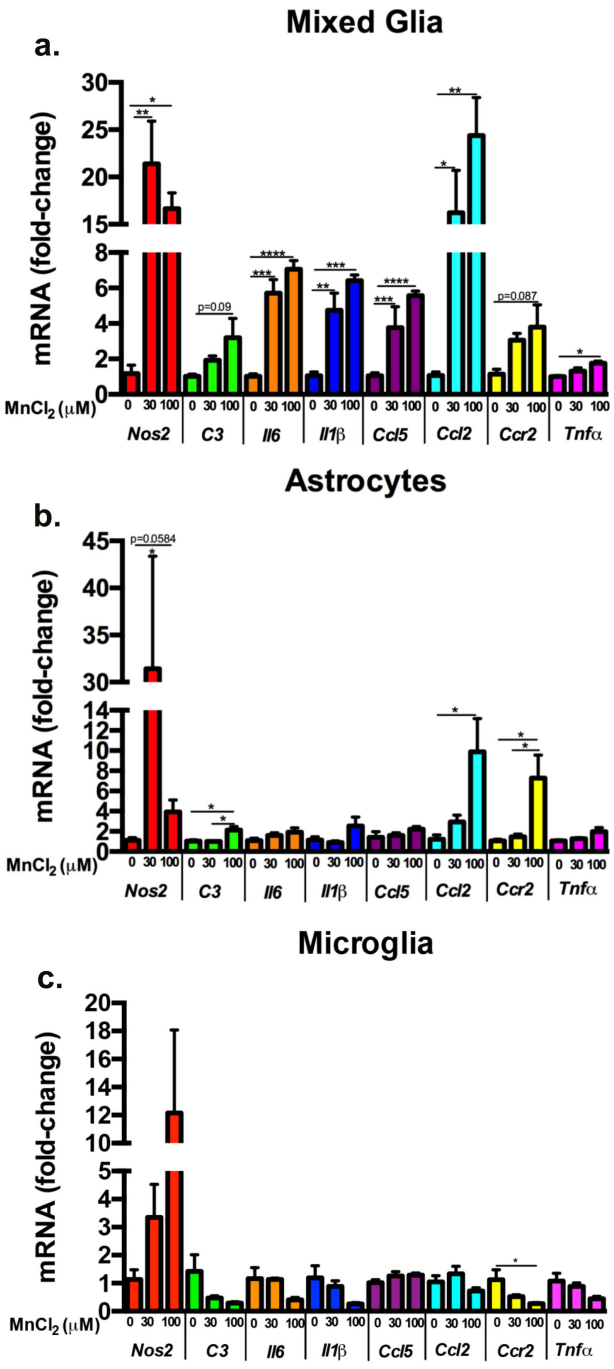

Figure 3.1. $MnCl_2$-exposed mixed glia express more inflammatory gene expression compared to astrocytes or microglia alone. Inflammatory gene expression exhibited dose-dependently in **(a)** mixed glia **(b)** pure astrocytes and **(c)** pure microglia.

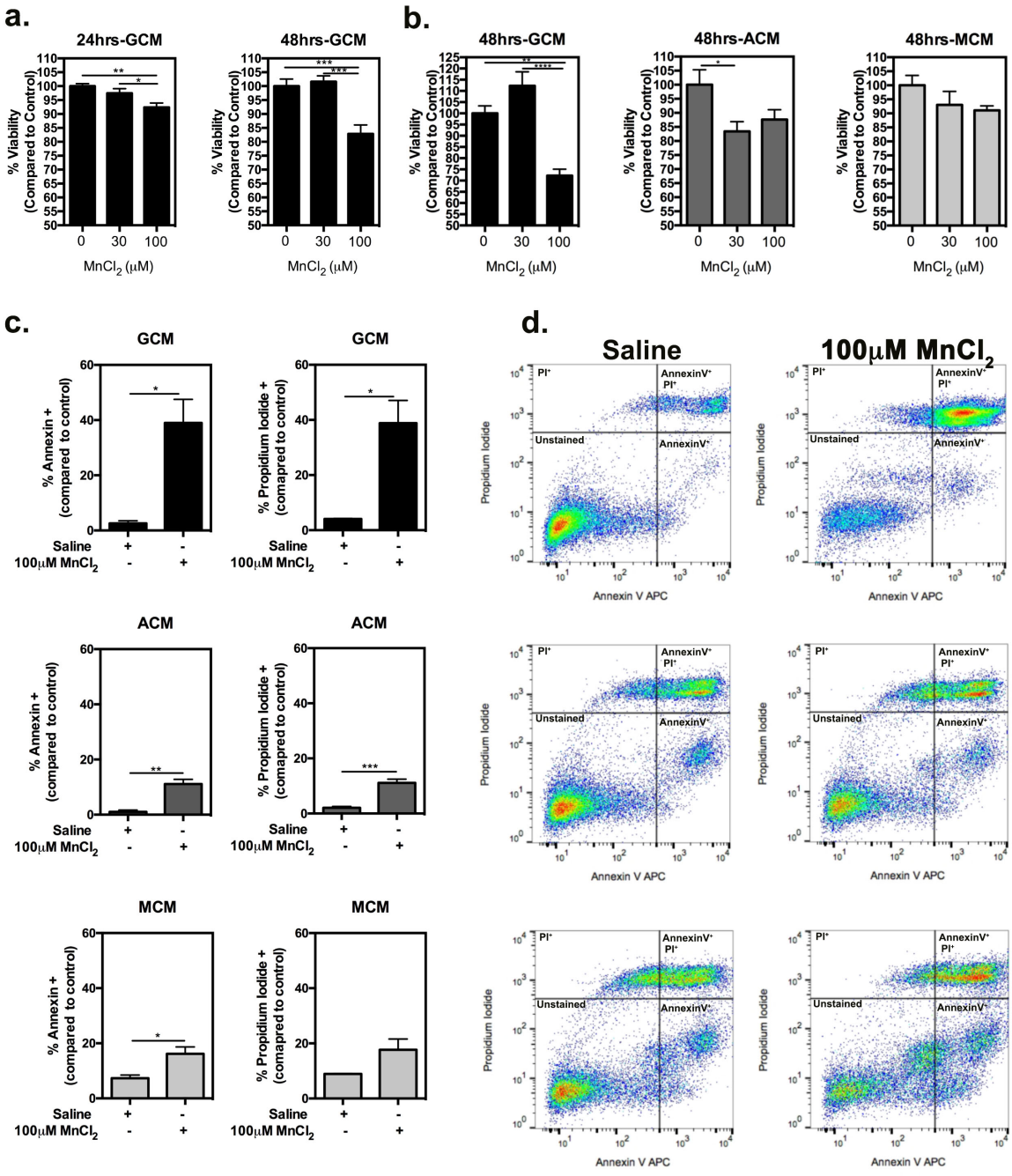

Figure 3.2. GCM (upon 100μM $MnCl_2$ exposure) causes more neuronal cell death in an N2A cell line at 48 hours than 24 hours, and more so than ACM and MCM.
(a) 24 hour exposure of GCM shows a dose-dependent decrease in N2A viability (left), while 48 hour (right) exposure at 100**μ**M shows a drastic decrease in N2A viability, suggesting 48 hours to be most optimal **(b)** GCM results in less neuronal viability compared to ACM or MCM. **(c-d, top)** Flow cytometric analysis shows GCM-100uM $MnCl_2$ exposure results in more apoptotic (+annexin) and more dead (+propidium iodide) neurons compared to **(c-d, middle)** ACM or **(c-d, bottom)** MCM.

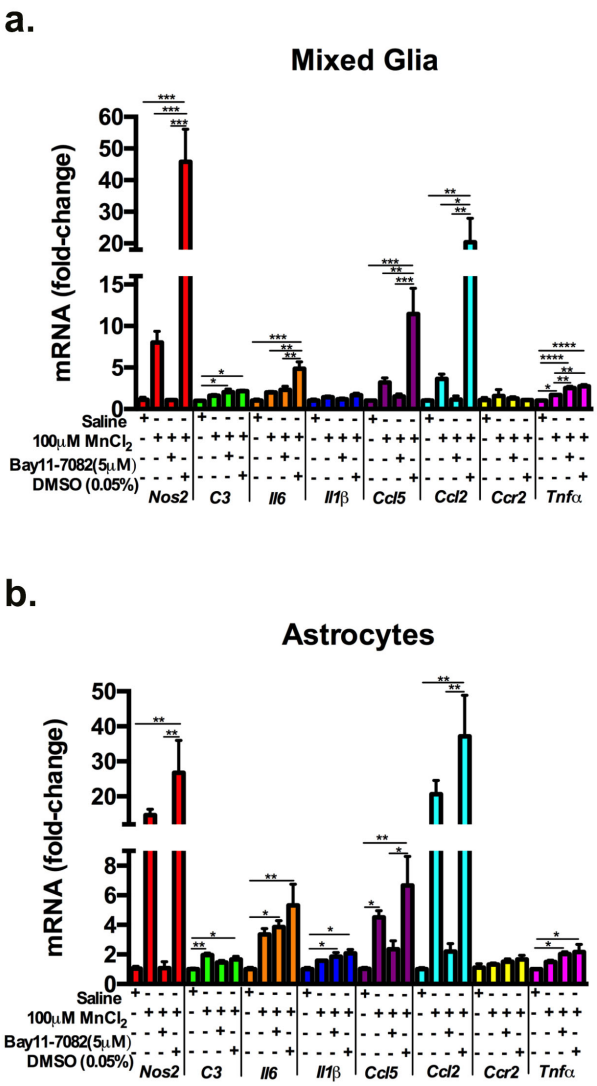

Figure 3.3. Pharmacologic inhibition of NF-kB decreases inflammatory gene expression upon 100uM $MnCl_2$ exposure. (a). Upon treatment with the NF-κB inhibitor, Bay 11-7082 (Bay-11) [(E)- 3-(4-methylphenyl) sulfonylprop-2-enenitrile], most inflammatory gene expression in mixed glia, induced by 100μM $MnCl_2$, is suppressed. **(b).** $MnCl_2$ exposure in pure astrocytes is less potent compared to mixed glia, additionally; NF-kB inhibition is less effective in decreasing some inflammatory gene expression.

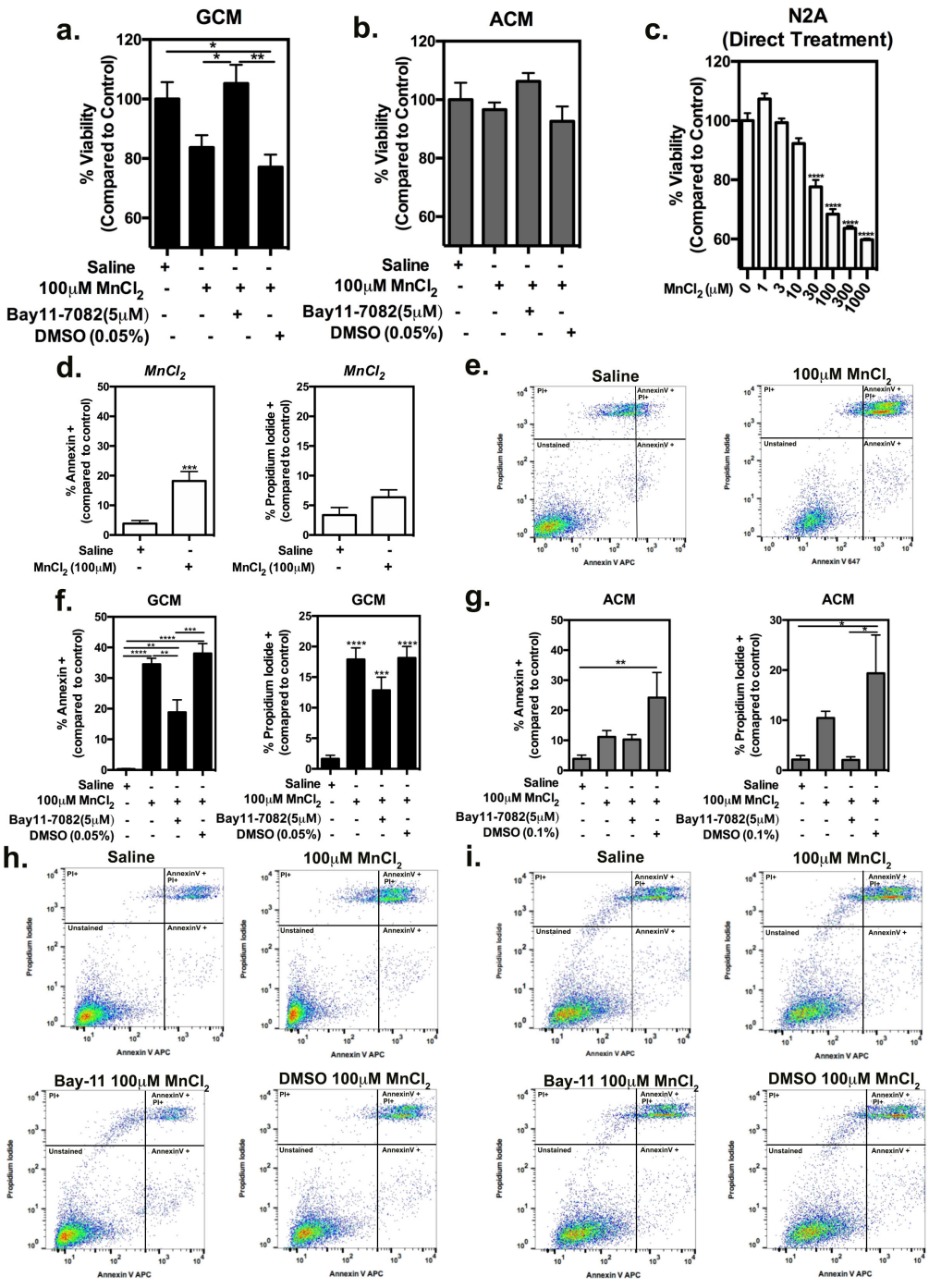

Figure 3.4. Pharmacologic inhibition of NF-κB in glia is neuroprotective in an N2A neuronal cell line. Pharmacologic inhibition (Bay11 treatment) of NF-κB in mixed glial cultures preserves N2A viability upon 100 **μ**M $MnCl_2$ **(a)** GCM treatment, while in astrocytes **(b)** ACM, is less potent. **(c).** A lethal concentration curve (LC50) of $MnCl_2$ to N2A cells. **(d-e)** As measured by flow cytometry, direct treatment with 100 **μ**M $MnCl_2$ to N2A cells results in less annexin and PI stain compared to **(f,h)** GCM and **(g,i)** ACM, which also shows NF-κB inhibition to effectively decrease annexin and PI stain in both cell populations.

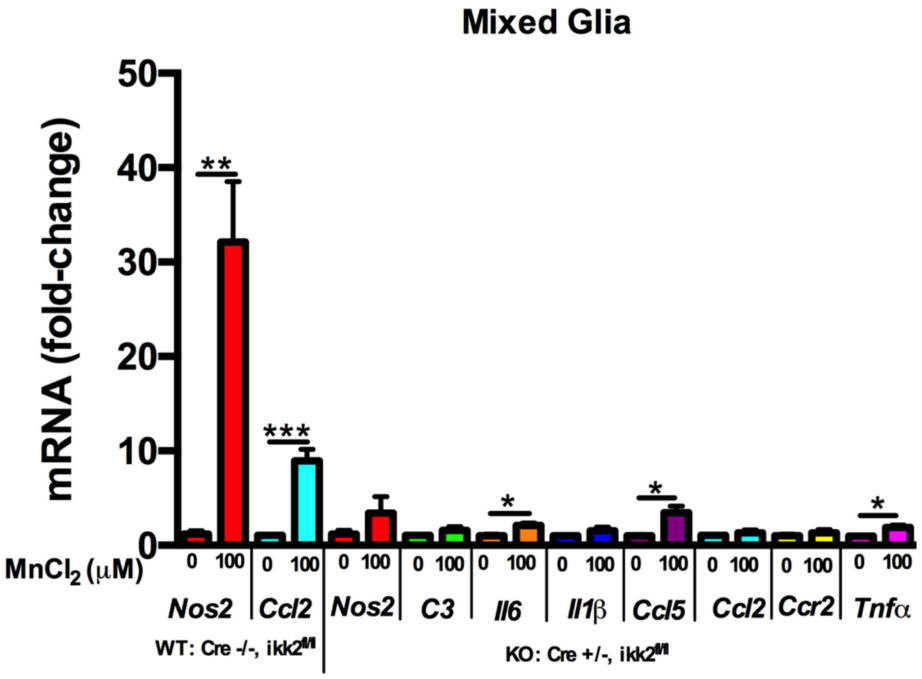

Secreted Cytokine Concentration (pg/ml)

Group	IFNγ	IL1β	IL6	CCL2	CCL3	CCL5	TNFα
IKK KO							
GCM							
Saline	--	43.64	15.573	29.87	2.04	8.493	1.708
100μM $MnCl_2$	--	46.74	7.058*	16.19	1.9	6.28	1.43

-- Result lower than limit of detection
*p<0.05 compared to saline (control)

Figure 3.5. Genetic inhibition of IKK in astrocytes (in a mixed glial population) decreases inflammatory gene expression regardless of 100uM $MnCl_2$ exposure. IKK inhibition decreases inflammatory gene expression

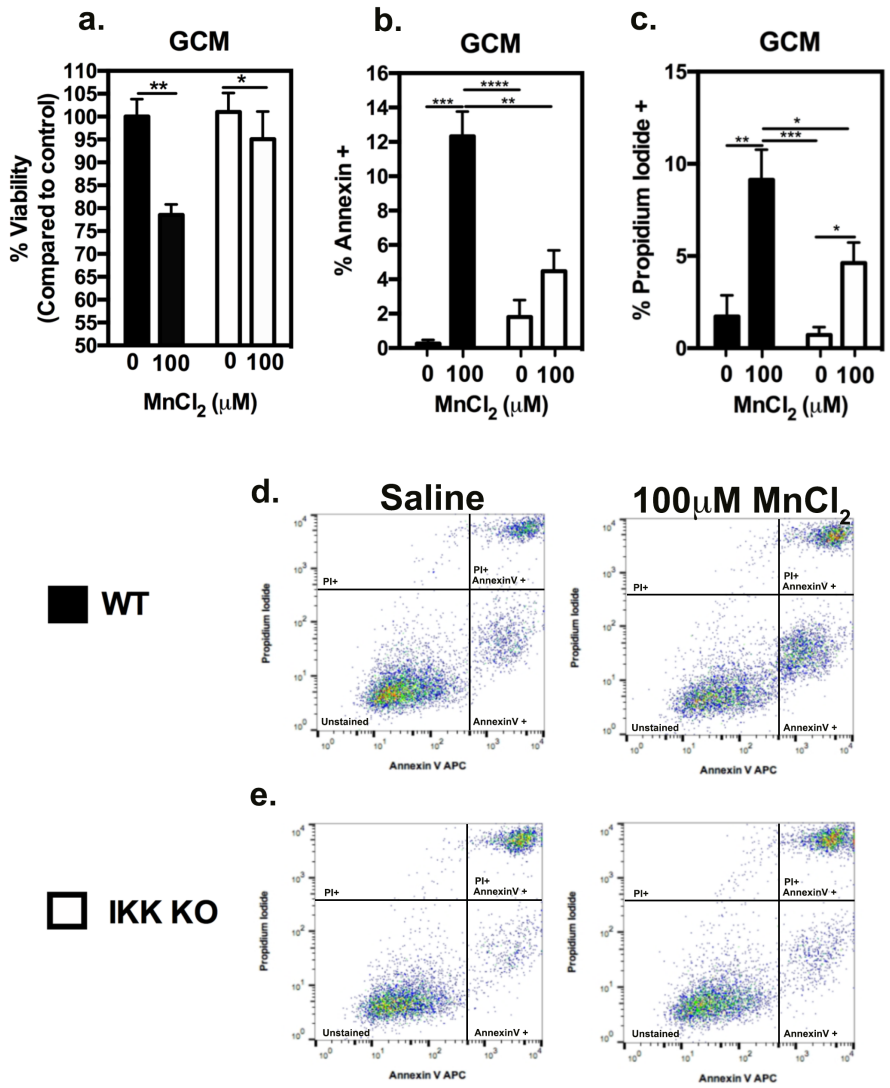

Figure 3.6. Genetic inhibition of IKK in astrocytes (in a mixed glial population) is neuroprotective in an N2A neuronal cell line. (a, black) GCM (from mixed glial cultures containing WT astrocytes treated with 100uM $MnCl_2$) decreases N2A viability ~25% compared to control, while **(a, white)** GCM from mixed glial cultures containing IKK KO astrocytes treated with 100uM $MnCl_2$ is more neuroprotective only causing a decrease of N2A viability by ~5% compared to control **(b-c, black)** GCM (WT) causes an increase in Annexin and PI positive stain in N2A cells, while **(b-c, white)** GCM (IKK KO) is more neuroprotective causing less Annexin and PI positive staining.

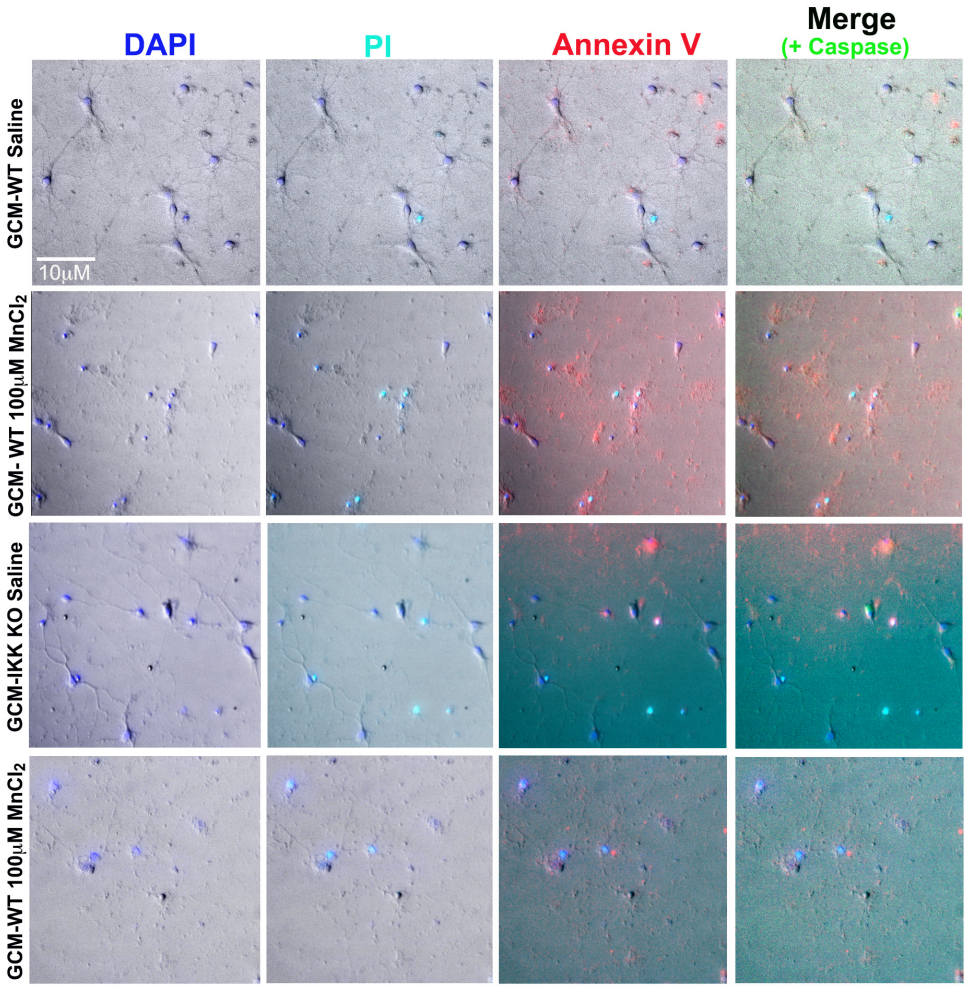

Figure 3.7. Representative images of live-cell imaging show that genetic inhibition of IKK in astrocytes (in a mixed glial population) is neuroprotective in primary neurons. (Top row) GCM (from mixed glial cultures containing WT astrocytes and microglia treated with Saline) exposure visually shows less PI, Annexin V or Caspase (left to right) positive staining of primary neurons, while GCM (from mixed glial cultures containing WT astrocytes treated with 100uM $MnCl_2$) depicts a marked increase in PI, Annexin V and Caspase positive staining in primary neurons. GCM (from glial cultures containing IKK KO astrocytes and WT microglia treated with Saline or 100uM $MnCl_2$) visually shows less of an increase in PI, Annexin V, and Caspase positive staining compared to GCM from WT mixed glial cultures.

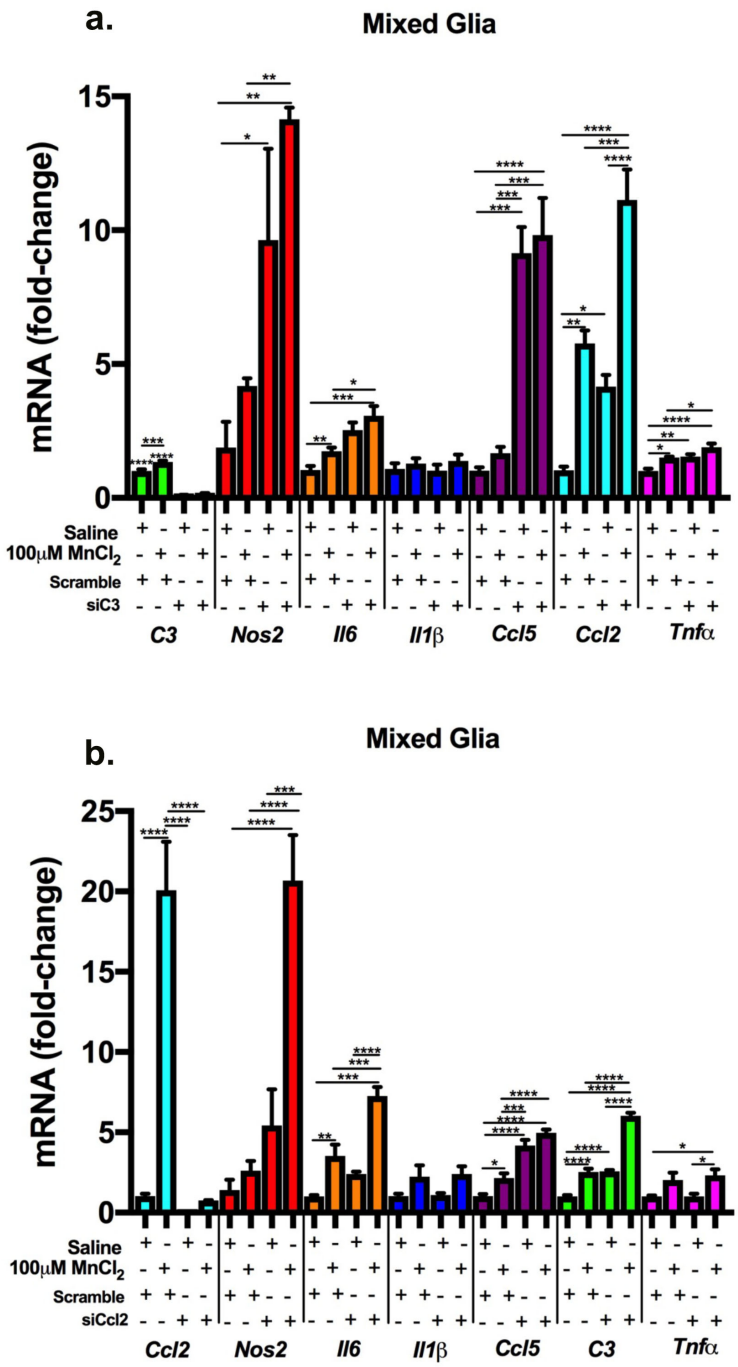

Figure 3.8. KD of astrocyte-specific inflammatory genes, *C3* and *Ccl2*, in mixed glia exacerbates Mn-induced inflammatory gene expression. (a) *C3* KD and **(b)** *Ccl2* KD cause mRNA fold-change in Mn-exposed mixed glia to increase more so than scramble saline control treated mixed glia.

CHAPTER 4

GLIAL-GLIAL SIGNALING MECHANISMS IN MODELS OF NEUROINFLAMMATION

4.1 INTRODUCTION

Prolonged inflammatory signaling by glial cells is an important etiological factor in the progression of neurodegenerative disease such as Parkinson's (PD) and manganism (Spranger et al., 1998; Teismann and Schulz, 2004). Production of inflammatory mediators by glia is highly regulated by the transcription factor, nuclear factor-κB (NF-κB) (Mosley et al., 2006), which is associated with overproduction of inflammatory cytokines, chemokines and genes such as inducible nitric oxide synthase (iNOS/NOS2) and reactive oxidative and nitrosative species (ROS/RNS) (Frank-Cannon et al., 2009; Nagatsu and Sawada, 2005).

Although the cause of idiopathic PD is not fully understood, it is linked both to genetic predisposition (Harischandra et al., 2015) (Harischandra et al., 2015), as well as to environmental neurotoxicants like Mn and viral and bacterial infections (Guilarte, 2010; Moreno et al., 2009; Olanow, 2004; Smith et al., 2015; Zhang et al., 2010). Exposure to high levels of Mn causes the neurodegenerative disorder, manganism, which was first described as early as 1837 (Couper) and presents with motor symptoms resembling PD. Research has only recently begun to determine how glial activation and neuroinflammation are associated with Mn-induced neuronal injury (Sidoryk-Wegrzynowicz and Aschner, 2013). Understanding how these inflammatory factors are regulated in glial cells during Mn exposure is critical to elucidating mechanisms underlying glial-neuronal signaling associated with neurotoxicity, as discussed in Chapter 3 (Popichak et al.,

in progress), which emphasizes how neuroinflammatory signaling between microglia and astrocytes impacts neuronal viability and apoptosis during Mn exposure.

Evidence for the involvement of activated glia in the progression of neurodegenerative diseases is extensive (Frakes et al., 2014; Hirsch et al., 2003; Rothe et al., 2017; Teismann and Schulz, 2004). Microglial activation is associated with Mn-induced-injury and neurotoxicity (Filipov and Dodd, 2012), however the role of intercellular signaling between microglia and astrocytes in Mn-induced neurodegeneration is less understood. NF-κB activation in glia results from neurotoxic exposure such as Mn, MPTP and LPS, leading to neuroinflammation (Carbone et al., 2008; Carbone et al., 2009; Filipov et al., 2005; Moreno et al., 2008).

Inhibiting neuroinflammation is a potential target for treating neurodegenerative diseases but there are no approved drugs that do so. Pharmacological attempts at disease modification for PD have failed in clinical trials for lack of efficacy, relegating patients to symptomatic therapies designed to augment dopamine function, which only temporarily alleviate motor symptoms. Moreover, long-term use of L-DOPA is associated with impairment of voluntary movement due to drug-induced dyskinesia, which is debilitating to quality of life (Lang and Lozano, 1998a; Lang and Lozano, 1998b; Panneton et al., 2010). In contrast to idiopathic PD, L-DOPA is generally ineffective in treating Mn-induced parkinsonism (Lu et al., 1994).

Molecular targets for blocking neuroinflammation are therefore highly studied as a potential therapeutic modality for suppressing neuroinflammation and thereby preventing further loss of dopamine neurons. Once such approach involves the NR4A family of orphan nuclear receptors, which are an important class of transcription factors necessary for development and homeostasis of neurons (Hammond et al., 2015; Saucedo-Cardenas and Conneely, 1996). They are also shown to inhibit the expression of NF-κB-regulated inflammatory genes in glial cells

(McEvoy et al., 2017; Rothe et al., 2017; Safe et al., 2015), demonstrated by one study in which NR4A2/Nurr1 regulates inflammatory gene expression in glial cells by inhibiting NF-κB activation (Saijo et al., 2009b). Inhibition of NR4A receptors could therefore be an effective means of inhibiting expression of NF-κB-regulated neuroinflammatory genes in glia and could serve as a potential target for pharmacologic intervention in neurological diseases such as PD and manganism. However, the endogenous ligands for these receptors are not known, making identification of pharmacological activators a high priority research target.

Selected diindolylmethane compounds (C-DIMs) have been shown to activate or inactivate nuclear receptors, including Nurr1 and Nur77, in cancer cells (Chintharlapalli et al., 2005; Cho et al., 2010; Cho et al., 2007; Inamoto et al., 2010; Inamoto et al., 2008; Lee et al., 2014; Top, 2016; Yu et al., 2015) but their capacity to directly activate these receptors in glial cells is not known. Because these compounds also suppress astrocyte inflammatory signaling *in vitro* (Carbone et al., 2008; Carbone et al., 2009; McMorrow and Murphy, 2011), we postulated that NR4A receptors inhibited inflammatory activation of astrocytes through an NF-κB-dependent mechanism. This suggests that pharmacological targeting of these receptors could be a viable strategy to mitigate glial activation and thereby slow the progression of neurodegeneration in diseases such as PD and manganism.

Here, it is demonstrated that C-DIM compounds inhibit NF-κB-mediated glial activation in *in vitro* and *in vivo* in models of neuroinflammation. We initially demonstrated that the diindolylmethane compound, 1,1-bis (3'-indolyl)-1-(*p*-*t*-butylphenyl) methane (C-DIM4), suppressed NF-κB-dependent expression of inducible nitric oxide synthase (iNOS/NOS2) and NO production in astrocytes exposed to 1-methyl-4-phenyl-1, 2,3,6-tetrahydropyridine (MPTP) by inhibiting binding of NF-κB/p65 to the NOS2 promoter, ultimately preventing inflammatory

gene activation. Subsequent experiments demonstrated that one diindolylmethane analog with Nurr1 activity, C-DIM12, has favorable pharmacokinetics and shows neuroprotective efficacy *in vivo*, as well as inhibiting inflammatory gene expression in microglia and inducing dopaminergic gene expression in neurons *in vitro* (De Miranda et al., 2013; De Miranda et al., 2015a; De Miranda et al., 2015b; Hammond et al., 2015). These studies demonstrate the importance of Nurr1 in regulating inflammatory gene expression in glia and homeostatic/trophic function in dopaminergic neurons. Furthermore, our laboratory utilized immunopurified murine microglia and astrocytes to show that Mn-induced NF-κB activation in microglia is essential for amplifying inflammatory activation of astrocytes, which establishes that glial-glial communication is critical to neuroinflammation during exposure to Mn. These studies support the findings that glial activation is directly involved in neuronal injury (Verkhratsky, 2007) and although it is known that microglia communicate directly with astrocytes, how astrocytes regulate neuronal cell fate during neurotoxic insults is less well understood.

Challenging glial cells with neurotoxins such as MPTP or inflammatory agents such as TNF and lipopolysaccharide (LPS) results in increased morphological indices of glial activation as well as increases in inflammatory gene expression. *In vivo* models of MPTP neurotoxicity demonstrate that glial activation accompanies neurodegeneration, based upon multiple experimental approaches including immunofluorescence (IF) and western blot for protein expression indicative of activated glial phenotypes, as well as genomic approaches including qRT arrays. Each of these experimental modalities provides information patterns of gene expression associated with the NF-κB pathway that regulate glial inflammatory phenotype. Furthermore, studies in our laboratory demonstrated that inflammatory activation of glia could be inhibited pharmacologically using selected diindolylmethane compounds that exert anti-

inflammatory effects in various models of inflammatory injury through nuclear specific mechanisms. Moreover, the mechanism of inhibition appears to require selected NR4A receptors, as determined by RNAi and chromatin immunoprecipitation (ChIP) experiments. The following data describe several approaches to identify patterns of gene expression and protein-DNA interactions that modulate NF-κB signaling in glial cells that regulate inflammatory phenotype.

4.2 MATERIALS AND METHODS

Materials. DIM-C-pPhtBu (C-DIM4), DIM-C-pPhOCH3 (C-DIM5), DIM-C-pPhOH (C-DIM8), and DIM-C-pPhCl (C-DIM12) were synthesized and characterized as described previously (Qin et al., 2004). For animal studies, working concentrations of C-DIM12 were diluted in corn oil and sonicated in hot water bath until solubilized. MPTP (Sigma, St. Louis MO) was solubilized at final working concentration in saline (0.9% $NaCl_2$). Probenecid (Sigma, St. Louis MO) was prepared in 5% sodium bicarbonate/MilliQ water to final working concentration (pH 7.5). All general chemical reagents including cell culture media, antibiotics, and fluorescent antibodies and dyes were purchased from Life Technologies (Carlsbad, CA) or Sigma Aldrich (St. Louis, MO) unless otherwise stated. TNFα and IFNγ were purchased from R&D Systems (Minneapolis, MN). All antibodies, unless otherwise stated, including Nurr1 and Nur77 were purchased from Santa Cruz Biotechnology (Santa Cruz, CA) and horseradish peroxidase conjugated goat anti-mouse and goat anti-rabbit secondary antibodies were purchased from Cell Signaling (Danvers, MA). For immunofluorescence studies, antibodies against glial fibrillary acidic protein (GFAP), anti-FLAG, Beta-actin and p65 were purchased from Sigma Chemical Co. (St. Louis, MO) and Santa Cruz Biotechnology (Santa Cruz, CA) respectively. Antibodies used for ChIP analysis of

p65 were purchased from Santa Cruz Biotechnology (Santa Cruz, CA) and Abcam (Cambridge, MA). Reagents utilized for transfection experiments were purchased from Mirus Bio (Madison, WI) for TransIT-X2 System reagent and Invitrogen (Carlsbad, CA) for Lipofectamine reagent. The NF-κB-293T-GFP-Luc reporter (HEK) cell line was purchased from System Biosciences (Mountain View, CA).

Animals and Treatment Regimen. Inbred C57/Bl6 male mice (~24 weeks of age; 25-30 grams in weight) were acquired by Charles River Laboratories (Wilmington, MA) and housed on 12-hour light/dark cycles in a temperature controlled room (maintained at 22-24°C) with access to standard chow and water *ad libitum*. Mice were administered C-DIM12 (25mg/kg) or corn oil (vehicle control) by oral gavage. Mice were dosed with MPTPp twice weekly for two weeks, with each dose delivered 2 days apart. On the day of dosing, probenecid was delivered in the morning by intraperitoneal injection (100 mg/kg) and then MPTP (20 mg/kg) or saline (0.9%NaCl) was administered 4 hrs later by subcutaneous injection, per our previously published protocol (De Miranda et al. 2014). C-DIM12 or corn oil was administered daily by intragastric gavage (14 doses total) throughout the treatment period. At the conclusion of the study, mice were anesthetized under deep isoflurane anesthesia and transcardially perfused with 0.1M phosphate buffered saline (PBS)-cacodylate/heparin (10 U/mL) and 3% paraformaldehyde/PBS. Post perfusion, brains were dissected and stored in paraformaldehyde at 4 °C overnight, and then stored in sodium-cacodlyate-PBS (pH 7.2) containing 15-30% sucrose at 4°C until processed for cryosectioning. For neurochemical sample collection, animals were also administered deep isoflurane before rapid removal of striatum and ventral midbrain for flash freezing in liquid

nitrogen. Brain samples were then transferred to -80°C storage until processed for RNA, protein and HPLC analysis.

Primary Cell Isolation. Cortical glia were isolated from day-1 old C57Bl/6 or transgenic mouse pups according to procedures described previously (Aschner and Kimelberg, 1991), and purity confirmed through immunofluorescent (IF) staining using antibodies against GFAP and IBA1 (Carbone et al., 2009). Briefly, pups were euthanized by decapitation under isofluorane anesthesia and cortices (astrocytes) were rapidly dissected out, and meninges removed. Tissue was subject to digestion with Dispase (1.5 U/ml), and selection of astrocytes was performed by complete media change 24 hrs after plating to remove non-astroglial cell types. Astrocyte cultures were maintained at 37°C and 5% CO2 in minimum essential media supplemented with 10% heat-inactivated fetal bovine serum and a penicillin (0.001 mg/ml), streptomycin (0.002 mg/ml), and neomycin (0.001) antibiotic cocktail. Cell media was changed 24 hr prior to all treatments. All animal procedures were approved by the Colorado State University Institutional Animal Care and Use Committee and were conducted in accordance with published NIH guidelines.

Gene Knockdown Assays. RNA interference (siRNA, small interfering RNA) sequences were acquired from Integrated DNA Technologies (IDT DNA, Coralville, IA). Nurr1 and Nur77 RNAi duplexes were designed against splice common variants of the target gene and were validated using a dose-response assay with increasing concentrations of the suspended oligo (900-1200 ng/ml) using a standard scrambled dicer- substrate RNA (DsiRNA) as control. BV2 microglia cells were transfected with RNAi oligonucleotides using the TransIT-X2 delivery

system (Mirus Bio, Madison, WI) 48 hr before treatment with LPS, with or without C-DIM12 (10 μM) treatment or vehicle control (DMSO) for 24 hr. Separate siRNA systems were used to ensure specific knockdown of Nurr1 and Nur77 mRNA, while limiting off-target effects on other nuclear receptor family members (Nur77 or Nurr1, respectively, and Nor1). The Nurr1 dsiRNA duplex sequences are (5'→3') CUAGGUUGAAGAUGUUAUAGGCACT; AGUGCCUAUAACAUCUUCAACCUAGAA (IDT DsiRNA; denoted siNurr1), the Nur77 DsiRNA duplex sequences (5'→3') UCGUUGCUGGUGUUCCAUAUUGAGCUU; AGCAACGACCACAAGGUAUAACUCG (IDT DsiRNA; denoted siNur77) and the Tnf DsiRNA sequences are GGAUGAGAAGUUCCCAAAUGGCCTC; UCCCUACUCUUCAAGGGUUUACCGGAG (IDT DsiRNA; denoted siTnf), and the Scr siRNA sequences are CUAGGUUGAAGAUGUUAUAGGCACT; AGUGCCUAUAACAUCUUCAACCUAGAA (IDT DsiRNA; denoted Scramble).

Flow Cytometry. The estimated percent of glia in mixed glial, microglial, and astrocyte cultures were determined by immunophenotying using direct labeling with anti-GLAST-PE (Miltenyi Biotec, San Diego, CA), anti-Cd11b-FITC (BD Biosciences), anti- CD11b-PE (Stemcell Technologies), and anti-GLAST-488 (Novus Biologicals, Littleton, CO) followed by flow cyto- metric analysis. Cells were counted using a Bio-Rad TC10 automated cell counter, and 1×10^6 cells/mL were resus- pended in 100 μL of incubation buffer (PBS with 0.05% bo- vine serum albumin). Mixed glial cultures were labeled using the mouse anti-GLAST-PE (20 μg/mL) and mouse anti-CD11b-FITC (10 μg/mL) at room temperature for 1 h. Microglia cultures were incubated with CD11b-PE accord- ing to manufacturer instructions while astrocyte cultures were incubated with rabbit polyclonal anti-GLAST-488 (10 μg/mL) at room temperature for 1 h. After

labeling, the cells were washed twice in incubation buffer and resuspended at a final volume of 500 µL of PBS and stored at 37 °C until analysis. Flow cytometry was performed on a Beckman Coulter CyAn ADP flow cytometer operated with Summit software for data collection at Colorado State University's Flow Cytometry Core Facility. All further data analysis was done utilizing FlowJo software (version 10.1; FlowJo, Ashland, OR).

Gene Expression Assays. Midbrain tissue samples from each experimental group were homogenized and lysed using Qiashredder columns along with on-column and in solution DNase treatment (Qiagen; Hilden, Germany). RNA from glia treated with respective inflammatory insult and lysed brain tissue was isolated using the RNEasy Mini kit (Qiagen, Valencia, CA), and purity and concentration were determined using a Nanodrop ND-1000 spectrophotometer (NanoDrop Technologies, Wilmington, DE). Following purification, RNA (250-1000ng) was used as template for reverse transcriptase (RT) reactions using the iScript RT kit (BioRad, Hercules CA). The resulting cDNA was immediately profiled for gene expression according to the 2-ΔΔCT method (Livak and Schmittgen, 2001). Primer sequences of genes profiled are presented in Table format. Brain tissue samples from each experimental group were amplified using RT^2 profiler PCR arrays (Qiagen; Hilden, Germany) for NF-κB signaling pathway target genes (PAMM-025ZG-4) and Parkinson's disease associated genes (Cat#: PAMM-124ZG-4) for a total analysis of 168 genes. Both sets of 384-well pathway array plates were run according the manufacturer's protocol on a Lightcycler 480 real time PCR instrument (Roche; Branford, CT, USA). Gene expression fold change was analyzed using the SAbiosciences software.

Western Blotting. Confluent treated glia or brain tissue were lysed with RIPA buffer, quantified via Pierce BCA Protein Assay kit (Thermo Scientific), and combined with SDS-PAGE loading buffer (1x final concentration), and equal volumes/total protein were separated by standard SDS-PAGE using a 10% acrylamide gel (BioRad, Hercules CA) followed by semi-dry transfer to polyvinylidene fluoride (PVDF) membrane (Pall Corp., Pensacola, FL). All blocking and antibody incubations were performed in 5% non-fat dry milk in tris-buffered saline containing 0.2% Tween-20. Protein was visualized on film using enhanced chemiluminescence (Pierce, Rockford, IL) on a Chemidoc XRS imaging system (Biorad, Hercules, CA). Membranes were stripped of antibody and reprobed against ß-Actin to confirm consistent protein loading among sample groups. Raw TIFF files were analyzed for mean optical band density with ImageJ analysis software (Schneider *et al.*, 2012).

NF-κB Reporter Assays. The NF-kB-293T-GFP-Luc reporter cell line was purchased from System Biosciences (Mountain View, CA). For green fluorescent protein/49,6-diamidino-2-phenylindole (GFP/DAPI) expression assays, cells were grown in DMEM (Life Technologies) supplemented with 10% FBS and 1_ PSN (as described earlier) on 96-well black-walled plates (Thermo Scientific, Waltham, MA). Cells were plated 24 hours before treatment with 30 ng/ml TNFa in the presence or absence of 100 mM of C-DIM12 or 50 mM of Bay-11 (positive control) for 24 hours, or at specific times/dosages as described in the figure legends. Reporter cells were washed with 1_ phosphate-buffered saline (PBS) and stained with Hoechst 33342 (Molecular Probes/Life Technologies, Eugene, OR) in Fluorobrite DMEM (Life Technologies) incubated at 37°C, 5% CO_2 for 5 minutes, then washed again with 1_ PBS. The medium was replaced with fresh Fluorobrite DMEM before reading the plate at 488/519 nm for GFP fluorescence

expression and 345/478 nm for DAPI fluorescence expression on a Cytation3 Cell Imaging Multi-Mode Reader (BioTek Instruments, Winooski, VT). The GFP expression intensity values were divided over the DAPI expression intensity values for quanti- tative analysis. TNFa concentrations were based on a dose–response assay (0–100 ng/ml; Supplemental Fig. 1) for optimal induction of NF- kB–GFP expression.

Immunofluorescence Microscopy. Primary astrocytes or BV2 microglial cells were grown to confluence on 20 mm serum-coated glass coverslips and treated accordingly. Blocking and antibody hybridization was conducted in 1% goat/donkey serum in PBS, and all washes were conducted in PBS. Coverslips were mounted in Vectashield Mounting medium containing DAPI (Vector Laboratories, Burlingame, CA). Slides were imaged using a Zeiss Axiovert 200M inverted fluorescence microscope equipped with a Hammamatsu ORCA-ER–cooled charge-coupled device camera (Hammamatsu Photonics, Hamamatsu City, Japan) using Slidebook software (version 5.5; Intelligent Imaging Innovations, Denver, CO) and 6 – 8 microscopic fields were examined per treatment group over no less than three independent experiments. Quantification of protein was determined by measuring the fluorescence intensity of protein of interest expression within the boundary of each cell, defined by DAPI counterstain, and segmented using Slidebook 5.0 software function for fluorescence intensity minus background (F/F_O). All brain tissue processed for IF was frozen with OCT on microtome stage and sectioned/collected for ST (25 μm in thickness) and SN (40 μm in thickness) regions. Tissue sections were stored in cryoprotectant (30% sucrose, 30% ethylene glycol, 0.5M phosphate buffer; pH 7.2) at 20°C until selected for immunostaining. IF staining was conducted as previously described by Miller et al. 2011, and all antibody dilutions were 1:500, unless stated

otherwise (Miller *et al.*, 2011). For stereology, SN sections were immunostained with anti-tyrosine hydroxylase (Millipore AB152) and anti-MAP2 (Abcam AB5392). For gliosis, SN and ST sections were immunostained with either anti-IBA1 (1:250; Wako 016-20001) or anti-GFAP (Dako Z0334) and anti-tyrosine hydroxylase (Abcam AB76442). SN tissue was also immunostained with anti-TH and anti-Nurr1 (1:200; Santa Cruz SC991) for mean intensity measurements of Nurr1. All secondary antibodies used for IF were alexa flour 488, 555, and 647 (LifeTech, Carlsbad CA).

Microglial Morphology. Microglia were prepared and assessed for changes in morphology both *in vitro* in primary microglia and *in vivo* microglia in brain tissue by confocal imaging as described in (Kirkley et al., 2017) and (Hammond et al., 2018).

Chromatin Immunoprecipitation (ChIP). Glia were grown to confluence in 10-cm tissue culture plates and treated before cross-linking with 1% formaldehyde (Thermo Scientific) for 10 minutes. The remaining steps were adapted from the Chromatrap ChIP (chromatin immunoprecipitation) protocol, which accompanies the Chromatrap Pro-A Premium ChIP Kit (Chromatrap, Wrexham, United Kingdom). DNA was sheared into approximately 500 bp fragments before removing 10% (200 ng) for input controls, with 2 μg of chromatin was loaded into the immunoprecipitation reaction with 2 mg precipitating antibody (as suggested by Chromatrap), anticore- pressor for repressor element 1 silencing transcription factor [anti-CoREST], anti–nuclear receptor corepressor 2 [anti-NCOR2], and anti-histone deacetylase 3 [anti-HDAC3] from Abcam (Cambridge, United Kingdom); anti-Nurr1 (N-20; 991), and anti-p65 (372) from Santa Cruz Biotechnology. Immunopurified DNA was isolated via the QIAquick

PCR Purification Kit (Qiagen; suggested by Chromatrap). A 149-bp region of the NOS2 promoter proximal to the NF-kB site of transcription was amplified via quantitative PCR and performed with SYBR-Green Supermix (Bio-Rad Laboratories, Hercules, CA) and analyzed using the percentage of input method according to Life Technologies.

Modeling. Small molecule docking studies were conducted and analyzed according to procedures described in Chapter 2 and (Hammond et al., 2018).

Mn Experiments and Assays. Additional Mn treatments and assessments in primary microglia are more thoroughly described in (Kirkley et al., 2017).

Statistical Analysis. Experiments were performed at least three times, with replicates consisting of independent cultures using a minimum of four plates or cover slips per replicate study. Data was presented as the mean +/- SEM, unless noted otherwise. All experimental values from each mean were analyzed with a Grubb's (α=0.05) test for exclusion of significant outliers. Differences between three experimental groups were analyzed with a one-way ANOVA followed by a Tukey *post hoc* multiple comparisons test. Two group comparisons for densitometry analysis was conducted with an unpaired student's t-test followed by Welch's correction. A two-way ANOVA was performed when incorporating 'day' as an experimental variable for behavioral tests. For all experiments, $p < 0.05$ was considered significant, although the level of significance was often much greater. All statistical analyses were conducted using Prism (version 6.0; Graph Pad Software, San Diego, CA).

4.3 RESULTS

A novel diindolylmethane compound suppresses NOS2 gene expression in primary astrocytes by a nuclear, NF-κB-inhibitory mechanism.

To determine the anti-inflammatory efficacy of C-DIM compounds in primary cultures of astrocytes and microglia, we exposed mixed glial cultures to an oxidative and inflammatory challenge consisting of MPTP and the inflammatory cytokines TNFα and IFNγ in the presence or absence of C-DIM's (Carbone et al., 2009). These experiments demonstrated that the diindolylmethane compound 1,1-bis (3'-indolyl)-1-(*p*-*t*-butylphenyl) methane (C-DIM4) significantly decreased MPTP/IFN/TNF-induced NOS2 mRNA and protein expression as measured by qRTPCR and western blotting, respectively (Figure 4.1).

Detection of GFAP and 3-nitrotyrosine (3-NT) by immunofluorescence microscopy revealed an increase in nitration in MPTP/TNF/IFN treated astrocytes and suppressed nitration to control levels after co-treatment with C-DIM4 and the NOS2 inhibitor, 2-amino-5, 6-dihydro-6-methyl-4*H*-1, 3-thiazine (AMT) (data not shown). Furthermore, activation of NF-κB in response to MPTP/TNF/IFN insult was measured by live-cell fluorescence imaging using primary astrocytes isolated from transgenic mice, which express an EGFP reporter construct driven by multiple *cis*-acting NF-κB domains. NF-κB was activated in astrocytes exposed to MPTP/TNF/IFN, and suppressed with co- treatment with C-DIM4, whereas DMSO vehicle control had no effect (Figure 4.2).

To assess the mechanism of inhibition of C-DIM4, we used chromatin immunoprecipitation (ChIP) assays to identify patterns of transcription factor binding to the Nos2 promoter at NF-κB enhancer elements. Based on previous studies demonstrating a requirement for degradation of the nuclear corepressor 2 protein (NCoR2) at the p65 binding site

during NF-κB-dependent transactivation (Pascual et al., 2005), we tested binding of this factor, as well as that of p65 and PPARγ, to the proximal NF-κB response element. These studies demonstrated that treatment with MPTP+TNF/IFN cause binding of p65 to the proximal NF-κB enhancer element in the Nos2 promoter along with removal of the corepressor, NCoR2. Treatment with C-DIM4 resulted in the prevention of p65 binding but was without effect on binding of PPAR-γ or NCoR2 (Figure 4.3). We showed that C-DIM4 decreased expression of inflammatory genes by decreasing binding to 5'-flanking *cis* elements, but we wanted to determine whether this would affect neuronal health in a co-culture system. Once astrocytes were treated with MPTP/TNF/IFN+C-DIM4, we cultured them with primary striatal neurons and then assessed apoptotic activity by staining for caspase activity and annexin V binding in neurons as a result. We showed that C-DIM4 treatment significantly decreased apoptosis in primary neurons while DMSO did not affect MPTP/TNF/IFN-induced cell death (Figure 4.4).

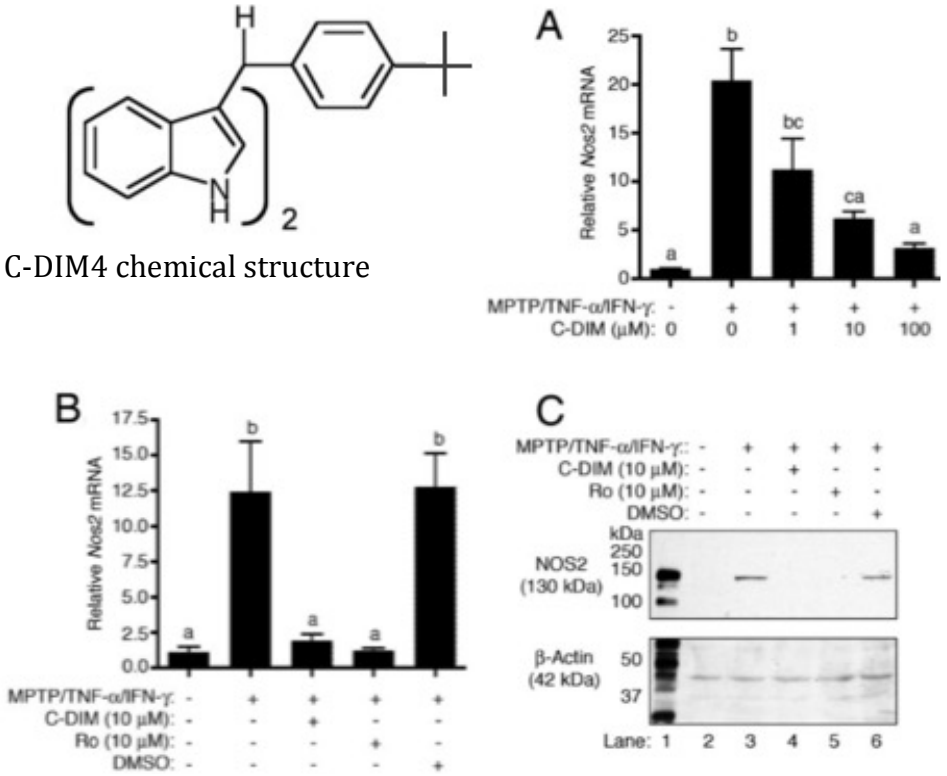

Figure 4.1. A) qRTPCR demonstrating dose-dependent suppression of *Nos2* mRNA by C-DIM4 in astrocytes challenged with MPTP, TNFα, and IFNγ. **B)** qRTPCR demonstrating equivalent suppression of *Nos2* mRNA by either C-DIM4 or rosiglitazone (known PPARγ agonist. **C)** Immunoblotting demonstrates suppression of NOS2 protein expression by either C-DIM4. Activated macrophage lysate was used as a positive control for identification of NOS2 (lane 1). (Carbone et al., 2009)

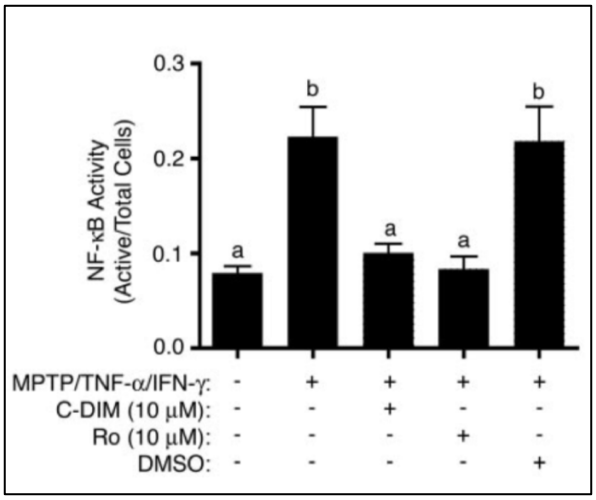

Figure 4.2. NF-κB is activated in astrocytes exposed to MPTP/TNFα/IFNγ, but co- treatment with either C-DIM4 or rosiglitazone suppresses this activation, whereas DMSO vehicle control had no effect. (Carbone et al., 2009)

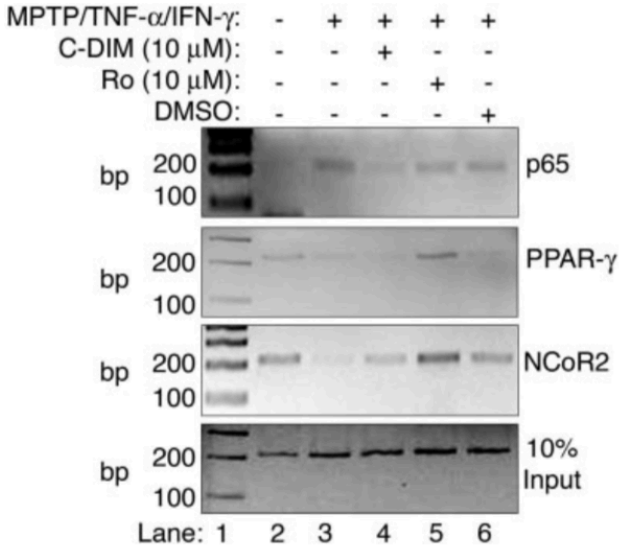

Figure 4.3. (Lane 3) ChIP reveals binding of p65 to the proximal NF-κB enhancer element in the *Nos2* promoter along with removal of NCoR2 after challenge of astrocytes with MPTP/TNFα/IFNγ. (Lane 4) C-DIM4 cotreatment resulted in the prevention of p65 docking with no effect on PPARγ recruitment or NCoR2 stabilization. (Lane 5) cotreatment of astrocytes with rosiglitazone did not affect p65 docking, resulted in recruitment of PPARγ and ensuing stabilization of NCoR2. These data demonstrate different mechanisms of *Nos2* gene suppression by C-DIM4 and rosiglitazone. (Carbone et al., 2009)

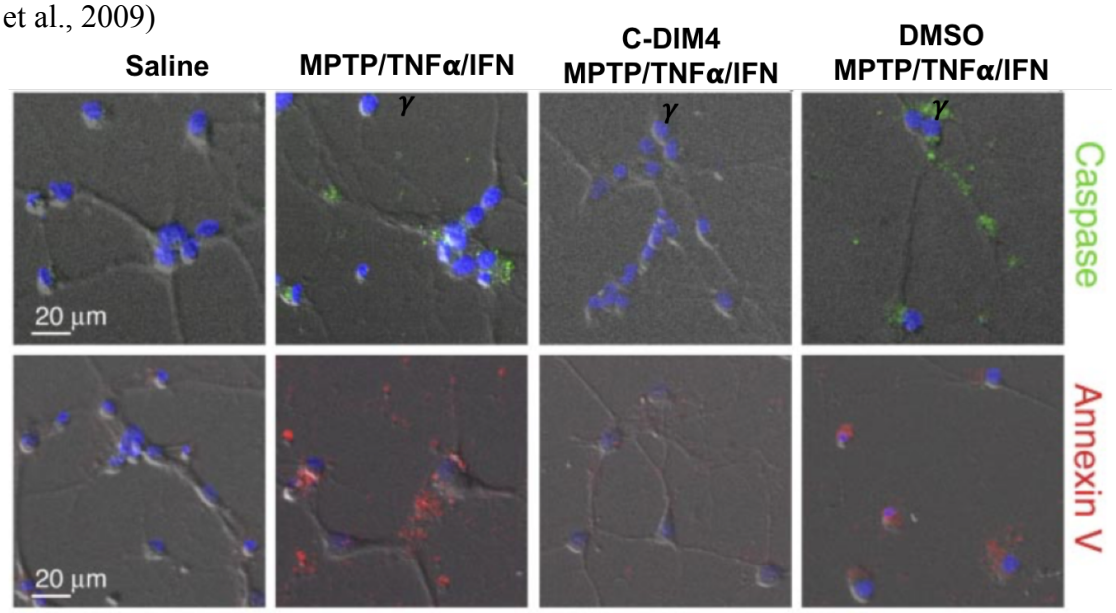

Figure 4.4. Representative images show caspase activity (green) and annexin V (red) binding in primary striatal neurons cocultured with astrocytes activated by exposure to MPTP/TNFα/IFNγ. Co- treatment of astrocytes with C-DIM4 before incubation with neurons suppressed neuronal apoptosis. (See Carbone et al., 2009 for quantitation graphs)

C-DIM compounds are neuroprotective and anti-inflammatory in an animal model of Parkinson's disease.

To further assess the anti-inflammatory and neuroprotective affects of C-DIMs, we dosed transgenic NF-κB/EGFP mice with MPTPp over 1 week and examined the capacity of selected C-DIM compounds to suppress ongoing loss of dopamine neurons and glial activation when administered after MPTPp (De Miranda et al., 2015b).

Progressive dopamine neuron loss by MPTPp in transgenic NF-κB/EGFP mice was determined by the quantification of tyrosine hydroxylase (TH)-positive and total (MAP2)-positive neuronal cell bodies in the substantia nigra (SN) and mean intensity of TH nerve terminals in the striatum (ST). Oral gavage administration of C-DIM5, C-DIM8, and C-DIM12 comparably attenuated dopamine neuronal loss in MPTPp14d compared to saline and drastically reduced the more moderate neuronal loss seen in MPTPp7d. Moreover, nitrotyrosine adducts (measured by 3-NT IF) and apoptotic marker, γH2AX, co-localize/increase in TH+ neurons in MPTPp treated groups, however, C-DIM8 and C-DIM12 significantly ablated those effects, and C-DIM5 trended toward decreasing those effects. Furthermore, IF analyses revealed that exposure to MPTPp over time (7d, 14d, and 21d) decreased total Nurr1 intensity and TH co-localization with Nurr1, and all C-DIMs increased Nurr1 expression. Intrinsic expression of NF-κB/EGFP alone and co-localizing with GFAP+ (astrocytes) and IBA-1+ (microglia) increased considerably, but more so in microglia. C-DIMs drastically decreased NF-κB/EGFP expression, and C-DIM12, specifically, decreased NF-κB/EGFP expression co-localizing with TH-positive neurons (Data not shown; see publication).

MPTPp7/14d increased astrocyte and microglial recruitment/activation indicated by increased GFAP and IBA-1 in IF analyses. All C-DIMs significantly decreased glial activation,

and C-DIM12 showed a greater trend in decreased glial activation compared to C-DIM5 and C-DIM8. To broaden assessment of NF- κB activation as a result of MPTPp exposure, we isolated RNA from SN of study mice and evaluated NF-κB-regulated inflammatory gene expression using a qRT array from SABiosciences. We showed that C-DIM5 and C-DIM12 decreased some inflammatory cytokines, but C-DIM12 was more significantly effective in reduction of inflammatory genes, *Tnf*, *Caspase 1*, and *Tlr4* (Figure 4.5).

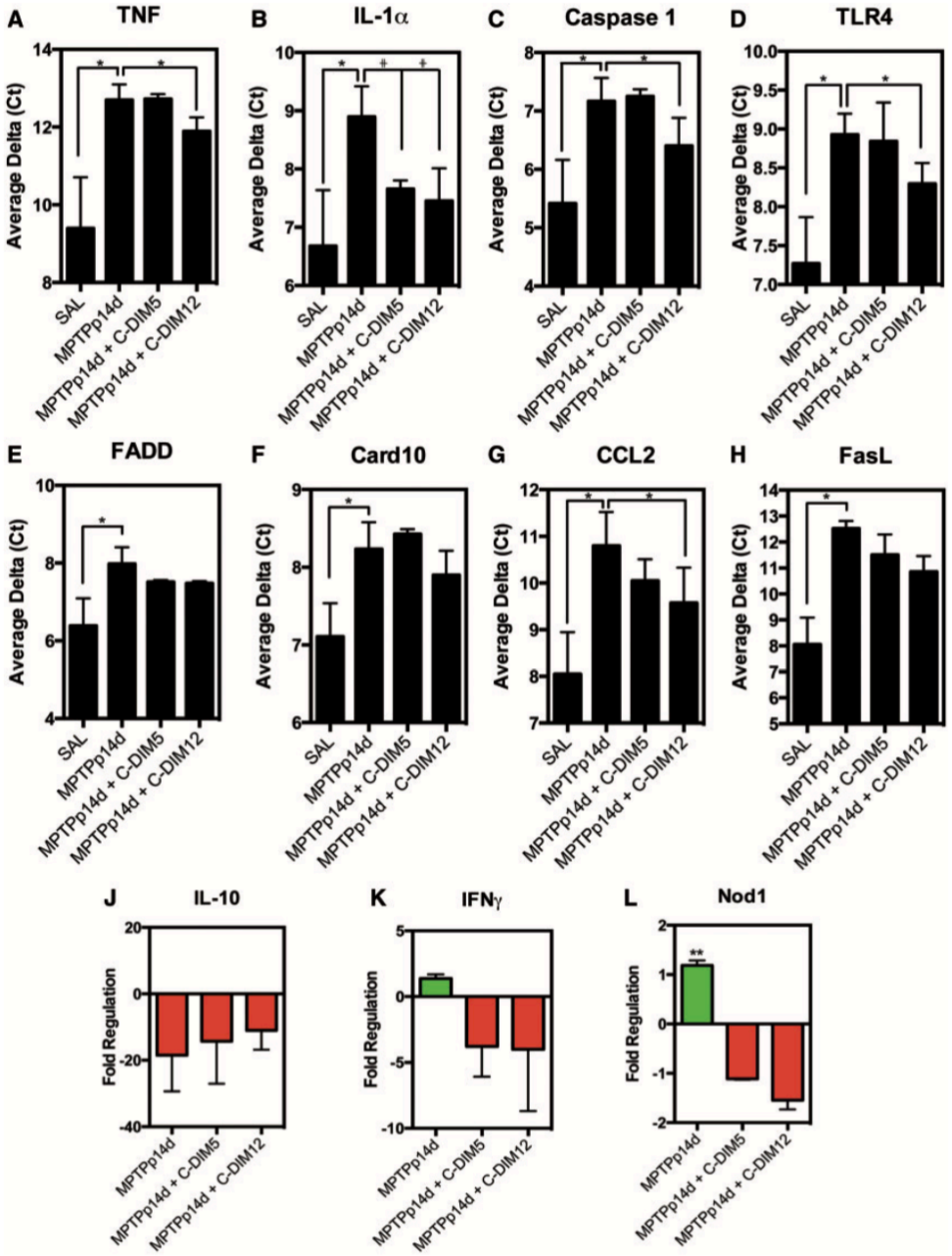

Figure 4.5. NF-κB-regulated inflammatory gene expression in the SN. RNA isolated from the SN of Saline, MPTPp14d, and C-DIM5- or C-DIM12-treated animals was analyzed using a real-time polymerase chain reaction (PCR) array of NF-κB pathway genes (SA Biosciences). **(A-H)** Average Delta CT values from real-time analysis show global increases in NF-κB-regulated genes from saline to MPTPp14d **(J-L)** Fold regulation over saline of IL-10 shows a trend for increased expression in C-DIM5 and C-DIM12 over MPTPp14d, whereas INFγ and Nod1 are increased in MPTPp14d but reduced in C-DIM5 and C-DIM12 treatments. (De Miranda et al., 2015b)

C-DIM12 inhibits LPS-induced glial activation by a nuclear-specific mechanism in BV2 microglial cells.

Based off of previous findings that C-DIM12 activates Nurr1 in various cancer cell lines (Inamoto et al., 2008; Lee et al., 2014; Safe et al., 2015) and is neuroprotective in *in vivo* efficacy studies in a mouse model of PD (De Miranda et al., 2013; De Miranda et al., 2015b), we wanted to ascertain whether C-DIM12 can directly inhibit inflammatory gene transcription in microglial cells by enhancing Nurr1-dependent transrepression of NF-κB at proinflammatory gene promoters (De Miranda et al., 2015a).

First, in an extensive study assessing LPS-induced inflammatory gene expression in primary murine mixed glia, we showed that 1μM or 10μM treatment of 14 C-DIM analogs structurally-and dose-dependently suppressed *Nos2* and *Il1β* mRNA expression (Table 3). Unpublished *Trail* and *Tnf* mRNA expression is shown in Figure 4.6, demonstrating less fold-change expression by LPS treatment, but overall, decreased inflammatory gene expression by all 14 C-DIM compounds.

Table 3. **Structure and dose-dependent suppression of LPS-induced inflammation by C-DIMs.** Primary murine mixed glial cultures were treated with saline or 1μg/ml LPS and 1μM or 10μM doses of one of 14 C-DIM analogs. Structural differences displayed as R-Group, and significant suppression of *Nos2* and *Il1β* mRNA levels from LPS control are indicated. (De Miranda et al., 2015a)

C-DIM	R-Group	NOS2 mRNA (Fold-Induction)		IL-1β mRNA (Fold-Induction)	
		Saline 1.0 ± 0.2	LPS 240.5 ± 24.4[a]	Saline 1.0 ± 0.2	LPS 175.7 ± 16.5[a]
		LPS +		LPS +	
		C-DIM (1 μM)	C-DIM (10 μM)	C-DIM (1 μM)	C-DIM (10 μM)
1	-CF_3	160.6 ± 13.1	50.8 ± 8.7[b]	167.6 ± 18.2[a]	34.1 ± 3.1[b]
2	-Br	175.5 ± 34.9	73.1 ± 23.1	129.4 ± 43.0	40.6 ± 3.7[b]
3	-F	133.8 ± 8.6	3.3 ± 1.5[b]	156.7 ± 10.6[a]	7.1 ± 1.8[b]
4	-*tert*-Butyl	107.8 ± 20.5	84.8 ± 8.0	125.3 ± 8.0	93.9 ± 10.2
5	-OCH_3	141.4 ± 24.0	14.7 ± 4.7[b]	142.6 ± 6.1[a]	15.4 ± 2.3[b]
6	-$N(CH_3)_2$	224.2 ± 68.0[a]	99.5 ± 21.7	164.9 ± 30.0[a]	65.1 ± 9.1
7	-H	184.9 ± 36.1[a]	12.4 ± 4.4[b]	142.9 ± 44.5[a]	12.6 ± 2.3[b]
8	-OH	189.3 ± 61.8[a]	0.7 ± 0.4[b]	136.2 ± 48.3[a]	9.3 ± 1.4[b]
9	-Phenyl	136.2 ± 47.7	180.9 ± 34.5[a]	137.4 ± 47.4[a]	127.2 ± 5.8
10	-CN	96.0 ± 21.6	34.5 ± 5.8[b]	140.1 ± 7.5[a]	23.8 ± 1.8[b]
11	-CH_3	140.0 ± 5.5	32.0 ± 6.8[b]	152.2 ± 15.7[a]	36.4 ± 3.5[b]
12	-Cl	180.4 ± 26.2	60.6 ± 17.5[b]	186.9 ± 27.6[a]	45.9 ± 8.9[b]
13	-$COOCH_3$	255.5 ± 78.8[a]	90.9 ± 7.8[b]	185.2 ± 11.5[a]	44.0 ± 15.2[b]
14	-I	242.9 ± 83.9[a]	122.7 ± 33.5[b]	161.4 ± 43.6[a]	72.4 ± 15.0

[a]Different from control group ($P < 0.05$).
[b]Different from LPS group ($P < 0.05$).

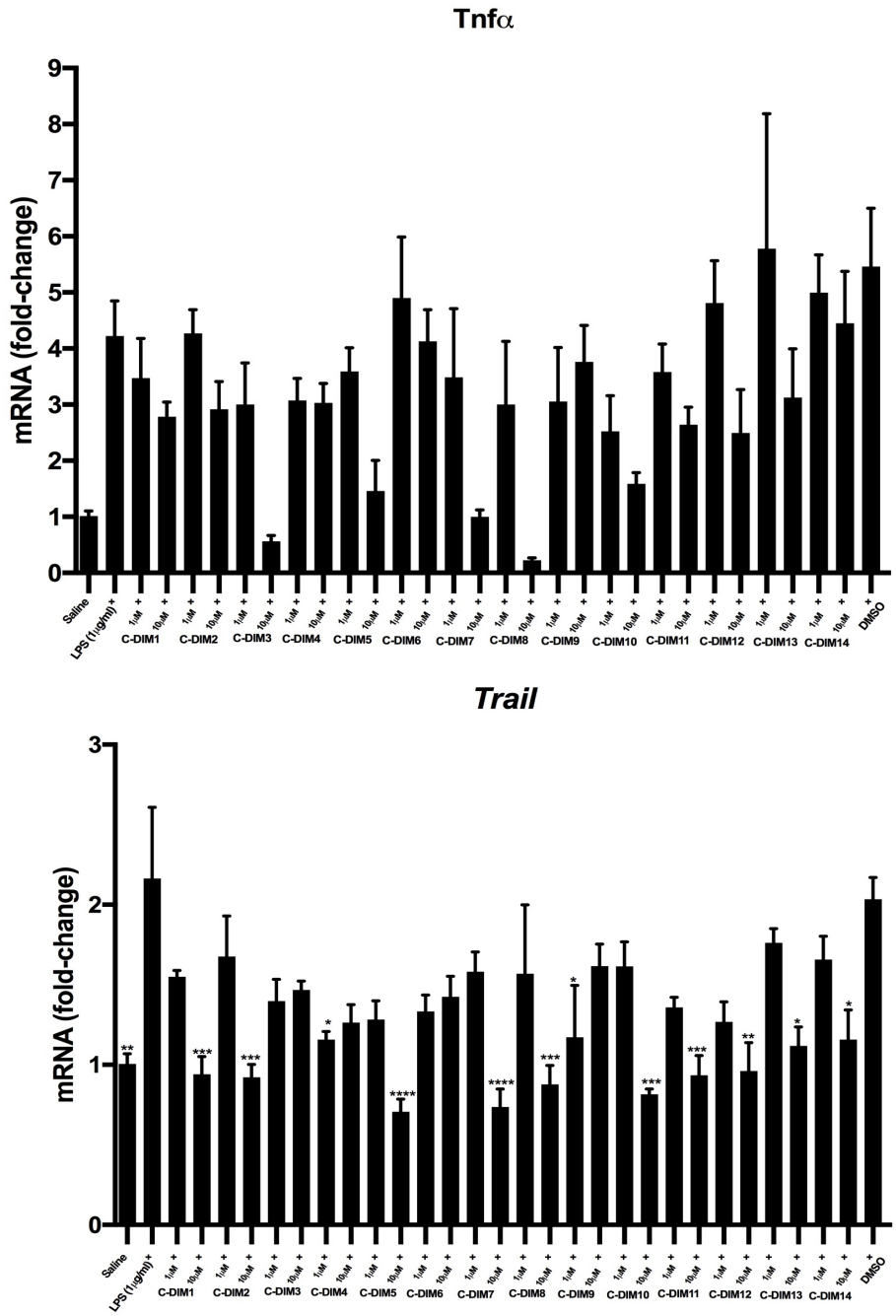

Figure 4.6. Structure and dose-dependent suppression of LPS-induced inflammation by C-DIMs in primary murine mixed glial cultures treated with saline or 1μg/ml LPS and 1μM or 10μM doses of one of 14 C-DIM analogs. Significant suppression of *Tnfα* and *Trail* mRNA levels from LPS control indicated with *.

Upon further examination, we showed that C-DIM5 (see Chapter 2) and C-DIM12 dose-dependently decreased LPS-induced *Nos2* and *Il1β* after 8 hours treatment in primary murine mixed glial cultures. We then determined that the optimal time point for maximal inflammatory gene expression due to LPS exposure in a BV2 microglial cell line was 24hrs (Figure 4.7), which was used in ensuing experimentation studying anti-neuroinflammatory efficacy of C-DIM12.

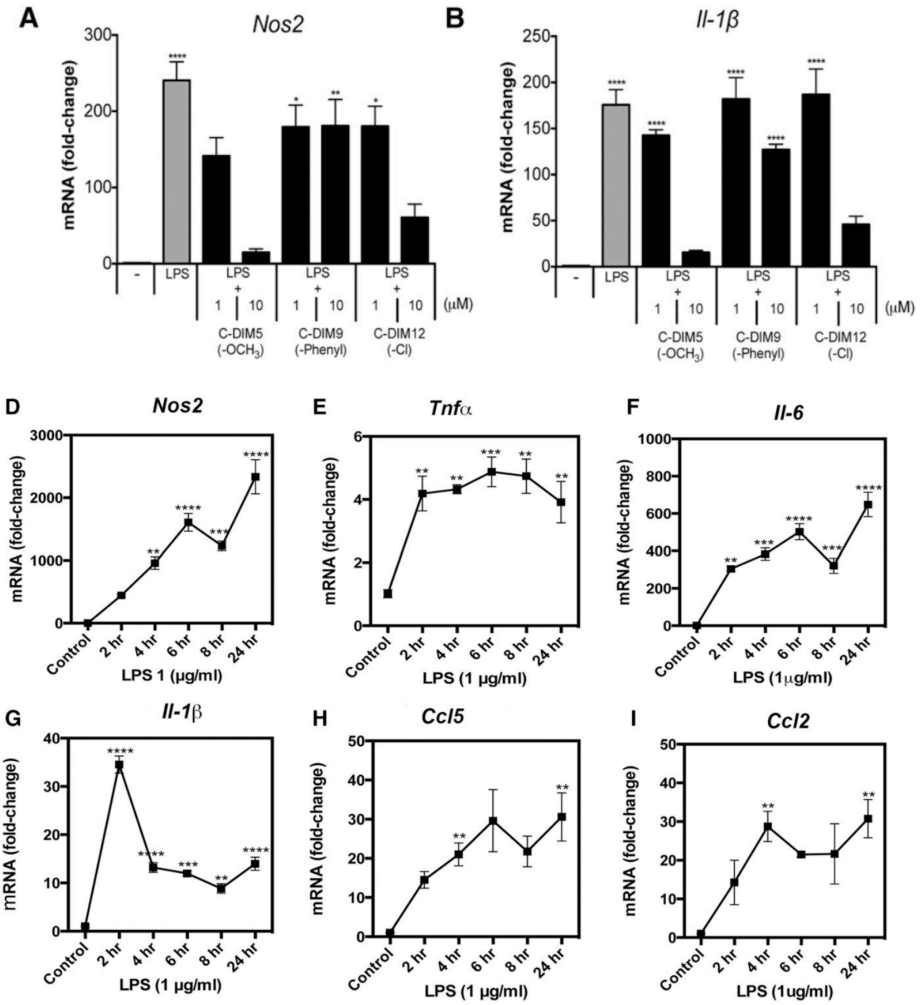

Figure 4.7. **(A-B)** C-DIM suppression of inflammatory genes, *Nos2* and *Il1B,* in glia is structure dependent in primary murine mixed glial cultures treated with saline or 1 μg/ml LPS and 1μM or 10μM of C-DIM5, C-DIM9, or C-DIM12 for 8 hours. **(D–I)** BV-2 microglia were treated with saline or 1μg /ml LPS over a 24-hour time point, and RNA was collected for real-time PCR analysis of cytokine mRNA expression. Statistical significance is expressed as mean compared with saline control. (De Miranda et al., 2015)

To determine the most anti-inflammatory concentration of C-DIM12 in BV2 microglial cells, qRTPCR analysis showed C-DIM12 dose-dependently decreased LPS-induced neuroinflammatory gene expression after 24hrs, demonstrating 10μM to be an efficacious concentration (Figure 4.8).

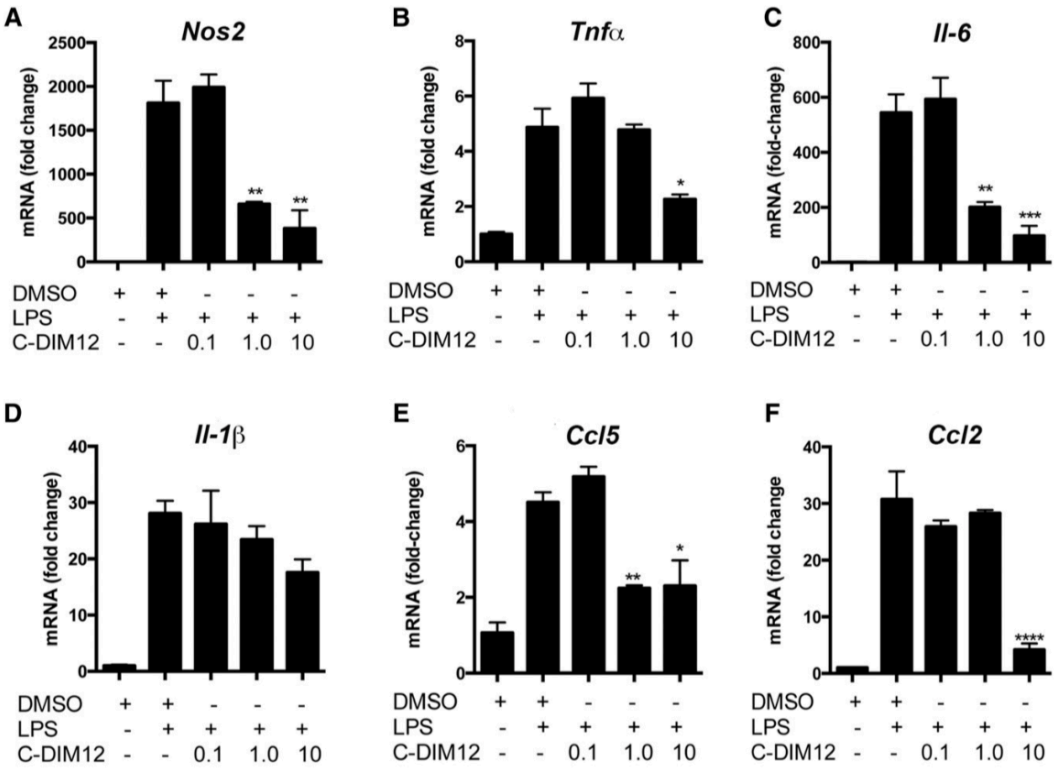

Figure 4.8. Dose-dependent suppression of inflammatory genes in BV-2 microglia **(A–F)** BV-2 microglia were pretreated for 1 hour with 0.1, 1.0, or 10μM C-DIM12 followed by 24 hours of LPS (1μg/ml). (De Miranda et al., 2015)

Altogether, we showed that C-DIM12 decreased LPS-induced NF-κB expression (data not shown) and NF-kB-regulated, neuroinflammatory gene expression in a BV2 microglial cell line. To identify how C-DIM12 does this, and based off of previous studies in cancer cells, we interrogated the involvement of Nurr1, which is known to function as a constitutive inhibitor of NF-κB activation in several cell types (Beard et al., 2015; Bonta et al., 2006; Saijo et al., 2009b). To do so, we knocked down (KD) *Nurr1* in BV2 cells, without any effects on the other NR4A

receptors or corepressors. KD of *Nurr1* inhibited the suppressive effects of C-DIM12 on expression of inflammatory genes in LPS-treated BV2 cells (Figure 4.9).

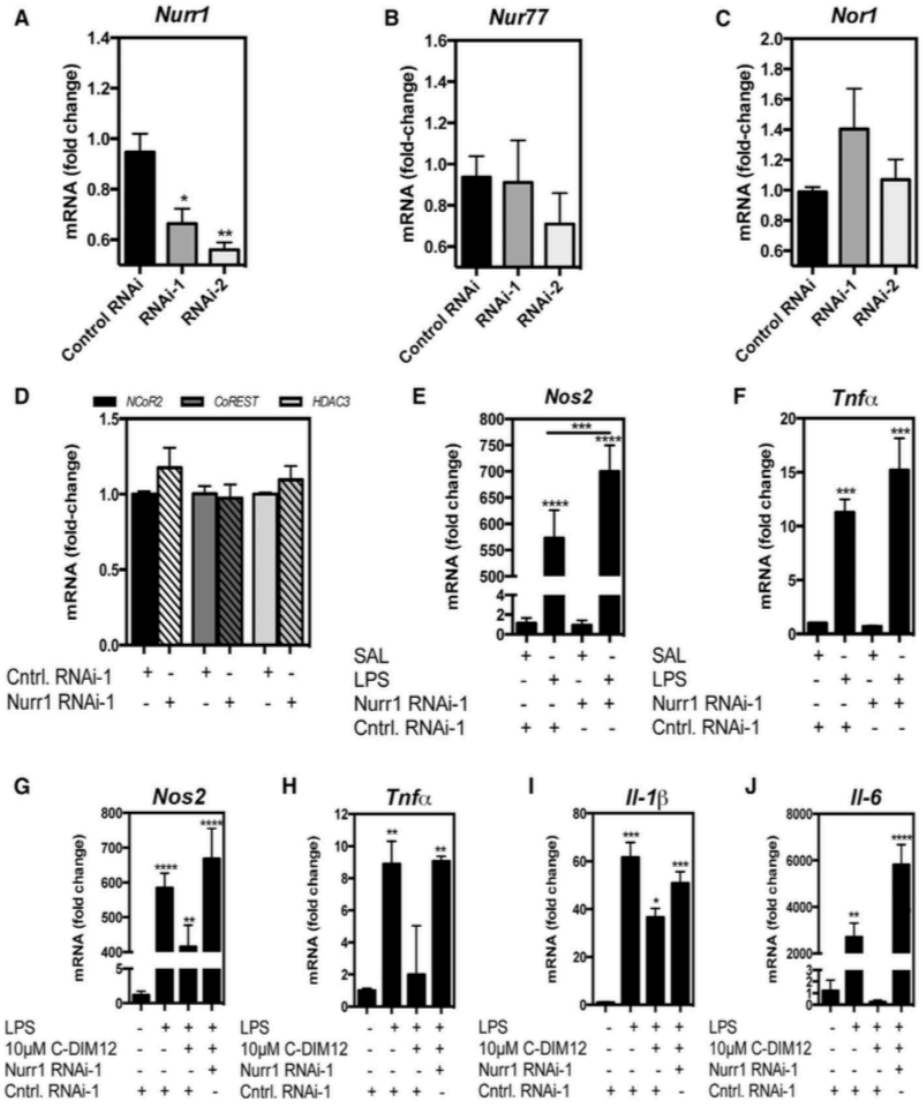

Figure 4.9. C-DIM12–dependent inhibition of inflammatory gene expression requires Nurr1. **(A-C)** BV-2 microglia were transfected with two different sequences of siRNA (denoted RNAi-1, RNAi-2) or scrambled RNAi (control RNAi). (D) *NCor2, CoRest, Hdac3* mRNA were unaffected by Nurr1 KD. **(E-F)** Following Nurr1 KD, BV-2 microglia were treated with saline or 1μg/ml LPS for 24 hours and assessed for mRNA expression of *Nos2* and *Tnfα*. **(G-J)** Following Nurr1 KD, BV-2 cells were treated with 10μM C-DIM12 (1 hour pretreatment) and 1μg/ml LPS treatment and assessed for mRNA expression of *Nos2, Tnfα, Il1β, and Il6*. Statistical significance compared to saline control (*) (De Miranda et al., 2015).

Using immunofluorescence microscopy, we demonstrated that C-DIM12 did not inhibit NF-κB translocation from the cytoplasm to the nucleus following LPS treatment (Figure 4.10). Because previous studies demonstrated that GSK3β is necessary for the phosphorylation of p65 and recruitment of Nurr1 to bind p65 (Saijo et al., 2009a), we treated BV2 cells with a GSK3β inhibitor, SB216763, and determined the effect on C-DIM12-dependent inhibition of inflammatory gene expression. Treatment with SB216763 caused a decrease in phosphorylated p65, as determined by western blot, that was associated with increased inflammatory gene expression following treatment with LPS compared to cells treated only with vehicle (DMSO). In the presence of SB216763, C-DIM12 was unable to block LPS-induced expression of neuroinflammatory genes in BV-2 cells, indicating that GSK3β-dependent phosphorylation of p65 is required for binding of Nurr1 to p65 following activation by C-DIM12.

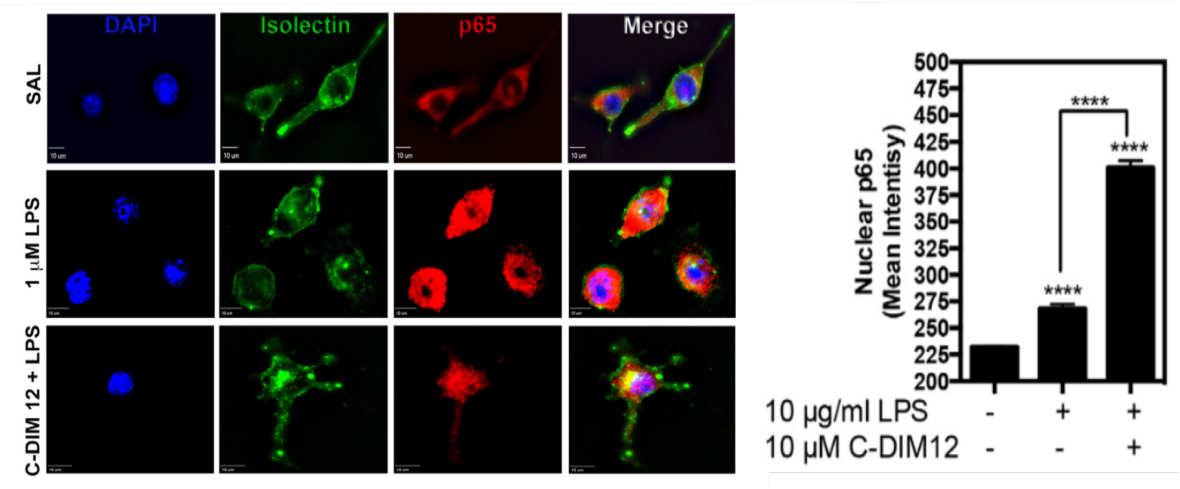

Figure 4.10. C-DIM12 does not prevent p65 translocation. **(A)** BV-2 cells were treated with 10μM C-DIM12 for 1 hour followed by saline or 1μg/ml LPS for 30 minutes and fixed for immunofluorescence to examine p65 translocation with DAPI (blue), isolectin (green), p65 (red). **(B)** p65 nuclear expression was quantified by mean fluorescence intensity encompassing the nuclei (DAPI boundary; background subtracted). (De Miranda et al., 2015)

Nurr1 can move between the nucleus and cytoplasm during inflammatory stimuli to regulate gene expression. We therefore examined the expression and subcellular localization of Nurr1 in primary microglia during treatment with LPS and C-DIM12 via immunofluorescence (IF) analysis. Primary microglia showed an increase in nuclear Nurr1 due to LPS treatment, which was further increased by co-treatment with C-DIM12. This was further supported by RT-qPCR showing increased *Nurr1* mRNA in cells treated with LPS and with LPS+C-DIM12. The same RNA used to assess *Nurr1* mRNA was also examined for expression of *Nos2* and *Il6* following LPS treatment, which indicated decreased expression of these genes in the LPS+C-DIM12 treatment group (Figure 4.11; unpublished representative images).

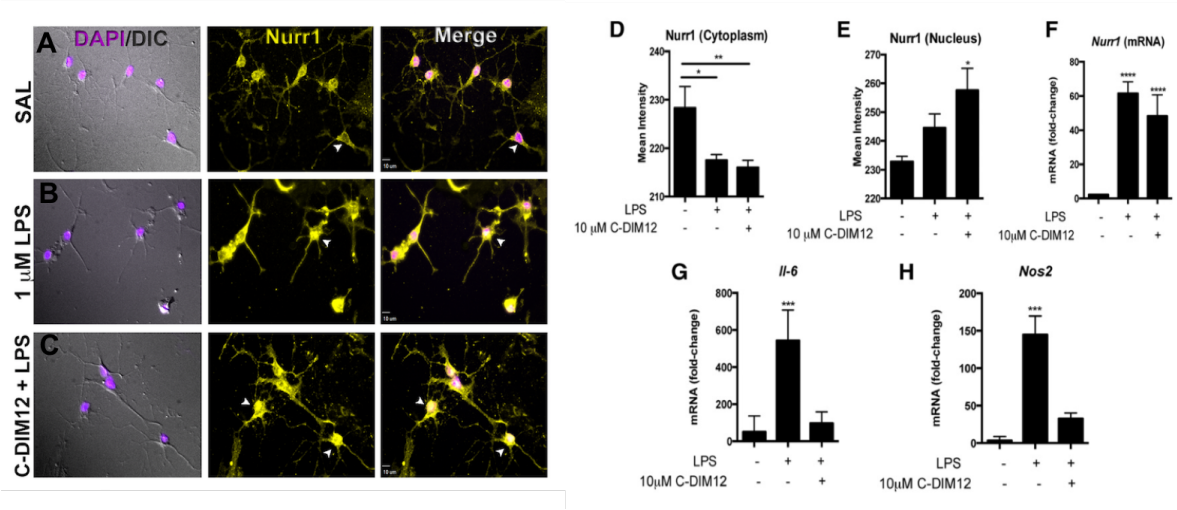

Figure 4.11. Nurr1 translocation and expression following LPS and C-DIM12 treatment. **(A–C)** Representative images of primary mouse microglia treated with 10μM C-DIM12 for 1 hour followed by 1μg/ml LPS for 24 hours. Cells were fixed and imaged for immunofluorescence of Nurr1 (red), CD11b (green) and DAPI (blue). **(D-E)** Quantification of Nurr1 protein translocation from the cytoplasm to the nucleus. **(F)** *Nurr1* mRNA levels in BV-2 microglia treated with 1μg/ml LPS, or 1μg/ml LPS + 10μM C-DIM12 for 24 hours. **(G-H)** *Il6* and *Nos2* mRNA levels from the same samples corresponding to *Nurr1* mRNA (De Miranda et al., 2015).

Given the data demonstrating that the mechanism of inhibition of p65 by C-DIM12 likely occurred in the nucleus, we used chromatin immunoprecipitation (ChIP) analysis to identify patterns of transcription factor binding to the proximal NF-kB binding site in the Nos2 promoter during treatment with LPS in the presence and absence of C-DIM12. Treatment with LPS over a period of 24 hrs caused an increase in binding of p65 to the proximal NF-kB binding site in the Nos2 promoter, as well as decreased binding of Nurr1 and the nuclear co-repressor proteins, NCoR2 and CoREST. C-DIM12 changed the patterns of transcription factor binding, causing an increase in the association of Nurr1 to the p65 binding, with a comcomitant loss of p65 binding and an increase in binding of NCoR2 and CoREST. These changes in association with DNA *cis* elements occurred in the absence of an change in the overall protein expression p65, Nurr1, NCoR2, CoREST and HDAC3 between the LPS and LPS+C-DIM12 treatment groups. This was consistent with the constant patterns of p65 and Nurr1 expression by IF and mRNA analyses, respectively (Figure 4.12).

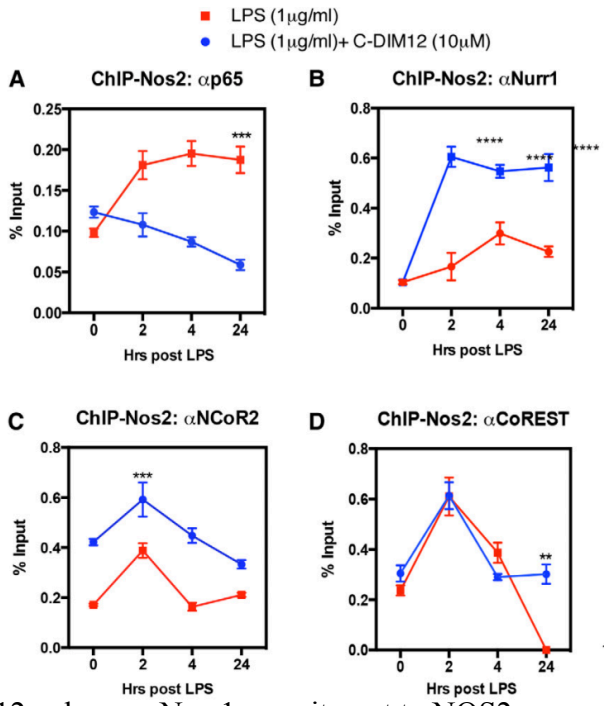

Figure 4.12. C-DIM12 enhances Nurr1 recruitment to NOS2 promoter, decreases p65 binding, and stabilizes binding of nuclear corepressors. BV-2 cells were treated with 10μM C-DIM12 for 1 hour followed by 1μg/ml LPS over a 24-hour time point and assessed at the *Nos2* promoter using ChIP. **(A)** The amount of p65 bound to the *Nos2* promoter was measured in LPS or LPS + C-DIM treatments. **(B)** The level of Nurr1 bound to the *Nos2* promoter with or without C-DIM12 over a 24-hour time course with LPS. **(C-D)** ChIP assessment of nuclear corepressor NCOR2 and corepressor complex CoREST bound to the *Nos2* promoter (De Miranda et al., 2015).

Pharmacodynamic efficacy of C-DIM12 in an *in vivo* model of Parkinson's disease.

We previously demonstrated that NR4A1/Nur77 or NR4A2/Nurr1 activating C-DIM compounds are neuroprotective against MPTP *in vivo*, based on an oral dose of 50mg/kg (De Miranda et al., 2013; De Miranda et al., 2015b). To ascertain whether a lower dose would be as efficacious, we conducted a pharmacokinetic study with C-DIM12 at 25 mg/kg over a time course of 24hrs. Plasma and midbrain samples were collected and analyzed by LC-MS for levels of C-DIM12 similar to previously published studies from our laboratory (De Miranda et al., 2013). These analyses demonstrated that C-DIM12 reached peak concentration at 4hrs in both plasma and brain, while half-life in the brain was about 15 minutes longer in brain tissue compared to plasma (Hammond et al., 2018).

Once it was determined that a single oral dose of 25 mg/Kg resulted in significant levels of C-DIM12 in plasma and brain, we determined the neuroprotective efficacy against loss of dopaminergic neurons induced by sub-acute treatment with MPTP and probenecid (MPTPp) over 14 days. C-DIM12 showed neuroprotective effects as demonstrated by preservation of TH+ (dopamine neurons) and MAP2+ (total neuron) cell counts, which were effectively depleted from MPTPp14d exposures alone (data not shown; see (Hammond et al., 2018).

Glial activation in PD is known to occur (Liddelow et al., 2017; Zhang et al., 2005), so we therefore assessed microglial and astrocyte activation by quantifying IBA-1 and GFAP positive cells, respectively, in both the SN and ST. MPTPp resulted in a significant increase in IBA-1 and GFAP positive cells and MPTPp+C-DIM12 decreased significantly decreased those numbers. Also, microglial activation was assessed based off of skeletonized analysis of phenotypic change in morphology from M2 anti-inflammatory phenotype to an inflammatory M1 phenotype in which the number of branched cytoplasmic processes decreases and activated microglia adopt a more amoeboid/phagocytic-like morphology. MPTPp+C-DIM12 groups had decreased numbers of an "activated" phenotype compared to MPTPp, as determined by number of branches, number of junctions, branch length and number of branch endpoints per IBA-1 positive cell (data not shown).

Neuroinflammatory gene expression is mediated by NF-κB and is upregulated in PD post-mortem brain tissue, essential for glial signaling and altered by Nurr1 activation (Hirsch and Hunot, 2009; Kirkley et al., 2017; Smith et al., 2015). Therefore, two extensive qPCR array experiments were conducted to broadly assess gene expression in the SN associated with the NF-κB pathway and Parkinson's disease. Heat map analyses of 168 genes from both arrays showed that gene expression in the MPTPp+C-DIM12 group clustered most closely with the control

group and that patterns of gene expression in the MPTPp group statistically differed from either the control or MPTPp+C-DIM12 groups, thereby demonstrating that C-DIM12 affected NF-κB regulated genes more prominently than genes associated with PD, although statistical significance was limited (Figure 4.13). And since it's known that Nur77 and Nurr1 are closely regulated in models of inflammation (Bonta et al., 2006; Wei et al., 2016), we assessed mRNA expression of both receptors in SN tissue from the array studies. We showed that C-DIM12 significantly increased *Nurr1* and *Nur77* mRNA expression compared to decreased levels seen in MPTPp (Figure 4.14), also supported by protein data that showed C-DIM12 increased Nurr1 protein expression compared to the loss seen in the MPTPp group.

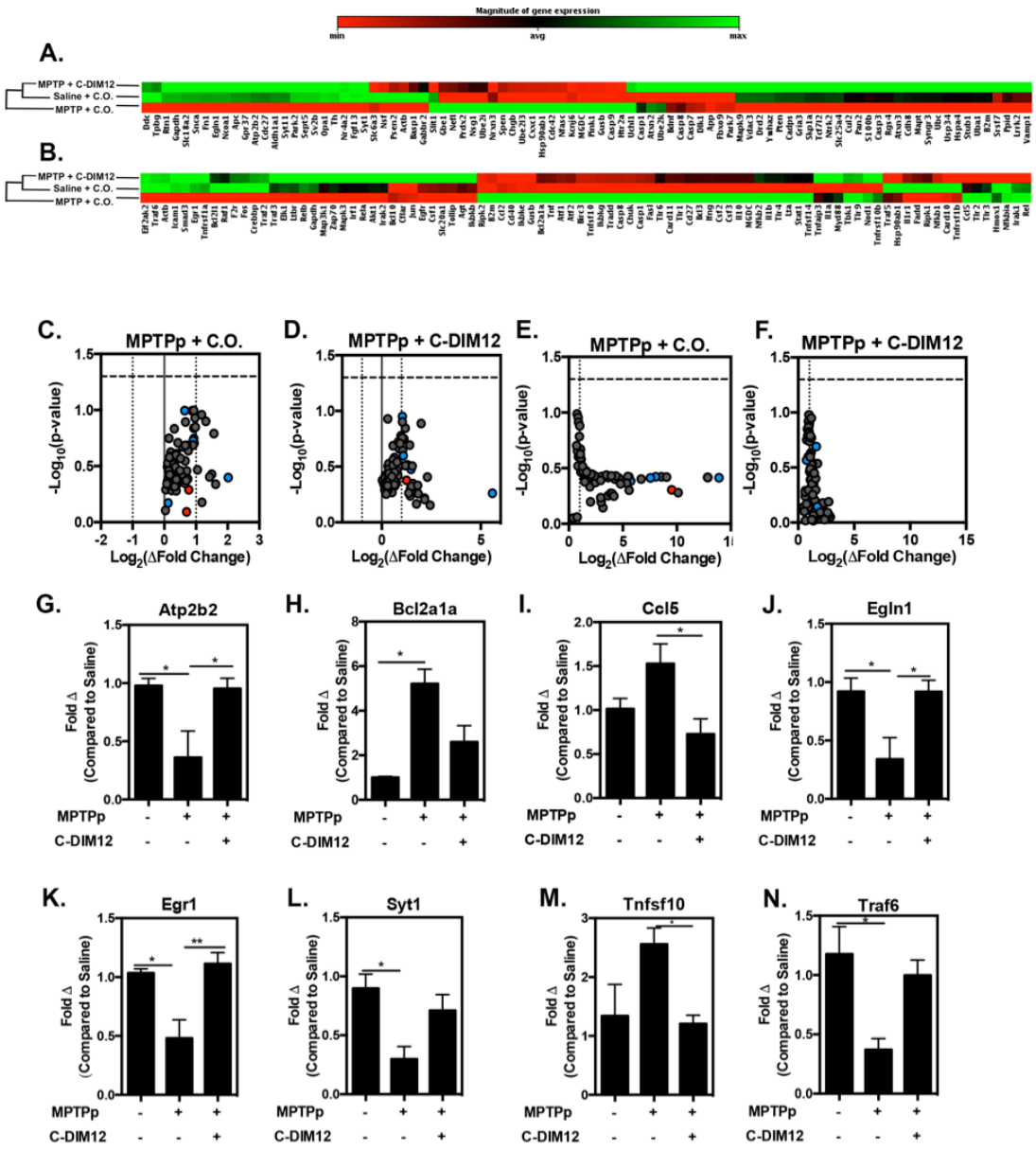

Figure 4.13. PD-associated and NF-κB-regulated gene expression is preserved in MPTPp+C-DIM12 SN. Ontology dendogram heat map of 84 **(A)** PD associated genes and **(B)** NF-κB-regulated genes from mouse SN depicts MPTP+C-DIM12 gene expression patterns to statistically cluster with saline gene expression patterns (red=increased gene expression, green=decreased gene expression). Volcano plots from **(C-D)** PD and **(E-F)** NF-κB arrays show statistically significant fold-change difference from control in MPTP and MPTP+C-DIM12 groups (red=minimum expression; green=maximum expression). Graphs of **(G-R)** individual genes extrapolated from arrays, which depict significant fold-change differences (Hammond et al., 2018).

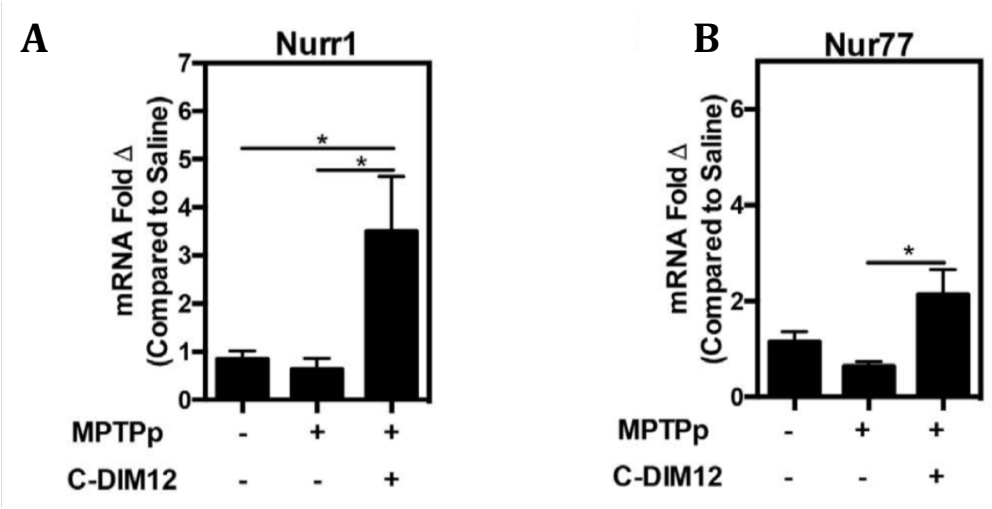

Figure 4.14. NR4A expression is increased by C-DIM12. Quantitative RT PCR data of mRNA isolated from MPTP+C-DIM12 SN tissue depicts higher expression of **(A)** *Nurr1* than **(B)** *Nur77*, although both are statistically significant (Hammond et al., 2018).

Microglia exacerbate glial activation in an *in vitro* model of Mn toxicity.

Though the circumstances involved in neuronal loss as a result of manganese neurotoxicity are poorly understood, activated glia are largely implicated as the primary source of increased inflammatory gene expression and neuroinflammatory injury (Tjalkens et al., 2017; Zhao et al., 2009). In this study, we elucidated the mechanistic function of microglia and neuroinflammatory effects associated with manganese (Mn) toxicity (Kirkley et al., 2017).

Initially, we assessed the purity of microglia and astrocytes isolated from mixed glial cultures via a column-free immunopurification method by IF and flow cytometric analysis. Mixed cultures contained approximately 68% astrocytes, determined by number of GFAP+ astrocytes and morphology, and about 30% microglia. Purified cultures revealed to be either 97% pure microglia or 91% pure astrocytes (Figure 4.15).

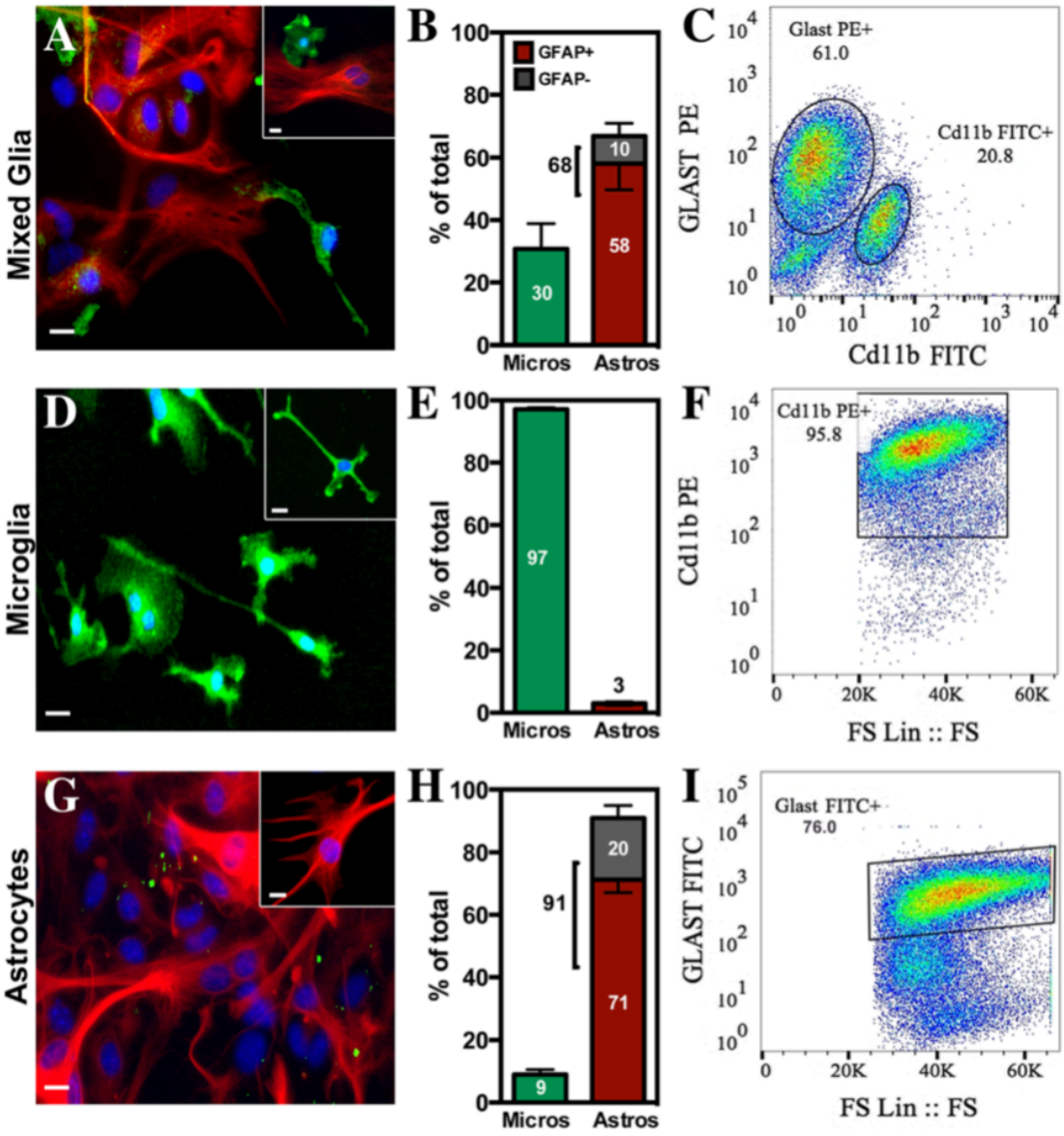

Figure 4.15. Column-free immunomagnetic separation generates highly pure cultures of microglia. **(A-C)** Mixed glia, **(D-F)** microglial, and **(G-I)** astrocyte cultures were assessed for total glial composition via immunofluorescence for GFAP-positive (red) and IBA-1-positive (green) cells or via flow cytometry for Cd11b and GLAST (Kirkley et al., 2017).

To determine dose-and time-dependent effects of Mn on inflammatory gene expression in purified microglia, we measured mRNA expression of *Nos2*, *Tnf*, *Il1β*, *Il6*, and *caspase 1*. Based on these results, the remaining experiments in microglia were conducted using 100μM Mn at a 24hr time point. We measured mRNA expression of inflammatory M1 genes (*cluster of differentiation (Cd) 86, Cd32,* and *Cd16)* and anti-inflammatory M2 genes (*brain-derived neurotrophic factor (Bdnf), insulin-like growth factor (Igf-1),* and *Cd206*) in Mn-treated microglia. We showed mixed response in that 100μM Mn up-regulated *Cd86* and *Igf-1* and down-regulated the remaining 4 genes. Additionally, quantitative image analysis of microglial morphology showed that Mn altered microglial phenotype from a resting state to an activated phenotype characterized by less branching, branch length, and branch endpoints (data not shown; see (Kirkley et al., 2017)).

Once microglia were treated with Mn, either the resultant conditioned media (MCM) containing residual/non-metabolized Mn and microglial factors was placed on purified astrocytes or a co-culture system of microglia seeded on top of astrocytes was established to assess the effects that microglial signaling from Mn exposure has on astrocyte response. Prior to that, the amount of Mn remaining in MCM media was assessed via microglia cell uptake via cellular fura-2 manganese extraction assay (CFMEA) or by measuring Mn levels in media, showing that microglia uptake 70% of Mn present in media leaving behind 30% in the medium (data not shown).

MCM and co-culture experiments showed that 100μM Mn alone only moderately induced inflammatory gene expression in pure astrocytes, but with either the presence of microglia (co-culture system) or with only 100μM Mn MCM (conditioned media experiments), inflammatory gene expression in astrocytes was significantly increased. Since MCM from

microglia treated with 100μM Mn would only contain ~30 μM Mn (due to microglial metabolism of 70% Mn), and astrocyte gene expression from direct treatment of 100μM Mn was so much less compared to MCM, we assessed what additional microglial inflammatory factors were released into the MCM. Multi- or single-plex chemiluminescent ELISA showed that the primary inflammatory proteins released by Mn-exposed microglia were IL-6, CCL2, and CCL5. Additionally, mixed glial cultures produced more TNF from Mn-treatment than pure microglia or pure astrocytes alone. Furthermore, via IF, we showed that Mn-treated microglia express more NOS2 than control (data not shown).

To assess the role that NF-κB plays in Mn-induced inflammatory gene expression in microglia, we treated microglia with the NF-κB inhibitor, Bay-11. The LPS-treated BV2 microglial cell line and 100μM Mn-treated primary microglia showed increased *Nos2* mRNA expression, however, Bay-11-treatment in both models significantly inhibited that increased expression. *Tnf* and *caspase 1* mRNA expression from Mn treatment in microglia was suppressed by Bay-11 treatment as well. Inflammatory cytokine production from Mn-treated microglia was significantly suppressed due to Bay-11 treatment, also. Inflammatory mRNA expression in astrocytes resultant from MCM treatment was moderately decreased from MCM (100μM Mn+Bay-11 treated microglia), and statistically significant for both *Tnf* and *Ccl5* compared to the DMSO (vehicle control for Bay-11) group, which did not suppress inflammatory gene expression.

TNF involvement in glial-glial signaling was more extensively assessed through knockdown (KD) experiments due to its increased mRNA and protein expression in both microglia and astrocytes as a result of either direct Mn treatment or MCM experiments. TNF KD in LPS-treated BV2s and Mn-treated microglia decreased *Tnf* mRNA expression in both, and

decreased TNF cytokine release in MCM. TNF KD minimally decreased cytokine production of IL-6, CCL2, and CCL5, while TNF KD in MCM experiments did significantly decrease inflammatory gene expression of *Tnf, Il1β,* and *Ccl2* in astrocytes (Figure 4.16).

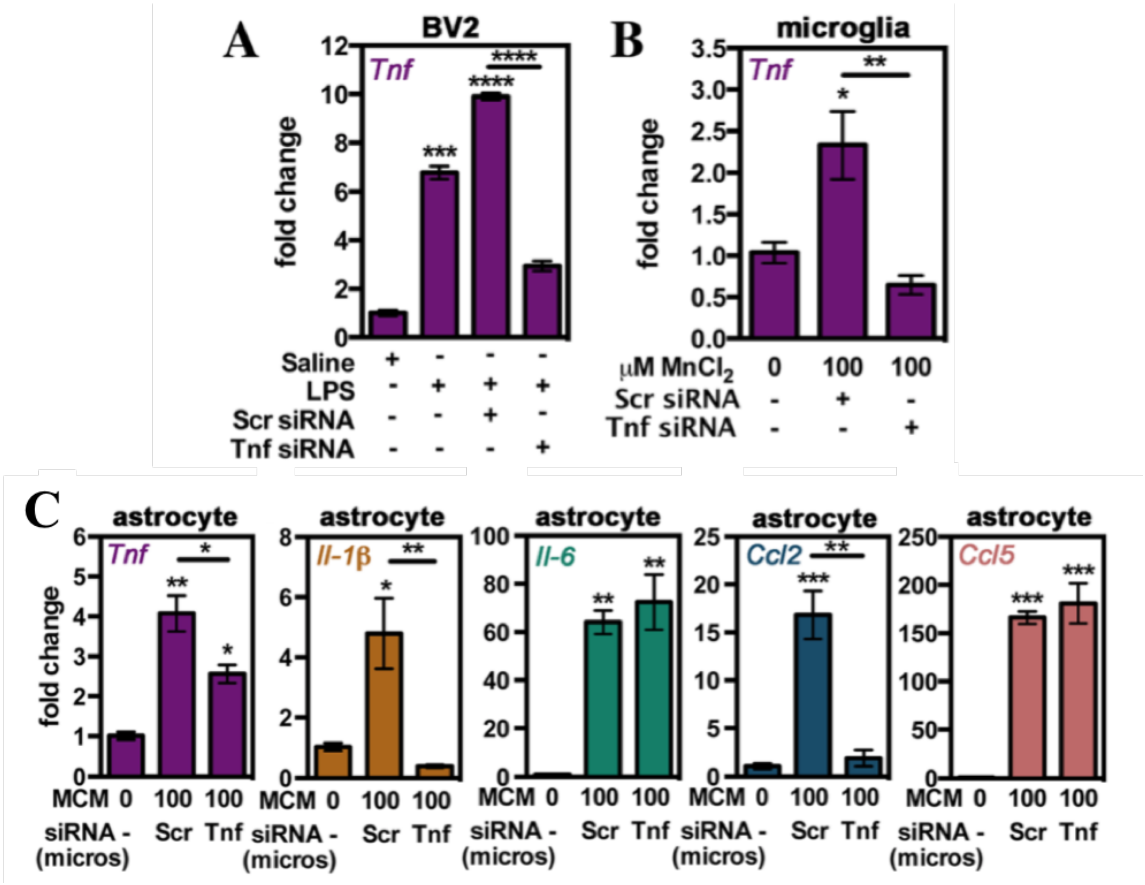

Figure 4.16. Release of TNF by Mn-activated microglia partly regulates inflammatory microglia-astrocyte crosstalk. Tnf knockdown in microglia was achieved through use of siRNA treatment 48 h prior to MCM experiments. Knockdown of Tnf was assessed in **(A)** BV2 microglial cells treated with lipopolysaccharide (1 μg/mL) for 24 h after Tnf KD. **(B)** Knockdown of Tnf in primary microglia treated with Mn via qPCR. **(C)** Levels of inflammatory gene expression in astrocytes treated with MCM of microglia transfected with Scr siRNA or Tnf siRNA were determined via qPCR for **(left to right)** *Tnf, Il-1β, Il-6, Ccl2, and Ccl5*. Expression data is represented by mRNA fold change ± SEM. Asterisks indicate significance. (Kirkley et al., 2017).

4.4 DISCUSSION

Glial activation is central to neuroinflammation and occurs early in the pathogenesis of neurodegenerative diseases such as PD and Mn neurotoxicity (Hirsch and Hunot, 2009; Wyss-Coray and Mucke, 2002). By being able to further elucidate glial-glial and glial-neuronal signaling mechanisms involved in models of neurotoxicity, we may be able to mitigate the damaging effects of glial activation and ultimately contribute to the development of disease-modifying treatment strategies in neurodegenerative disease. These studies from our laboratory showed that glial activation in models of inflammation could be halted by pharmacologic inhibition of NF-κB.

Chronic inflammation and glial activation has been consistently observed in PD models as well as postmortem brain tissue from PD patients (Tansey et al., 2007; Teismann and Schulz, 2004). Since these characteristics may provide a realistic target for slowing the progression of neuronal injury, this laboratory has explored nuclear orphan receptor ligands as candidates for halting inflammation. We have shown that C-DIM compounds can suppress manganese-induced NOS expression (Tjalkens et al., 2008), and in one such study we showed that C-DIM4 suppresses NF-κB-dependent expression of inducible NOS2 and NO production in astrocytes exposed to MPTP/cytokines through a mechanism, which inhibits p65/ NF-κB from binding the NOS2 promoter. This ultimately prevented NF-κB-dependent inflammatory gene activation, consistent with other studies, which implicate NF-κB involvement in glial activation (Pekny and Nilsson, 2005; Zhang et al., 2010). These findings were further explored and supported in our laboratory in PD *in vivo* models, which examined the efficacy of C-DIM compounds to reduce the loss of dopamine neurons and decrease associated inflammatory activation of astrocytes and microglia in the MPTPp model of PD.

Previous studies from our laboratory by De Miranda et al., demonstrated that MPTPp treatment caused progressive loss of dopaminergic neurons in the SN by IF and IHC staining of not just TH, but also total neuronal numbers (MAP2 stain), establishing a true loss of neurons and not just the phenotypic decrease in TH expression. This solidifies the characteristics necessary to establish neuroprotective efficacy in therapeutic studies such as this. Additionally, inflammatory gene activation in glia is attributed to neurodegeneration in neurotoxic models (Teismann and Schulz, 2004; Zhang et al., 2009; Zhang et al., 2005; Zhao et al., 2009); so we screened multiple C-DIM compounds in their ability to suppress LPS-induced inflammatory gene expression to further identify specific compounds worth pursuing in animal studies (De Miranda et al., 2015a). By doing this we found that C-DIM5 (see Chapter 2; Popichak et al., submitted 4-2-18), C-DIM8, and C-DIM12 optimally decreased inflammatory gene expression by inhibiting NF-κB activation, through NR4A-dependent mechanisms consistent with other research studies in cancer cells (Lee et al., 2014; Qin et al., 2004; Yoon et al., 2011).

The De Miranda et al study, which assessed neuroprotective efficacy by C-DIM5, C-DIM8, and C-DIM12, did so by showing that these compounds inhibited MPTPp-induced neuronal loss, decreased loss of dopamine terminal proteins, and prevented neuronal apoptosis and dysfunction. Furthermore, Nurr1 translocation and expression in TH+ neurons was increased due to these compounds, in support with other studies that show Nurr1 to be involved in neuronal regulation (Hammond et al., 2015; Kadkhodaei et al., 2013). More intriguingly, however, is that this study demonstrated a correlation with increased NF-κB-eGFP expression and recruitment of IBA-1+ microglia and GFAP+ astrocytes in an MPTPp model, all significantly decreased by these C-DIM compounds. This study began to elucidate the mechanism by which these compounds, specifically C-DIM12, inhibit NF-κB-mediated

inflammatory gene and eGFP expression, however, the glial-specific Nurr1 mechanism is further established in the De Miranda et al study from 2015.

The nuclear receptor Nurr1 is described as a potential therapeutic target for the mitigation of damaging effects due to glial activation, but compounds, up to this point, capable of inhibiting NF-κB-regulated neuroinflammation through Nurr1 activation have gone unidentified (Kim et al., 2015; Wang et al., 2015). The De Miranda et al 2015 study examined C-DIM12 for a number of reasons including its structurally dependent suppression of inflammatory gene expression in primary glia and its significant distribution to the brain after oral dosing (De Miranda et al., 2013), further supported by our laboratory (Hammond et al., 2018) and the *in vivo* PD study above, which demonstrated C-DIM12 attenuation of dopamine neuron loss and decreased glial activation and cytokine induction more significantly overall compared to other C-DIM compounds. Altogether, these data indicated that C-DIM12 suppresses NF-κB-induced gene expression in BV2 microglia cells through transcriptional repression by Nurr1, a mechanism established by a previous group (Saijo et al., 2009b). These data are similar to C-DIM12 studies in cancer cells, which have also elucidated a Nurr1-specific mechanism (Inamoto et al., 2008; Li et al., 2012).

Not surprisingly, C-DIM12 failed to inhibit p65 translocation from the cytoplasm to the nucleus, suggesting that its mechanism of NF-κB inhibition is nuclear, and thereby prevents transcriptional activation of NF-κB-regulated genes by a direct effect on transcriptional activity of nuclear proteins. Increased p65 expression from LPS+C-DIM12 treatment may be due to the increased recruitment of Nurr1 directly bound to p65. Furthermore, KD of Nurr1 resulted in loss of inflammatory gene suppression by C-DIM12 suggesting that Nurr1 is needed for the transrepressive activity of C-DIM12 to occur. ChIP assays also revealed that LPS+C-DIM12

decreased the amount of p65 protein and increased Nurr1 and corepressor proteins bound to the NOS2 promoter, without drastically effecting overall protein expression. Altogether, this suggests that C-DIM12 enhances Nurr1-mediated recruitment of corepressors that facilitate trans repression of inflammatory genes in BV2 microglial cells.

These studies not only highlight the importance of glial activation in a PD model and in LPS-induced activation of microglia but also demonstrate that the anti-inflammatory effects of C-DIM12 occur through a Nurr1-specific mechanism. Another study from our laboratory pursued a more extensive examination of the efficacy of C-DIM12 at a less concentrated dose (25mg/kg versus 50mg/kg) of oral administration in an MPTPp mouse model (Hammond et al., 2018), demonstrating a dose-dependent increase in brain levels, further confirming the effectiveness of this analog (De Miranda et al., 2013).

This study also demonstrated that C-DIM12 was neuroprotective in an MPTPp model by diminishing the number of total neurons (MAP2+) and dopaminergic neurons (TH+) lost in the SN. Consistent with the former C-DIM12 animal study, more extensive behavioral analyses showed that C-DIM12 decreased MPTPp-induced cognitive and locomotor dysfunction. C-DIM12 also preserved protein expression of TH, and the dopamine transporter proteins, DAT and VMAT2.

Glial activation contributes to neurodegeneration as a result of MPTP exposure (Sugama et al., 2003) by exacerbation of neuronal loss (Sriram et al., 2006). In support with those studies, we showed that C-DIM12 significantly reduced microglial (IBA-1+) and astroglial (GFAP+) numbers in association with C-DIM12 preservation of DA neuronal loss. Furthermore, C-DIM12 conserved ramified/resting microglial morphology, overall demonstrating that C-DIM12 modulates both glial cell types in a neurotoxic model of neuroinflammation. In conjunction with

this, we also demonstrated that C-DIM12 global gene expression patterns statistically cluster with control gene patterns in NF-κB and PD qRT arrays, further suggesting that C-DIM12-Nurr1 transcriptional activation might modulate glial-glial and glial-neuronal signaling through NF-κB-dependent gene expression. Lastly, computational modeling and transactivation studies showed the that increased theoretical probability that C-DIM12 binds the coactivator site of Nurr1 is feasible, and likely results in modulation of transcriptional activity, as discussed in the previous De Miranda et al studies.

Taken together, these last three studies demonstrated that C-DIM12 crosses the blood brain barrier, suppresses glial activation, protects against DA neuronal cell body loss, preserves DA terminals, improves neurobehavioral function and decreases NF-κB regulated neuroinflammatory gene expression in the MPTPp mouse model of PD by modulating transcriptional activity of Nurr1. Given these findings, C-DIM12 is a functional Nurr1 ligand with distinct effects in neurons and glia that could represent a disease-modifying treatment strategy for PD.

Exposure of high levels of Mn can cause the Parkinson-like disorder, manganism. Research has only recently begun to identify glial involvement in Mn-associated glial activation and inflammation often associated with increased levels of inflammatory cytokines and mediators (Sidoryk-Wegrzynowicz and Aschner, 2013; Tjalkens et al., 2017). Understanding how these inflammatory factors are regulated in glial cells from Mn exposure is critical to elucidating mechanisms underlying glial-neuronal signaling associated with neurotoxicity further explored in Chapter 3 (Popichak et al., in progress) and the Kirkley et al., 2017 study. They emphasize neuroinflammatory signaling between microglia and astrocytes, as well as glial-neuronal signaling in neurotoxic models, alluded to in the previous C-DIM12 studies.

Additionally, studies assessing C-DIM12 efficacy in two models, an arthritic model assessing TNF-induced inflammation in primary synovial fibroblasts from murine joints (addressing reviewer comments), and another model evaluating LPS-induced activation in a RAW macrophage cell line simulating an increased systemic inflammatory response (to be submitted) have specifically shown that the Nurr1-dependent mechanism involved in NF-κB-associated inflammation of PD and LPS is translational.

We showed that Mn activated microglia by causing increased NF-κB-regulated inflammatory gene expression and increased levels of cytokines and chemokines including IL-6, TNF, CCL2, and CCL5, consistent with other studies which assessed microglial role in Mn toxicity (Filipov et al., 2005; Moreno et al., 2009), as well as changes in morphology indicating a transition to a mixed M1/M2 phenotype and a de-ramified morphology using methods consistent with those of Hammond et al. (2018). Also, conditioned media from Mn-exposed microglia (MCM) and exposure to Mn in the presence of co-cultured microglia increased astrocytic expression of *Tnf*, *Il-1β*, *Il-6*, *Ccl2*, and *Ccl5* mRNA determined by qPCR analyses, in support with one such study which demonstrates that microglial activation induces an inflammatory phenotype in astrocytes (Liddelow et al., 2017). Additionally, pharmacological inhibition with Bay 11-7082 of NF-κB in microglia abolished microglial-induced astrocyte activation, and siRNA knockdown of Tnf in microglia moderately decreased NF-κB-mediated inflammation in astrocytes, suggesting that Mn-induced NF-κB activation in microglia specifically plays an essential role in amplifying astrocyte activation. Future studies from this laboratory, currently in the writing process, will elucidate some of these unknown mechanisms. Our laboratory has developed and demonstrated that an astrocyte-specific NF-κB/IKKβ knockout mouse strain (discussed in Chapter 3; Popichak et al., in progress) is significantly neuroprotective in an MPTP

mouse PD model (Kirkley et al., in progress); illuminating the crucial role that astrocytes (and NF-κB in astrocytes) play in glial inflammation and neurodegeneration.

CHAPTER 5

DISCUSSION & FINAL CONCLUSIONS

The endpoint of neurodegenerative disorders such as Parkinson's disease (PD) is neuronal cell death and permanently decreased neurological function. By the time the symptoms of PD manifest, 60-80% of neurons are already lost. There are no treatments capable of halting neurodegeneration in PD and related disorders nor are there biomarkers that could enable earlier diagnosis prior to permanent loss of neurons. By being able to identify characteristics, such as glial activation, that act in advance of neuronal cell death, the opportunity for early diagnosis and the potential for new therapeutic targets arise. Research, including that discussed in Chapters 2-4, provides insight into mechanisms of glial activation in *in vitro* models of neurodegeneration based on the use of selectively neurotoxic agents such as MPTP (Chapter 2), manganese (Chapter3) and LPS (Chapter 4) toxicity, as well as in *in vivo* models of MPTP neurotoxicity (Chapter 4).

Glia release inflammatory factors as means of cellular communication and immune function, or neuroinflammation, which can contribute to neurodegeneration and additional activation of surrounding glia. The transcription factor, Nuclear Factor-kappa B (NF-κB), is activated in glia in response to neurotoxic exposures such as the PD-inducing drug MPTP, inflammatory cytokines, and manganese (Mn).

We first examined NF-κB-regulated inflammatory gene expression in mixed glia as a result of MPTP/TNF/IFN exposure, an established model from our laboratory, and then identified a unique mechanism of inflammatory gene inhibition in astrocytes by a novel

diindolylmethane compound (C-DIM5). We also demonstrated that selected transcription factors belonging to the Nuclear Receptor 4A family, including NR4A1/Nur77 and NR4A2/Nurr1, inhibit NF-κB in a number of inflammatory models. Computational molecular modeling showed that C-DIM5 binds both receptors, with a greater propensity toward Nur77. C-DIM5, in an MPTP/TNF/IFN *in vitro* model of primary mixed glia, suppressed NF-κB-regulated inflammatory gene expression, caused an increase in *Nur77* mRNA expression and protein production of both Nur77 and Nurr1. Especially interesting is the observed increase of nuclear Nurr1, persistent sequestration of nuclear Nur77 and failure to inhibit p65/ NF-κB translocation from the cytoplasm to the nucleus of MPTP/TNF/IFN-treated astrocytes; implicating a nuclear-specific mechanism of inhibition. More surprisingly, however, was the compensatory increase of each nuclear receptor upon knockdown (KD) of the other, and furthermore, increased inflammatory gene expression by C-DIM5 in Nur77 KD astrocytes. KD of Nurr1 removed inhibitory effects of C-DIM5, but KD of both receptors eliminated inhibitory effects of C-DIM5 altogether, suggesting compensatory regulation of Nur77 and Nurr1 as well as dual activation by C-DIM5. These data and others presented by our laboratory support further pursuit of C-DIM5 in animal studies. Compensatory NR4A regulation in primary astrocytes is a novel biological finding, which presents a new target for inflammatory modulation in models of neurotoxicity.

Understanding glial-glial and glial-neuronal communication signals in a model of Mn neurotoxicity is extensively evaluated in our laboratory. Relatively low levels of Mn increased expression of NF-κB-regulated genes in primary mixed glia, purified astrocytes and in purified microglia, however mixed glia demonstrated more inflammatory gene expression than either pure cell population suggesting that mixed glia release signals and inflammatory mediators which exacerbate inflammatory gene signaling. Conditioned media from all three cell

populations, after Mn exposure, once applied to neuronal cultures, caused decreased neuronal viability and increased apoptotic and cell death markers, however glia conditioned media was more potent compared to astrocyte conditioned media or microglia conditioned media, causing more neuronal cell death than either cell type alone. Intriguingly, pharmacologic inhibition of NF-κB in mixed glia and pure astrocytes effectively decreased inflammatory gene expression and demonstrated neuroprotection in conditioned media experiments with neurons. However, astrocyte-specific genetic inhibition of NF-κB (IKK) in mixed glial cultures (Figure 5.2) almost completely suppressed inflammatory gene expression and was largely neuroprotective in conditioned media experiments, not only emphasizing the capacity of NF-κB to cause glial activation, but further implicating astrocytes as the key mediators in glial-glial signaling and glial-neuronal signaling leading to neuronal cell death (Figure 5.1).

Earlier published studies from our laboratory established the model of MPTP/TNF/IFN exposure in primary astrocyte cultures and demonstrated that one C-DIM analog (C-DIM4), had activity towards the nuclear receptor, PPARγ, and also demonstrated anti-inflammatory activity in glial cells by inhibiting NF-κB (Carbone et al., 2009). These data provided the basis for studying other diindolylmethane compounds in models of neuroinflammation, including *in vivo* studies of MPTP neurotoxicity (De Miranda et al., 2015b; Hammond et al., 2018). These studies demonstrated increased glial recruitment and proliferation to sites of neurodegeneration as well as increased NF-κB-eGFP expression. Additionally, inflammatory gene expression from brain tissue was assessed utilizing individual and broad-scale qRT-PCR array studies, which showed that another diindolylmethane compound (C-DIM12) decreased NF-κB-regulated inflammatory gene expression similar to control levels and pattern of expression, similar to gene expression patterns in the C-DIM5 *in vitro* study. These data further demonstrated that C-DIM12 binds and

activates Nurr1 in glia, suggesting that this is the mechanism, which C-DIM12 inhibits NF-κB expression and decreases glial activation thereby inhibiting neurodegeneration. Furthermore, an *in vitro* LPS model in BV2 microglia (De Miranda et al., 2015a) confirmed the mechanism of action of C-DIM12 to be Nurr1-specific and directly inhibitory of NF-κB in a microglial cell line. Collectively, these data highlight glial-mediated inflammation as a result of NF-κB activation suggesting an innovative target of treatment, including activation of the nuclear receptor, Nurr1 by C-DIM12 activation (Figure 5.2).

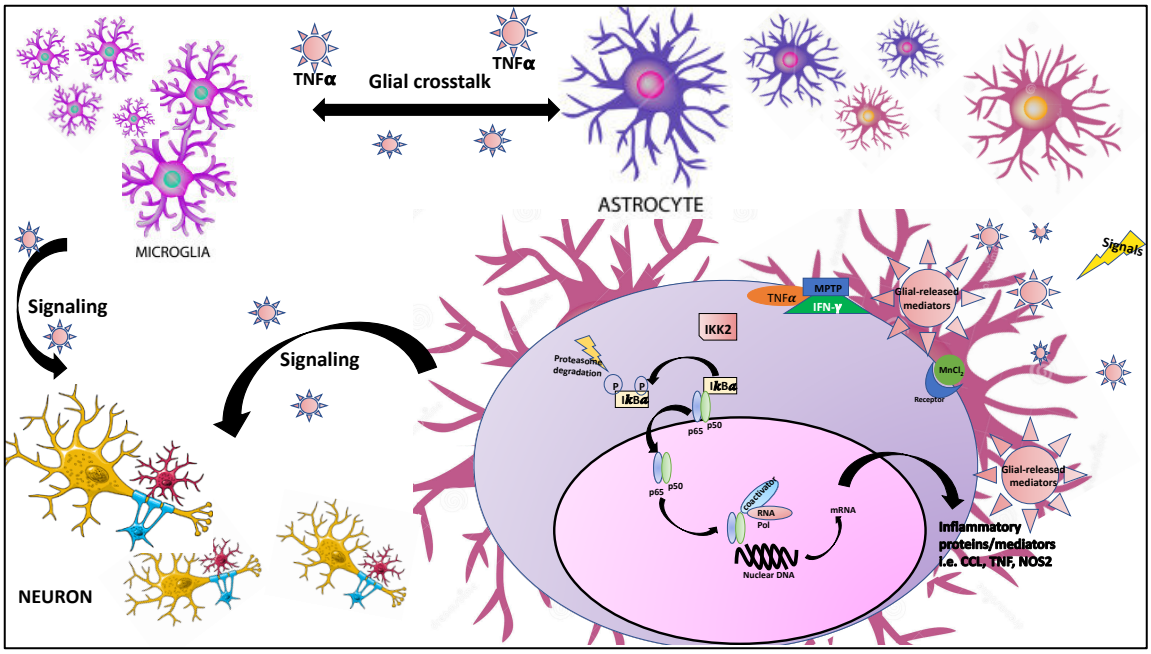

Figure 5.1. Schematic depicting glial-glial and glial-neuronal signaling following neurotoxin-dependent activation of NF-κB in astrocytes.

Another study demonstrated glial-glial communication but it was done so in an *in vitro* model of Mn exposure (Kirkley et al., 2017). This study demonstrated that microglial activation as a result of Mn treatment amplified the inflammatory response of astrocytes in conditioned medium and co-culture experiments by measuring NF-κB-regulated gene expression in both cell types. Furthermore, pharmacologic inhibition of NF-κB in microglia diminished inflammatory

response in both microglia as well as astrocytes in conditioned-media experiments, as did TNFα KD, not only emphasizing NF-κB activation as a large contributor to inflammatory gene expression in glia, but also underscoring the importance of microglial-glial communication in exacerbation of glial activation.

These data highlight the importance of glial-glial and glial-neuronal communication in models of neurotoxicity. In doing so, they shed light on key players involved in neuroinflammation including glial activation mediated by NF-κB as well as NR4A family members, Nur77 and Nurr1, and their potential as therapeutic targets to potentially inhibit inflammation (Figure 5.2).

Because glial responses to inflammatory-causing exposures can affect neuronal health and viability depending on the degree of glial activation and the severity of the toxic exposure, examining the pathways and signaling events regulating crosstalk between glia will be critical to develop more successful avenues in the treatment of neuroinflammation. We provided evidence that glial-glial crosstalk through NF-κB signaling plays an essential role in inflammatory responses to toxic exposures (Figure 5.1), however continued research exploring how glial communication affects neuronal injury in these models and others will help our understanding of how glial-glial interactions regulate neuroinflammatory mechanisms in Mn neurotoxicity and other neurotoxic insults.

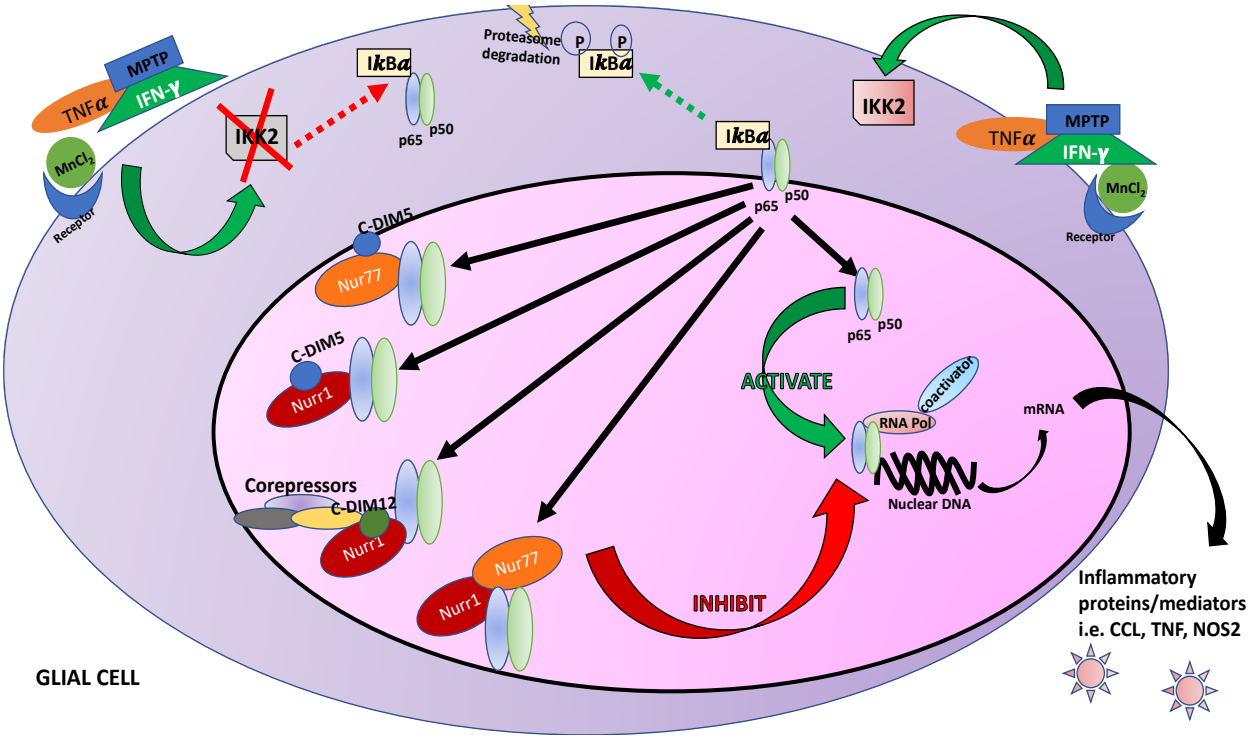

Figure 5.2. NF-κB is a proposed target of pharmacological and genetic inhibition in toxic models in glia. Hypothesized nuclear-specific mechanisms by which C-DIM5 and C-DIM12 activate Nur77/Nurr1 and Nurr1, respectively, to inhibit NF-κB from binding inflammatory gene promoters. Additionally, astrocyte-specific IKK2 KO prevents translocation and activation of NF-κB altogether. Furthermore, a proposed mechanism that Nurr1 and Nur77 dimerize prior to binding NF-κb is depicted.

REFERENCES

Aschner, J.L., and M. Aschner. 2005. Nutritional aspects of manganese homeostasis. *Mol Aspects Med*. 26:353-362.

Aschner, M. 2000. Manganese: brain transport and emerging research needs. *In* Environ Health Perspect. Vol. 108 Suppl 3. 429-432.

Aschner, M., and J.L. Aschner. 1991. Manganese neurotoxicity: cellular effects and blood-brain barrier transport. *Neurosci Biobehav Rev*. 15:333-340.

Aschner, M., K.M. Erikson, and D.C. Dorman. 2005. Manganese dosimetry: species differences and implications for neurotoxicity. *In* Crit. Rev. Toxicol. Vol. 35. 1-32.

Aschner, M., M. Gannon, and H.K. Kimelberg. 1992. Manganese uptake and efflux in cultured rat astrocytes. *J Neurochem*. 58:730-735.

Aschner, M., T.R. Guilarte, J.S. Schneider, and W. Zheng. 2007. Manganese: Recent advances in understanding its transport and neurotoxicity. *In* Toxicology and Applied Pharmacology. Vol. 221. 131-147.

Aschner, M., and H.K. Kimelberg. 1991. The use of astrocytes in culture as model systems for evaluating neurotoxic-induced-injury. *Neurotoxicology*. 12:505-517.

Baltazar, M.T., R.J. Dinis-Oliveira, M. de Lourdes Bastos, A.M. Tsatsakis, J.A. Duarte, and F. Carvalho. 2014. Pesticides exposure as etiological factors of Parkinson's disease and other neurodegenerative diseases—A mechanistic approach. *In* Toxicology Letters. Vol. 230. Elsevier Ireland Ltd. 85-103.

Barhoumi, R., J. Faske, X. Liu, and R.B. Tjalkens. 2004. Manganese potentiates lipopolysaccharide-induced expression of NOS2 in C6 glioma cells through mitochondrial-dependent activation of nuclear factor kappaB. *Brain Res Mol Brain Res*. 122:167-179.

Beard, J.A., A. Tenga, and T. Chen. 2015. The interplay of NR4A receptors and the oncogene-tumor suppressor networks in cancer. *Cell Signal*. 27:257-266.

Bechade, C., S. Colasse, M.A. Diana, M. Rouault, and A. Bessis. 2014. NOS2 expression is restricted to neurons in the healthy brain but is triggered in microglia upon inflammation. *Glia*. 62:956-963.

Billingsley, K.J., S. Bandres-Ciga, S. Saez-Atienzar, and A.B. Singleton. 2018. Genetic risk factors in Parkinson's disease. Cell and Tissue Research. 1-12.

Bjørklund, G., M.S. Chartrand, and J. Aaseth. 2017. Manganese exposure and neurotoxic effects in children. *In* Environmental Research. Vol. 155. 380-384.

Block, M.L., and L. Calderon-Garciduenas. 2009. Air pollution: mechanisms of neuroinflammation and CNS disease. *Trends Neurosci*. 32:506-516.

Block, M.L., and J.S. Hong. 2005. Microglia and inflammation-mediated neurodegeneration: multiple triggers with a common mechanism. *Prog Neurobiol*. 76:77-98.

Böhm, H.J. 1994. The development of a simple empirical scoring function to estimate the binding constant for a protein-ligand complex of known three-dimensional structure. *In* J. Comput. Aided Mol. Des. Vol. 8. 243-256.

Bonta, P.I., C.M. van Tiel, M. Vos, T.W.H. Pols, J.V. van Thienen, V. Ferreira, E.K. Arkenbout, J. Seppen, C.A. Spek, T. van der Poll, H. Pannekoek, and C.J.M. de Vries. 2006. Nuclear receptors Nur77, Nurr1, and NOR-1 expressed in atherosclerotic lesion macrophages

reduce lipid loading and inflammatory responses. *In* Arterioscler. Thromb. Vasc. Biol. Vol. 26. 2288-2294.

Bowler, R.M., W. Koller, and P.E. Schulz. 2006. Parkinsonism due to manganism in a welder: Neurological and neuropsychological sequelae. *In* Neurotoxicology. Vol. 27. 327-332.

Brooks, B.R., I. Brooks, C L, J. Mackerell, A D, L. Nilsson, R.J. Petrella, B. Roux, Y. Won, G. Archontis, C. Bartels, S. Boresch, A. Caflisch, L. Caves, Q. Cui, A.R. Dinner, M. Feig, S. Fischer, J. Gao, M. Hodoscek, W. Im, K. Kuczera, T. Lazaridis, J. Ma, V. Ovchinnikov, E. Paci, R.W. Pastor, C.B. Post, J.Z. Pu, M. Schaefer, B. Tidor, R.M. Venable, H.L. Woodcock, X. Wu, W. Yang, D.M. York, and M. Karplus. 2009. CHARMM: The biomolecular simulation program. *In* J. Comput. Chem. Vol. 30. 1545-1614.

Carbone, D.L., J.A. Moreno, and R.B. Tjalkens. 2008. Nuclear factor kappa-B mediates selective induction of neuronal nitric oxide synthase in astrocytes during low-level inflammatory stimulation with MPTP. *In* Brain Research. Vol. 1217. 1-9.

Carbone, D.L., K.A. Popichak, J.A. Moreno, S. Safe, and R.B. Tjalkens. 2009. Suppression of 1-methyl-4-phenyl-1,2,3,6-tetrahydropyridine-induced nitric-oxide synthase 2 expression in astrocytes by a novel diindolylmethane analog protects striatal neurons against apoptosis. *Mol Pharmacol*. 75:35-43.

Carmignoto, G., and M. Gomez-Gonzalo. 2010. The contribution of astrocyte signalling to neurovascular coupling. *Brain Res Rev*. 63:138-148.

Chang, J.Y., and L.Z. Liu. 1999. Manganese potentiates nitric oxide production by microglia. *Brain Res Mol Brain Res*. 68:22-28.

Chao, C.C., S. Hu, T.W. Molitor, E.G. Shaskan, and P.K. Peterson. 1992. Activated microglia mediate neuronal cell injury via a nitric oxide mechanism. *J Immunol*. 149:2736-2741.

Chen, C.J., Y.C. Ou, S.Y. Lin, S.L. Liao, S.Y. Chen, and J.H. Chen. 2006. Manganese modulates pro-inflammatory gene expression in activated glia. *Neurochem Int*. 49:62-71.

Chen, Y., Y. Jin, H. Zhan, J. Chen, Y. Chen, H. Meng, J. Jin, L. Yu, X. Cao, and Y. Xu. 2017. Proteomic analysis of the effects of Nur77 on lipopolysaccharide-induced microglial activation. *Neurosci Lett*. 659:33-43.

Chintharlapalli, S., R. Burghardt, S. Papineni, S. Ramaiah, K. Yoon, and S. Safe. 2005. Activation of Nur77 by selected 1,1-Bis(3'-indolyl)-1-(p-substituted phenyl)methanes induces apoptosis through nuclear pathways. *J Biol Chem*. 280:24903-24914.

Cho, I.H., J. Hong, E.C. Suh, J.H. Kim, H. Lee, J.E. Lee, S. Lee, C.H. Kim, D.W. Kim, E.K. Jo, K.E. Lee, M. Karin, and S.J. Lee. 2008. Role of microglial IKKbeta in kainic acid-induced hippocampal neuronal cell death. *Brain*. 131:3019-3033.

Cho, S.D., S.O. Lee, S. Chintharlapalli, M. Abdelrahim, S. Khan, K. Yoon, A.M. Kamat, and S. Safe. 2010. Activation of nerve growth factor-induced B alpha by methylene-substituted diindolylmethanes in bladder cancer cells induces apoptosis and inhibits tumor growth. *Mol Pharmacol*. 77:396-404.

Cho, S.D., K. Yoon, S. Chintharlapalli, M. Abdelrahim, P. Lei, S. Hamilton, S. Khan, S.K. Ramaiah, and S. Safe. 2007. Nur77 agonists induce proapoptotic genes and responses in colon cancer cells through nuclear receptor-dependent and nuclear receptor-independent pathways. *Cancer Res*. 67:674-683.

Collipp, P.J., S.Y. Chen, and S. Maitinsky. 1983. Manganese in infant formulas and learning disability. *Ann Nutr Metab*. 27:488-494.

Couper, J. On the effects of black oxide of manganese when inhaled into the lungs. *British Annals of Medicine, Pharmacy, Vital Statistics, and General Science*:41-42.

De Miranda, B.R., J.A. Miller, R.J. Hansen, P.J. Lunghofer, S. Safe, D.L. Gustafson, D. Colagiovanni, and R.B. Tjalkens. 2013. Neuroprotective efficacy and pharmacokinetic behavior of novel anti-inflammatory para-phenyl substituted diindolylmethanes in a mouse model of Parkinson's disease. *J Pharmacol Exp Ther*. 345:125-138.

De Miranda, B.R., K.A. Popichak, S.L. Hammond, B.A. Jorgensen, A.T. Phillips, S. Safe, and R.B. Tjalkens. 2015a. The Nurr1 Activator 1,1-Bis(3'-Indolyl)-1-(p-Chlorophenyl)Methane Blocks Inflammatory Gene Expression in BV-2 Microglial Cells by Inhibiting Nuclear Factor kappaB. *Mol Pharmacol*. 87:1021-1034.

De Miranda, B.R., K.A. Popichak, S.L. Hammond, J.A. Miller, S. Safe, and R.B. Tjalkens. 2015b. Novel para-phenyl substituted diindolylmethanes protect against MPTP neurotoxicity and suppress glial activation in a mouse model of Parkinson's disease. *Toxicol Sci*. 143:360-373.

Di Monte, D.A., M. Lavasani, and A.B. Manning-Bog. 2002. Environmental factors in Parkinson's disease. *In* Neurotoxicology. Vol. 23. 487-502.

Doetsch, F. 2003. The glial identity of neural stem cells. *Nat Neurosci*. 6:1127-1134.

Fang, S.C., A.J. Mehta, J.Q. Hang, E.A. Eisen, H.L. Dai, H.X. Zhang, L. Su, and D.C. Christiani. 2003. Cotton dust, endotoxin and cancer mortality among the Shanghai textile workers cohort: a 30-year analysis. *In* Occup Environ Med. Vol. 70. 722-729.

Feig, M., A. Onufriev, M.S. Lee, W. Im, D.A. Case, and C.L. Brooks. 2004. Performance comparison of generalized born and Poisson methods in the calculation of electrostatic solvation energies for protein structures. *In* J. Comput. Chem. Vol. 25. 265-284.

Ferreira, M., and J. Massano. 2016. An updated review of Parkinson's disease genetics and clinicopathological correlations. *In* Acta Neurol Scand. Vol. 135. 273-284.

Filipov, N.M., and C.A. Dodd. 2012. Role of glial cells in manganese neurotoxicity. *J Appl Toxicol*. 32:310-317.

Filipov, N.M., R.F. Seegal, and D.A. Lawrence. 2005. Manganese potentiates in vitro production of proinflammatory cytokines and nitric oxide by microglia through a nuclear factor kappa B-dependent mechanism. *Toxicol Sci*. 84:139-148.

Flaig, R., H. Greschik, C. Peluso-Iltis, and D. Moras. 2005. Structural Basis for the Cell-specific Activities of the NGFI-B and the Nurr1 Ligand-binding Domain. *In* Journal of Biological Chemistry. Vol. 280. 19250-19258.

Frakes, A.E., L. Ferraiuolo, A.M. Haidet-Phillips, L. Schmelzer, L. Braun, C.J. Miranda, K.J. Ladner, A.K. Bevan, K.D. Foust, J.P. Godbout, P.G. Popovich, D.C. Guttridge, and B.K. Kaspar. 2014. Microglia induce motor neuron death via the classical NF-kappaB pathway in amyotrophic lateral sclerosis. *Neuron*. 81:1009-1023.

Frank-Cannon, T.C., L.T. Alto, F.E. McAlpine, and M.G. Tansey. 2009. Does neuroinflammation fan the flame in neurodegenerative diseases? *Mol Neurodegener*. 4:47.

Gehrmann, J., Y. Matsumoto, and G.W. Kreutzberg. 1995. Microglia: intrinsic immuneffector cell of the brain. *Brain Res Brain Res Rev*. 20:269-287.

Gensel, J.C., K.A. Kigerl, S.S. Mandrekar-Colucci, A.D. Gaudet, and P.G. Popovich. 2012. Achieving CNS axon regeneration by manipulating convergent neuro-immune signaling. *Cell Tissue Res*. 349:201-213.

Giordano, G., D. Pizzurro, K. VanDeMark, M. Guizzetti, and L.G. Costa. 2009. Manganese inhibits the ability of astrocytes to promote neuronal differentiation. *Toxicol Appl Pharmacol*. 240:226-235.

Gonzalez-Scarano, F., and G. Baltuch. 1999. Microglia as mediators of inflammatory and degenerative diseases. *Annu Rev Neurosci*. 22:219-240.
Guilarte, T.R. 2010. Manganese and Parkinson's disease: a critical review and new findings. *Environ Health Perspect*. 118:1071-1080.
Halliwell, B. 2006. Oxidative stress and neurodegeneration: where are we now? *In* Journal of Neurochemistry. Vol. 97. 1634-1658.
Hammond, S.L., K.A. Popichak, X. Li, L.G. Hunt, E.H. Richman, P. Damale, E. Chong, D.S. Backos, S. Safe, and R.B. Tjalkens. 2018. The Nurr1 ligand,1,1-bis(3'-indolyl)-1-(p-chlorophenyl)methane, modulates glial reactivity and is neuroprotective in MPTP-induced parkinsonism. *In* Journal of Pharmacology and Experimental Therapeutics.
Hammond, S.L., S. Safe, and R.B. Tjalkens. 2015. A novel synthetic activator of Nurr1 induces dopaminergic gene expression and protects against 6-hydroxydopamine neurotoxicity in vitro. *In* Neuroscience Letters. Vol. 607. Elsevier Ireland Ltd. 83-89.
Harant, H., and I.J. Lindley. 2004. Negative cross-talk between the human orphan nuclear receptor Nur77/NAK-1/TR3 and nuclear factor-kappaB. *Nucleic Acids Res*. 32:5280-5290.
Harischandra, D.S., H. Jin, V. Anantharam, A. Kanthasamy, and A.G. Kanthasamy. 2015. alpha-Synuclein protects against manganese neurotoxic insult during the early stages of exposure in a dopaminergic cell model of Parkinson's disease. *Toxicol Sci*. 143:454-468.
Hirsch, E.C., T. Breidert, E. Rousselet, S. Hunot, A. Hartmann, and P.P. Michel. 2003. The role of glial reaction and inflammation in Parkinson's disease. *Ann N Y Acad Sci*. 991:214-228.
Hirsch, E.C., and S. Hunot. 2000. Nitric oxide, glial cells and neuronal degeneration in parkinsonism. *In* Trends Pharmacol. Sci. Vol. 21. 163-165.
Hirsch, E.C., and S. Hunot. 2009. Neuroinflammation in Parkinson's disease: a target for neuroprotection? *Lancet Neurol*. 8:382-397.
Hong, C.Y., J.H. Park, R.S. Ahn, S.Y. Im, H.S. Choi, J. Soh, S.H. Mellon, and K. Lee. 2004. Molecular mechanism of suppression of testicular steroidogenesis by proinflammatory cytokine tumor necrosis factor alpha. *Mol Cell Biol*. 24:2593-2604.
Hua, M.S., and C.C. Huang. 1991. Chronic occupational exposure to manganese and neurobehavioral function. *J Clin Exp Neuropsychol*. 13:495-507.
Inamoto, T., B.A. Czerniak, C.P. Dinney, and A.M. Kamat. 2010. Cytoplasmic mislocalization of the orphan nuclear receptor Nurr1 is a prognostic factor in bladder cancer. *Cancer*. 116:340-346.
Inamoto, T., S. Papineni, S. Chintharlapalli, S.D. Cho, S. Safe, and A.M. Kamat. 2008. 1,1-Bis(3'-indolyl)-1-(p-chlorophenyl)methane activates the orphan nuclear receptor Nurr1 and inhibits bladder cancer growth. *In* Molecular Cancer Therapeutics. Vol. 7. 3825-3833.
Jain, A.N. 1996. Scoring noncovalent protein-ligand interactions: a continuous differentiable function tuned to compute binding affinities. *In* J. Comput. Aided Mol. Des. Vol. 10. 427-440.
Jankovic, J. 2008. Parkinson's disease: clinical features and diagnosis. *J Neurol Neurosurg Psychiatry*. 79:368-376.
Kadkhodaei, B., A. Alvarsson, N. Schintu, D. Ramsköld, N. Volakakis, E. Joodmardi, T. Yoshitake, J. Kehr, M. Decressac, and A. Björklund. 2013. Transcription factor Nurr1

maintains fiber integrity and nuclear-encoded mitochondrial gene expression in dopamine neurons. *In* Proc Natl Acad Sci U S A. Vol. 110. National Acad Sciences. 2360-2365.
Kalia, L.V., and A.E. Lang. 2015. Parkinson's disease. *Lancet*. 386:896-912.
Karin, M. 1999. How NF-kappaB is activated: the role of the IkappaB kinase (IKK) complex. *Oncogene*. 18:6867-6874.
Karin, M. 2005. Inflammation-activated protein kinases as targets for drug development. *Proc Am Thorac Soc*. 2:386-390; discussion 394-385.
Karin, M., and Y. Ben-Neriah. 2000. Phosphorylation meets ubiquitination: the control of NF-[kappa]B activity. *In* Annu. Rev. Immunol. Vol. 18. 621-663.
Kim, C.-H., B.-S. Han, J. Moon, D.-J. Kim, J. Shin, S. Rajan, Q.T. Nguyen, M. Sohn, W.-G. Kim, M. Han, I. Jeong, K.-S. Kim, E.-H. Lee, Y. Tu, J.L. Naffin-Olivos, C.-H. Park, D. Ringe, H.S. Yoon, G.A. Petsko, and K.-S. Kim. 2015. Nuclear receptor Nurr1 agonists enhance its dual functions and improve behavioral deficits in an animal model of Parkinson's disease. *In* Proceedings of the National Academy of Sciences. Vol. 112. 8756-8761.
Kim, Y., B.N. Kim, Y.C. Hong, M.S. Shin, H.J. Yoo, J.W. Kim, S.Y. Bhang, and S.C. Cho. 2009. Co-exposure to environmental lead and manganese affects the intelligence of school-aged children. *Neurotoxicology*. 30:564-571.
Kim, Y.S., S.S. Kim, J.J. Cho, D.H. Choi, O. Hwang, D.H. Shin, H.S. Chun, M.F. Beal, and T.H. Joh. 2005. Matrix metalloproteinase-3: a novel signaling proteinase from apoptotic neuronal cells that activates microglia. *J Neurosci*. 25:3701-3711.
Kimelberg, H.K. 2004. The problem of astrocyte identity. *Neurochem Int*. 45:191-202.
Kirkley, K.S., K.A. Popichak, M.F. Afzali, M.E. Legare, and R.B. Tjalkens. 2017. Microglia amplify inflammatory activation of astrocytes in manganese neurotoxicity. *J Neuroinflammation*. 14:99.
Koska, J.r., V.Z. Spassov, A.J. Maynard, L. Yan, N. Austin, P.K. Flook, and C.M. Venkatachalam. 2008. Fully Automated Molecular Mechanics Based Induced Fit Protein−Ligand Docking Method. *In* J. Chem. Inf. Model. Vol. 48. 1965-1973.
Kurakula, K., D.S. Koenis, C.M. van Tiel, and C.J.M. de Vries. 2014. NR4A nuclear receptors are orphans but not lonesome. *In* BBA - Molecular Cell Research. Vol. 1843. Elsevier B.V. 2543-2555.
Lang, A.E., and A.M. Lozano. 1998a. Parkinson's disease. First of two parts. *In* N. Engl. J. Med. Vol. 339. 1044-1053.
Lang, A.E., and A.M. Lozano. 1998b. Parkinson's disease. Second of two parts. *In* N. Engl. J. Med. Vol. 339. 1130-1143.
Lange, J.H., I. Niehaus, and K.W. Thomulka. 2003. Is Endotoxin an Environmental Cause of Parkinson’s Disease? *In* Neuroepidemiology. Vol. 22. 313-313.
Lawson, L.J., V.H. Perry, P. Dri, and S. Gordon. 1990. Heterogeneity in the distribution and morphology of microglia in the normal adult mouse brain. *Neuroscience*. 39:151-170.
Lee, D.J., M.S. Hsu, M.M. Seldin, J.L. Arellano, and D.K. Binder. 2012. Decreased expression of the glial water channel aquaporin-4 in the intrahippocampal kainic acid model of epileptogenesis. *Exp Neurol*. 235:246-255.
Lee, S.-O., X. Li, E. Hedrick, U.-H. Jin, R.B. Tjalkens, D.S. Backos, L. Li, Y. Zhang, Q. Wu, and S. Safe. 2014. Diindolylmethane Analogs Bind NR4A1 and Are NR4A1 Antagonists in Colon Cancer Cells. *In* Molecular Endocrinology. Vol. 28. 1729-1739.

Lee, S.C., W. Liu, D.W. Dickson, C.F. Brosnan, and J.W. Berman. 1993. Cytokine production by human fetal microglia and astrocytes. Differential induction by lipopolysaccharide and IL-1 beta. *J Immunol*. 150:2659-2667.

Li, L., Y. Liu, H.Z. Chen, F.W. Li, J.F. Wu, H.K. Zhang, J.P. He, Y.Z. Xing, Y. Chen, W.J. Wang, X.Y. Tian, A.Z. Li, Q. Zhang, P.Q. Huang, J. Han, T. Lin, and Q. Wu. 2015a. Impeding the interaction between Nur77 and p38 reduces LPS-induced inflammation. *Nat Chem Biol*. 11:339-346.

Li, W., J. Liu, S.L. Hammond, R.B. Tjalkens, Z. Saifudeen, and Y. Feng. 2015b. Angiotensin II regulates brain (pro)renin receptor expression through activation of cAMP response element-binding protein. *In* Am J Physiol Regul Integr Comp Physiol. Vol. 309. R138-R147.

Li, X., S.-O. Lee, and S. Safe. 2012. Structure-dependent activation of NR4A2 (Nurr1) by 1,1-bis(3′-indolyl)-1-(aromatic)methane analogs in pancreatic cancer cells. *In* Biochemical Pharmacology. Vol. 83. 1445-1455.

Liddelow, S.A., K.A. Guttenplan, L.E. Clarke, F.C. Bennett, C.J. Bohlen, L. Schirmer, M.L. Bennett, A.E. Munch, W.S. Chung, T.C. Peterson, D.K. Wilton, A. Frouin, B.A. Napier, N. Panicker, M. Kumar, M.S. Buckwalter, D.H. Rowitch, V.L. Dawson, T.M. Dawson, B. Stevens, and B.A. Barres. 2017. Neurotoxic reactive astrocytes are induced by activated microglia. *Nature*. 541:481-487.

Lin, B., S.K. Kolluri, F. Lin, W. Liu, Y.H. Han, X. Cao, M.I. Dawson, J.C. Reed, and X.K. Zhang. 2004. Conversion of Bcl-2 from protector to killer by interaction with nuclear orphan receptor Nur77/TR3. *Cell*. 116:527-540.

Liu, B., H.M. Gao, and J.S. Hong. 2003. Parkinson's disease and exposure to infectious agents and pesticides and the occurrence of brain injuries: role of neuroinflammation. *Environ Health Perspect*. 111:1065-1073.

Liu, W., Y. Gao, and N. Chang. 2017. Nurr1 overexpression exerts neuroprotective and anti-inflammatory roles via down-regulating CCL2 expression in both in vivo and in vitro Parkinson's disease models. Elsevier Ltd. 1-8.

Liu, X., K.A. Sullivan, J.E. Madl, M. Legare, and R.B. Tjalkens. 2006. Manganese-induced neurotoxicity: the role of astroglial-derived nitric oxide in striatal interneuron degeneration. *Toxicol Sci*. 91:521-531.

Livak, K.J., and T.D. Schmittgen. 2001. Analysis of relative gene expression data using real-time quantitative PCR and the 2(-Delta Delta C(T)) Method. *Methods (San Diego, Calif.* 25:402-408.

Lozano, A.M., A.E. Lang, W.D. Hutchison, and J.O. Dostrovsky. 1998. New developments in understanding the etiology of Parkinson's disease and in its treatment. *In* Curr. Opin. Neurobiol. Vol. 8. 783-790.

Lu, C.S., C.C. Huang, N.S. Chu, and D.B. Calne. 1994. Levodopa failure in chronic manganism. *Neurology*. 44:1600-1602.

Lucchini, R.G., M. Aschner, Y. Kim, and M. Šarić. 2014. Chapter 45 – Manganese. *In* Handbook on the Toxicology of Metals. Elsevier. 975-1012.

McEvoy, C., M. de Gaetano, H.E. Giffney, B. Bahar, E.P. Cummins, E.P. Brennan, M. Barry, O. Belton, C.G. Godson, E.P. Murphy, and D. Crean. 2017. NR4A Receptors Differentially Regulate NF-kappaB Signaling in Myeloid Cells. *Front Immunol*. 8:7.

McMorrow, J.P., and E.P. Murphy. 2011. Inflammation: a role for NR4A orphan nuclear receptors? *In* Biochem. Soc. Trans. Vol. 39. 688-693.

Menezes-Filho, J.A., O. Novaes Cde, J.C. Moreira, P.N. Sarcinelli, and D. Mergler. 2011. Elevated manganese and cognitive performance in school-aged children and their mothers. *Environ Res*. 111:156-163.
Mistry, H.D., and P.J. Williams. 2011. The Importance of Antioxidant Micronutrients in Pregnancy. *In* Oxidative Medicine and Cellular Longevity. Vol. 2011. 1-12.
Morello, M., A. Canini, P. Mattioli, R.P. Sorge, A. Alimonti, B. Bocca, G. Forte, A. Martorana, G. Bernardi, and G. Sancesario. 2008. Sub-cellular localization of manganese in the basal ganglia of normal and manganese-treated rats An electron spectroscopy imaging and electron energy-loss spectroscopy study. *Neurotoxicology*. 29:60-72.
Moreno, J.A., K.M. Streifel, K.A. Sullivan, W.H. Hanneman, and R.B. Tjalkens. 2011. Manganese-induced NF-kappaB activation and nitrosative stress is decreased by estrogen in juvenile mice. *Toxicol Sci*. 122:121-133.
Moreno, J.A., K.M. Streifel, K.A. Sullivan, M.E. Legare, and R.B. Tjalkens. 2009. Developmental exposure to manganese increases adult susceptibility to inflammatory activation of glia and neuronal protein nitration. *Toxicol Sci*. 112:405-415.
Moreno, J.A., K.A. Sullivan, D.L. Carbone, W.H. Hanneman, and R.B. Tjalkens. 2008. Manganese potentiates nuclear factor-kappaB-dependent expression of nitric oxide synthase 2 in astrocytes by activating soluble guanylate cyclase and extracellular responsive kinase signaling pathways. *J Neurosci Res*. 86:2028-2038.
Mosley, R.L., E.J. Benner, I. Kadiu, M. Thomas, M.D. Boska, K. Hasan, C. Laurie, and H.E. Gendelman. 2006. Neuroinflammation, Oxidative Stress and the Pathogenesis of Parkinson's Disease. *Clin Neurosci Res*. 6:261-281.
Murphy, E.P., and D. Crean. 2015. Molecular Interactions between NR4A Orphan Nuclear Receptors and NF-kappaB Are Required for Appropriate Inflammatory Responses and Immune Cell Homeostasis. *Biomolecules*. 5:1302-1318.
Nagatsu, T., and M. Sawada. 2005. Inflammatory process in Parkinson's disease: role for cytokines. *Curr Pharm Des*. 11:999-1016.
Nakabayashi, K., S. Makino, S. Minagawa, A.C. Smith, J.S. Bamforth, P. Stanier, M. Preece, L. Parker-Katiraee, T. Paton, M. Oshimura, P. Mill, Y. Yoshikawa, C.C. Hui, D. Monk, G.E. Moore, and S.W. Scherer. 2004. Genomic imprinting of PPP1R9A encoding neurabin I in skeletal muscle and extra-embryonic tissues. *J Med Genet*. 41:601-608.
Nakajima, K., and S. Kohsaka. 1993. Functional roles of microglia in the brain. *Neurosci Res*. 17:187-203.
Nakanishi, H., H. Obaishi, A. Satoh, M. Wada, K. Mandai, K. Satoh, H. Nishioka, Y. Matsuura, A. Mizoguchi, and Y. Takai. 1997. Neurabin: a novel neural tissue-specific actin filament-binding protein involved in neurite formation. *J Cell Biol*. 139:951-961.
Neal, A.P.G., T. . 2012. Mechanisms of Heavy Metal Neurotoxicity: Lead and Manganese. *Drug Metab toxicol*. 5.
Neher, J.J., U. Neniskyte, J.W. Zhao, A. Bal-Price, A.M. Tolkovsky, and G.C. Brown. 2011. Inhibition of microglial phagocytosis is sufficient to prevent inflammatory neuronal death. *J Immunol*. 186:4973-4983.
O'Callaghan, J.P., and K. Sriram. 2005. Glial fibrillary acidic protein and related glial proteins as biomarkers of neurotoxicity. *Expert Opin Drug Saf*. 4:433-442.
Olanow, C.W. 2004. Manganese-induced parkinsonism and Parkinson's disease. *Ann N Y Acad Sci*. 1012:209-223.

Panneton, W.M., V.B. Kumar, Q. Gan, W.J. Burke, and J.E. Galvin. 2010. The neurotoxicity of DOPAL: behavioral and stereological evidence for its role in Parkinson disease pathogenesis. *PLoS One*. 5:e15251.
Park, E., and H.S. Chun. 2016. Melatonin Attenuates Manganese and Lipopolysaccharide-Induced Inflammatory Activation of BV2 Microglia. *Neurochem Res*.
Parkinson, J. 1817. An Essay on the Shaking Palsy. 66.
Parmalee, N.L., and M. Aschner. 2016. Manganese and aging. *In* Neurotoxicology. Vol. 56. Elsevier B.V. 262-268.
Parpura, V., M.T. Heneka, V. Montana, S.H. Oliet, A. Schousboe, P.G. Haydon, R.F. Stout, Jr., D.C. Spray, A. Reichenbach, T. Pannicke, M. Pekny, M. Pekna, R. Zorec, and A. Verkhratsky. 2012. Glial cells in (patho)physiology. *J Neurochem*. 121:4-27.
Parrill, A.L., and M.R. Reddy. 1999. Rational Drug Design. *In* Novel Methodology and Practical Applications. Amer Chemical Society. 374.
Pascual, G., A.L. Fong, S. Ogawa, A. Gamliel, A.C. Li, V. Perissi, D.W. Rose, T.M. Willson, M.G. Rosenfeld, and C.K. Glass. 2005. A SUMOylation-dependent pathway mediates transrepression of inflammatory response genes by PPAR-γ. *In* Nature. Vol. 437. 759-763.
Pekny, M., and M. Nilsson. 2005. Astrocyte activation and reactive gliosis. *Glia*. 50:427-434.
Pekny, M., U. Wilhelmsson, and M. Pekna. 2014. The dual role of astrocyte activation and reactive gliosis. *Neurosci Lett*. 565:30-38.
Perea, G., M. Navarrete, and A. Araque. 2009. Tripartite synapses: astrocytes process and control synaptic information. *Trends Neurosci*. 32:421-431.
Perl, D.P., and C.W. Olanow. 2007. The neuropathology of manganese-induced Parkinsonism. *J Neuropathol Exp Neurol*. 66:675-682.
Pringsheim, T., N. Jette, A. Frolkis, and T.D.L. Steeves. 2014. The prevalence of Parkinson's disease: A systematic review and meta-analysis. *In* Mov. Disord. Vol. 29. 1583-1590.
Qin, C., D. Morrow, J. Stewart, K. Spencer, W. Porter, R. Smith, 3rd, T. Phillips, M. Abdelrahim, I. Samudio, and S. Safe. 2004. A new class of peroxisome proliferator-activated receptor gamma (PPARgamma) agonists that inhibit growth of breast cancer cells: 1,1-Bis(3'-indolyl)-1-(p-substituted phenyl)methanes. *Mol Cancer Ther*. 3:247-260.
Racette, B.A. 2014. Manganism in the 21st century: The Hanninen lecture. *In* Neurotoxicology. Vol. 45. Elsevier B.V. 201-207.
Ransohoff, R.M., and V.H. Perry. 2009. Microglial physiology: unique stimuli, specialized responses. *Annu Rev Immunol*. 27:119-145.
Riojas-Rodriguez, H., R. Solis-Vivanco, A. Schilmann, S. Montes, S. Rodriguez, C. Rios, and Y. Rodriguez-Agudelo. 2010. Intellectual function in Mexican children living in a mining area and environmentally exposed to manganese. *Environ Health Perspect*. 118:1465-1470.
Rothe, T., N. Ipseiz, M. Faas, S. Lang, F. Perez-Branguli, D. Metzger, H. Ichinose, B. Winner, G. Schett, and G. Kronke. 2017. The Nuclear Receptor Nr4a1 Acts as a Microglia Rheostat and Serves as a Therapeutic Target in Autoimmune-Driven Central Nervous System Inflammation. *J Immunol*. 198:3878-3885.
Safe, S., U.-H. Jin, B. Morpurgo, A. Abudayyeh, M. Singh, and R.B. Tjalkens. 2015. Nuclear receptor 4A (NR4A) family – orphans no more. *In* Journal of Steroid Biochemistry and Molecular Biology. Elsevier Ltd. 1-13.

Saijo, K., A. Crotti, and C.K. Glass. 2013. Regulation of microglia activation and deactivation by nuclear receptors. *Glia*. 61:104-111.
Saijo, K., B. Winner, C.T. Carson, J.G. Collier, L. Boyer, M.G. Rosenfeld, F.H. Gage, and C.K. Glass. 2009a. A Nurr1/CoREST Pathway in Microglia and Astrocytes Protects Dopaminergic Neurons from Inflammation-Induced Death. *In* Cell. Vol. 137. Elsevier Ltd. 47-59.
Saijo, K., B. Winner, C.T. Carson, J.G. Collier, L. Boyer, M.G. Rosenfeld, F.H. Gage, and C.K. Glass. 2009b. A Nurr1/CoREST pathway in microglia and astrocytes protects dopaminergic neurons from inflammation-induced death. *Cell*. 137:47-59.
Santamaria, A.B. 2008. Manganese exposure, essentiality & toxicity. *Indian J Med Res*. 128:484-500.
Saucedo-Cardenas, O., and O.M. Conneely. 1996. Comparative distribution of NURR1 and NUR77 nuclear receptors in the mouse central nervous system. *J Mol Neurosci*. 7:51-63.
Schapira, A.H.V. 2011. Mitochondrial Pathology in Parkinson's Disease. *In* Mt Sinai J Med. Vol. 78. 872-881.
Sidoryk-Wegrzynowicz, M., and M. Aschner. 2013. Role of astrocytes in manganese mediated neurotoxicity. *BMC Pharmacol Toxicol*. 14:23.
Sigel, A.S., H.; Sigel, R.K.O. 2007. Metal Ions in Life Sciences. Wiley.
Smith, G.A., E.M. Rocha, T. Rooney, P. Barneoud, J.R. McLean, J. Beagan, T. Osborn, M. Coimbra, Y. Luo, P.J. Hallett, and O. Isacson. 2015. A Nurr1 Agonist Causes Neuroprotection in a Parkinson's Disease Lesion Model Primed with the Toll-Like Receptor 3 dsRNA Inflammatory Stimulant Poly(I:C). *In* PLoS ONE. Vol. 10. e0121072.
Sofroniew, M.V., and H.V. Vinters. 2010. Astrocytes: biology and pathology. *Acta Neuropathol*. 119:7-35.
Spranger, M., S. Schwab, S. Desiderato, E. Bonmann, D. Krieger, and J. Fandrey. 1998. Manganese augments nitric oxide synthesis in murine astrocytes: a new pathogenetic mechanism in manganism? *Exp Neurol*. 149:277-283.
Sriram, K., J.M. Matheson, S.A. Benkovic, D.B. Miller, M.I. Luster, and J.P. O'Callaghan. 2006. Deficiency of TNF receptors suppresses microglial activation and alters the susceptibility of brain regions to MPTP-induced neurotoxicity: role of TNF-alpha. *FASEB J*. 20:670-682.
St-Hilaire, M., E. Bourhis, D. Lévesque, and C. Rouillard. 2006. Impaired behavioural and molecular adaptations to dopamine denervation and repeated L-DOPA treatment in Nur77-knockout mice. *In* European Journal of Neuroscience. Vol. 24. 795-805.
Streifel, K.M., J. Miller, R. Mouneimne, and R.B. Tjalkens. 2013. Manganese inhibits ATP-induced calcium entry through the transient receptor potential channel TRPC3 in astrocytes. *Neurotoxicology*. 34:160-166.
Streifel, K.M., J.A. Moreno, W.H. Hanneman, M.E. Legare, and R.B. Tjalkens. 2012. Gene deletion of nos2 protects against manganese-induced neurological dysfunction in juvenile mice. *Toxicol Sci*. 126:183-192.
Streit, W.J. 2002. Microglia as neuroprotective, immunocompetent cells of the CNS. *Glia*. 40:133-139.
Suarez-Fernandez, M.B., A.B. Soldado, A. Sanz-Medel, J.A. Vega, A. Novelli, and M.T. Fernandez-Sanchez. 1999. Aluminum-induced degeneration of astrocytes occurs via apoptosis and results in neuronal death. *Brain Res*. 835:125-136.

Sugama, S., L. Yang, B.P. Cho, L.A. DeGiorgio, S. Lorenzl, D.S. Albers, M.F. Beal, B.T. Volpe, and T.H. Joh. 2003. Age-related microglial activation in 1-methyl-4-phenyl-1,2,3,6-tetrahydropyridine (MPTP)-induced dopaminergic neurodegeneration in C57BL/6 mice. *Brain Res*. 964:288-294.

Tanaka, M., M.E. Fuentes, K. Yamaguchi, M.H. Durnin, S.A. Dalrymple, K.L. Hardy, and D.V. Goeddel. 1999. Embryonic lethality, liver degeneration, and impaired NF-kappa B activation in IKK-beta-deficient mice. *In* Immunity. Vol. 10. 421-429.

Tansey, M.G., M.K. McCoy, and T.C. Frank-Cannon. 2007. Neuroinflammatory mechanisms in Parkinson's disease: potential environmental triggers, pathways, and targets for early therapeutic intervention. *Exp Neurol*. 208:1-25.

Teismann, P., and J.B. Schulz. 2004. Cellular pathology of Parkinson's disease: astrocytes, microglia and inflammation. *Cell Tissue Res*. 318:149-161.

THORN, J. 2002. Measurement Strategies for the Determination of Airborne Bacterial Endotoxin in Sewage Treatment Plants. *In* Annals of Occupational Hygiene. Vol. 46. 549-554.

Tjalkens, R.B., X. Liu, B. Mohl, T. Wright, J.A. Moreno, D.L. Carbone, and S. Safe. 2008. The peroxisome proliferator-activated receptor-γ agonist 1,1-bis(3′-indolyl)-1-(p-trifluoromethylphenyl)methane suppresses manganese-induced production of nitric oxide in astrocytes and inhibits apoptosis in cocultured PC12 cells. *In* Journal of Neuroscience Research. Vol. 86. 618-629.

Tjalkens, R.B., K.A. Popichak, and K.A. Kirkley. 2017. Inflammatory Activation of Microglia and Astrocytes in Manganese Neurotoxicity. *In* Advances in Neurobiology. Vol. 18. Springer International Publishing. 159-181.

Top. 2016. Nuclear receptor 4A1 (NR4A1) as a drug target for treating rhabdomyosarcoma (RMS). 1-13.

Verina, T., S.F. Kiihl, J.S. Schneider, and T.R. Guilarte. 2011. Manganese exposure induces microglia activation and dystrophy in the substantia nigra of non-human primates. *Neurotoxicology*. 32:215-226.

Verkhratski**, A.N., and A. Butt. 2013. Glial physiology and pathophysiology. Wiley-Blackwell, Chichester, West Sussex. xxxi, 527 p., 516 p. of col. plates pp.

Verkhratsky, A., and A. Butt. 2007. Glial Neurobiology: A Textbook. John Wiley & Sons Ltd. 215 pp.

Verkhratsky, A., L. Steardo, V. Parpura, and V. Montana. 2016. Translational potential of astrocytes in brain disorders. *Prog Neurobiol*. 144:188-205.

Verkhratsky, A.B., A. 2007. Glial Neurobiology.

Villarán, R.F., A.M. Espinosa-Oliva, M. Sarmiento, R.M. De Pablos, S. Argüelles, M.J. Delgado-Cortés, V. Sobrino, N. Van Rooijen, J.L. Venero, A.J. Herrera, J. Cano, and A. Machado. 2010. Ulcerative colitis exacerbates lipopolysaccharide-induced damage to the nigral dopaminergic system: potential risk factor in Parkinson`s disease. *In* Journal of Neurochemistry. Vol. 114. 1687-1700.

Wang, A., J. Rud, C.M. Olson, J. Anguita, and B.A. Osborne. 2009. Phosphorylation of Nur77 by the MEK-ERK-RSK Cascade Induces Mitochondrial Translocation and Apoptosis in T Cells. *In* The Journal of Immunology. Vol. 183. 3268-3277.

Wang, Q., Y. Liu, and J. Zhou. 2015. Neuroinflammation in Parkinson’s disease and its potential as therapeutic target. *In* Translational Neurodegeneration. Translational Neurodegeneration. 1-9.

Wang, Z., G. Benoit, J. Liu, S. Prasad, P. Aarnisalo, X. Liu, H. Xu, N.P.C. Walker, and T. Perlmann. 2003. Structure and function of Nurr1 identifies a class of ligand-independent nuclear receptors. *In* Nature. Vol. 423. 555-560.

Webster, C.M., M. Hokari, A. McManus, X.N. Tang, H. Ma, R. Kacimi, and M.A. Yenari. 2013. Microglial P2Y12 deficiency/inhibition protects against brain ischemia. *PLoS One*. 8:e70927.

Wei, X., H. Gao, J. Zou, X. Liu, D. Chen, J. Liao, Y. Xu, L. Ma, B. Tang, Z. Zhang, X. Cai, K. Jin, Y. Xia, and Q. Wang. 2016. Contra-directional Coupling of Nur77 and Nurr1 in Neurodegeneration: A Novel Mechanism for Memantine-Induced Anti-inflammation and Anti-mitochondrial Impairment. *Mol Neurobiol*. 53:5876-5892.

Weintraub, D., A.I. Tröster, C. Marras, and G. Stebbins. 2018. Initial cognitive changes in Parkinson's disease. *In* Mov. Disord. Vol. 29. 584.

Wingate, A.D., D.G. Campbell, M. Peggie, and J.S.C. Arthur. 2006. Nur77 is phosphorylated in cells by RSK in response to mitogenic stimulation. *In* Biochem. J. Vol. 393. 715-724.

Wood, R.J. 2009. Manganese and birth outcome. *In* Nutrition Reviews. Vol. 67. 416-420.

Woolf, A., R. Wright, C. Amarasiriwardena, and D. Bellinger. 2002. A child with chronic manganese exposure from drinking water. *Environ Health Perspect*. 110:613-616.

Wu, G., D.H. Robertson, C.L. Brooks, and M. Vieth. 2003. Detailed analysis of grid-based molecular docking: A case study of CDOCKER-A CHARMm-based MD docking algorithm. *In* J. Comput. Chem. Vol. 24. 1549-1562.

Wyss-Coray, T., and L. Mucke. 2002. Inflammation in neurodegenerative disease--a double-edged sword. *Neuron*. 35:419-432.

Xu, J., H. Dong, Q. Qian, X. Zhang, Y. Wang, W. Jin, and Y. Qian. 2017. Astrocyte-derived CCL2 participates in surgery-induced cognitive dysfunction and neuroinflammation via evoking microglia activation. *Behav Brain Res*. 332:145-153.

Yin, Z., D. Milatovic, J.L. Aschner, T. Syversen, J.B. Rocha, D.O. Souza, M. Sidoryk, J. Albrecht, and M. Aschner. 2007. Methylmercury induces oxidative injury, alterations in permeability and glutamine transport in cultured astrocytes. *Brain Res*. 1131:1-10.

Yoon, K., S.O. Lee, S.D. Cho, K. Kim, S. Khan, and S. Safe. 2011. Activation of nuclear TR3 (NR4A1) by a diindolylmethane analog induces apoptosis and proapoptotic genes in pancreatic cancer cells and tumors. *In* Carcinogenesis. Vol. 32. 836-842.

Yu, C., S. Cui, C. Zong, W. Gao, T. Xu, P. Gao, J. Chen, D. Qin, Q. Guan, Y. Liu, Y. Fu, X. Li, and X. Wang. 2015. The Orphan Nuclear Receptor NR4A1 Protects Pancreatic β-Cells from Endoplasmic Reticulum (ER) Stress-mediated Apoptosis. *In* Journal of Biological Chemistry. Vol. 290. 20687-20699.

Zhang, P., K.M. Lokuta, D.E. Turner, and B. Liu. 2010. Synergistic dopaminergic neurotoxicity of manganese and lipopolysaccharide: differential involvement of microglia and astroglia. *J Neurochem*. 112:434-443.

Zhang, P., T.A. Wong, K.M. Lokuta, D.E. Turner, K. Vujisic, and B. Liu. 2009. Microglia enhance manganese chloride-induced dopaminergic neurodegeneration: role of free radical generation. *Exp Neurol*. 217:219-230.

Zhang, S., Z. Zhou, and J. Fu. 2003. Effect of manganese chloride exposure on liver and brain mitochondria function in rats. *Environ Res*. 93:149-157.

Zhang, W., T. Wang, Z. Pei, D.S. Miller, X. Wu, M.L. Block, B. Wilson, W. Zhang, Y. Zhou, J.S. Hong, and J. Zhang. 2005. Aggregated alpha-synuclein activates microglia: a process leading to disease progression in Parkinson's disease. *FASEB J*. 19:533-542.

Zhao, F., T. Cai, M. Liu, G. Zheng, W. Luo, and J. Chen. 2009. Manganese induces dopaminergic neurodegeneration via microglial activation in a rat model of manganism. *Toxicol Sci*. 107:156-164.

Zota, A.R., A.S. Ettinger, M. Bouchard, C.J. Amarasiriwardena, J. Schwartz, H. Hu, and R.O. Wright. 2009. Maternal Blood Manganese Levels and Infant Birth Weight. *In* Epidemiology. Vol. 20. 367-373.